

EPA-650/3-74-003

October 1973

Ecological Research Series

WIND TUNNEL TESTS OF NEGATIVELY BOUYANT PLUMES



Office of Research and Development
U.S. Environmental Protection Agency
Washington, DC 20460

WIND TUNNEL TESTS OF NEGATIVELY BOUYANT PLUMES

by

T. G. Hoot, R. N. Meroney, and J. A. Peterka

Fluid Dynamics & Diffusion Laboratory
College of Engineering
Colorado State University
Fort Collins, Colorado 80521

Grant AP-01186
Program Element No. 1AA009

EPA Project Officer: Willaim H. Snyder

Meteorology Laboratory
National Environmental Research Center
Research Triangle Park, North Carolina 27711

Prepared for

OFFICE OF RESEARCH AND DEVELOPMENT
U.S. ENVIRONMENTAL PROTECTION AGENCY
WASHINGTON, D.C. 20460

October 1973

This report has been reviewed by the Environmental Protection Agency and approved for publication. Approval does not signify that the contents necessarily reflect the views and policies of the Agency, nor does mention of trade names or commercial products constitute endorsement or recommendation for use.

ABSTRACT

WIND TUNNEL TESTS OF NEGATIVELY BUOYANT PLUMES

This study reports the results of tests made of negatively buoyant emissions into a quiescent medium, laminar crosswind and turbulent boundary layer. Measurements included the maximum rise height, horizontal point of descent and behavior of emission concentrations.

TABLE OF CONTENTS

<u>Section</u>	<u>Page</u>
LIST OF TABLES	vi
LIST OF FIGURES	vii
LIST OF SYMBOLS	ix
I. INTRODUCTION	1
1.1 Negatively Buoyant Emissions	1
1.2 Plume Rise	3
1.3 Moist Plumes	5
1.4 Velocity and Concentration Distributions	6
II. PLUME RISE EQUATIONS	9
2.1 Vertical Plumes in a Quiescent Medium	9
2.2 Bent Over Negatively Buoyant Plume in a Laminar Crosswind	17
III. CONCENTRATION DETERMINATIONS	25
3.1 Plumes in a Laminar Crosswind	25
3.2 Dense Ground Source in a Turbulent Boundary Layer	27
3.2.1 Eulerian Diffusion Formulation	27
3.2.2 Lagrangian Formulations	29
3.2.3 Wind Tunnel Simulation of Diffusion	31
IV. EXPERIMENTAL MEASUREMENTS	33
4.1 Plume Rise	33
4.2 Concentration Measurements	35
4.2.1 Plumes in a Laminar Crosswind	35
4.2.2 Dense Ground Source in a Turbulent Boundary Layer	35
V. APPARATUS AND INSTRUMENTATION	37
5.1 Wind Tunnels	37
5.2 Velocity and Temperature Measurements	37
5.3 Gas Mixing and Smoke Visualization	38
5.4 Vortex Generators	39
5.5 Concentration Measurements	40
5.5.1 Measuring Apparatus	40
5.5.2 Tube and Gas Calibration	40
5.5.3 Concentration Calculations and Counting Statistics	41
VI. RESULTS OF EXPERIMENTS	43
6.1 Plume Rise	43
6.1.1 Vertical Plumes	43
6.1.2 Plumes in a Laminar Crosswind	44
6.1.3 Plume Rise in the Presence of a Cubical Structure	46

<u>Section</u>	<u>Page</u>
6.2 Concentrations	47
6.2.1 Plumes in a Laminar Crosswind	47
6.2.2 Dense Ground Source in a Turbulent Boundary Layer	48
6.2.3 Decay of Concentration in Buoyancy Dominated Plumes After Touchdown	49
VII. CONCLUSIONS	51
BIBLIOGRAPHY	52
TABLES	55
FIGURES	60

LIST OF TABLES

<u>Table</u>		<u>Page</u>
I	VERTICAL PLUMES SMOKE VISUALIZATION DATA	55
II	PLUMES IN A LAMINAR CROSSWIND SMOKE VISUALIZATION DATA	56

LIST OF FIGURES

<u>Figure</u>		<u>Page</u>
1	CSU Thermal Wind Tunnel	60
2	Flow Mixing and Visualization System	61
3	Vortex Generator Details	62
4	Velocity Profile Laminar Flow	63
5	Velocity Profile at Source, Turbulent Boundary Layer	64
6	Velocity Profiles, Tunnel Centerline, Turbulent Boundary Layer	65
7	Turbulence Intensities, Tunnel Centerline	66
8	Temperature Profiles, Thermal Stratification	67
9	Gradient Richardson Number, Thermal Stratification	68
10	Radiation Detection System	69
11	Smoke Photographs	70
12	Dimensionless Rise Height vs. Froude Number-Vertical Plumes	72
13	Dimensionless Rise Height vs. Rise Height Parameter	73
14	Dimensionless "Touchdown" Distance vs. "Touchdown Parameter"	74
15	Isopleths of Plume in Laminar Crosswind	75
16	Maximum Concentration vs. Downstream Distance Plumes in a Laminar Crosswind, $R=5$, $D_o=1/8"$	77
17	Maximum Concentration vs. Downstream Distance, Plumes in a Laminar Crosswind, $R=10$, $D_o=1/8"$	78
18	Maximum Concentration vs. Downstream Distance, Plumes in a Laminar Crosswind, $R=15$, $D_o=1/8"$	79
19	Maximum Concentration at Plume High Point vs. H/D_o	80

<u>Figure</u>		<u>Page</u>
20	Maximum Concentration at Plume Touchdown vs. Fall Parameter	81
21	Maximum Concentrations vs. Downstream Distance, Negatively Buoyant Ground Source, Neutral Stratification	82
22	Maximum Concentrations vs. Downstream Distance, Negatively Buoyant Ground Source, Inversion Stratification	83
23	Lateral Spread 50 Percent Concentration Neutral Stratification	84
24	Lateral Spread 50 Percent Concentration Inversion Stratification	85
25	Lateral Spread 10 Percent Concentration Neutral Stratification	86
26	Lateral Spread 10 Percent Concentration Inversion Stratification	87
27	Vertical Spread 50 Percent Concentration Neutral Stratification	88
28	Vertical Spread 50 Percent Concentration Inversion Stratification	89
29	Vertical Spread 10 Percent Concentration Neutral Stratification	90
30	Vertical Spread 10 Percent Concentration Inversion Stratification	91
31	Cross-sectional Distribution of Concentration, x=6 ft. Neutral Stratification	92
32	Decay of Plume Maximum Concentration Downstream from Touchdown Point	93

LIST OF SYMBOLS

b	Plume Radius
b_o	Stack Radius
D_o	Stack Diameter
e	Base of Natural Logarithm
F	Flux of Negative Buoyancy
F_R	"Vertical" Densimetric Froude Number Based on Stack Exit Velocity, Density and Density Difference
F_{RH}	"Horizontal" Densimetric Froude Number Based on Crosswind Velocity, Ambient Density and Stack Exit Density Difference
g	Gravitational Acceleration
H	Maximum Plume Rise Height Above Stack
h_s	Stack Height Above Ground
h_b	Building Height Above Ground
R	Velocity Ratio (Stack Exit Velocity Divided by Crosswind Velocity)
Ri	Richardson Number
Re	Reynolds Number
S	Distance Measured Along Plume Trajectory From Stack Exit
SG	Specific Gravity (Air = 1)
t	Time
T	Time of Maximum Plume Rise
T_o, T_r	Reference Temperatures
U	Boundary Layer Longitudinal Velocity
U	Plume Velocity
U_o	Stack Exit Velocity
V	Crosswind Velocity
W	Plume Vertical Velocity

X	Longitudinal Coordinate
\bar{X}	Longitudinal Coordinate of Plume Maximum Rise
X_D	Plume Touchdown Point (Longitudinal Coordinate)
y	Lateral Coordinate
z	Vertical Coordinate

Greek Letters

α, β	Dimensionless Entrainment Constants
γ	Ratio of Characteristic Length for Gaussian Concentration Distribution to that for Velocity Distribution
θ	Angle of Plume Trajectory with Horizontal
ν	Kinematic Viscosity
σ_y	Transverse Plume Standard Deviation
σ_z	Vertical Plume Standard Deviation
ρ	Plume Density
ρ_o	Plume Density at Stack Exit
ρ_A	Ambient Air Density
χ	Local Concentration
χ_o	Concentration at Stack Exit

Subscripts

O	Denotes Stack Exit Quantities
A	Denotes Ambient Quantities
D	Denotes Quantities at Plume Touchdown
M	Denotes Quantity at Plume Centerline

SECTION I

INTRODUCTION

Negatively buoyant emissions into the atmosphere have been reported by several observers. Scorer (23) reports the case of two power plants emitting wet-washed plumes with apparently insufficient elimination of free water, in which the subsequent evaporation of the free water cools the plume and causes it to sink. According to the report the plant itself is obscured from view on many occasions. Chesler and Jesser (8) and Bodurtha (3) have observed and discussed the descent of dense gases from stacks and relief valves.

The consequences of such behavior are potentially drastic. When the plume sinks rapidly to the ground, very little dilution will occur in comparison with normal emissions and high ground level concentrations of gases which may be toxic or explosive could result. In this report experimental results of the dynamic behavior of negatively buoyant emissions and the resulting concentration distributions are reported.

1.1 Negatively Buoyant Emissions

Previous experimental work with negatively buoyant emissions appears to be confined to three efforts. Bodurtha (3) conducted wind tunnel tests of emissions of freon-air mixtures into a crosswind. Various combinations of density, exit velocity, crosswind velocity and stack diameter were used in obtaining smoke pictures. The results were correlated by an expression for the maximum rise height:

$$H = 5.44 D_o^{0.5} R^{0.75}$$

In which H is the maximum rise height of the plume centerline, D_o is the stack diameter and R is the ratio of the exit velocity to the wind speed. This formula has the disadvantage of being dimensionally inhomogeneous and the absence of relative density terms makes its application questionable as the specific gravity approaches unity.

Turner (31) conducted experiments in which salt water jets were injected vertically into calm fresh water. Maximum rise heights were observed and correlated with various dimensionless parameters and an expression was reported equivalent to:

$$H/D_o = 1.74 F_R$$

In which H and D_o are as previously defined and F_R is the densimetric Froude number based on the ambient density and original density difference. This Froude number is defined as:

$$F_R = \frac{\sqrt{\rho_A} U_o}{\sqrt{g D_o (\rho_o - \rho_A)}}$$

where ρ_A = Ambient Density

U_o = Exit Velocity

ρ_o = Exit Density

D_o = Exit Diameter

This definition of the Froude number implies the Boussinesq assumption for density in the inertial terms of the equations of motion; thus it can be considered applicable in the density range in which that assumption is valid. Although the constant of proportionality is reported by Turner as equal to 1.74, a plot of values given in the original article indicates the value of this constant was determined graphically to be 3.1.

Holly and Grace (15) conducted tests of salt water jets injected vertically into a fresh water open channel in which maximum rise heights and downstream concentrations were measured. Expressions obtained for rise height and concentration distribution were:

$$\frac{H-D}{D_0} = (3.47 \times 10^{\frac{-0.148F_R}{R}})$$

and

$$\epsilon_m = (31. \times 10^{\frac{0.4F_R}{R}}) \left(\frac{X}{X_0}\right)^{.68}$$

In which H is the top edge of the jet and D the jet diameter at maximum rise height, ϵ_m is the least dilution (reciprocal of dimensionless concentration), X is downstream distance and X_0 the distance to the point where the jet descends to the channel bottom. The least dilution expression was stated to apply to both the regions upstream and downstream from $X = X_0$.

1.2 Plume Rise

A large amount of work has been completed upon the rise of buoyant plumes. The beginning point for most of the recent work is the classic paper of Morton, Taylor and Turner (19) which examines the rise of a buoyant plume in a quiescent medium. The analysis was based on the conservation of volume, mass and momentum with assumptions of self similarity, circular plume cross section and simple proportionality of volumetric entrainment rate to plume velocity. Either Gaussian or "top hat" profiles of velocity and buoyancy flux may be assumed with appropriate modifications of the equations. With the assumption of a

"virtual point source" located below the actual exit, the model predicts a "straight sided" plume.

The "bent-over" plume rise models of Briggs (4) and Csanady (10) incorporate this theory for the initial stage of buoyant, bent-over rise which predicts a $2/3$ power parabola as the plume trajectory. In both models a second stage is introduced in which the rate of volumetric entrainment is related to the turbulent energy dissipation per unit mass. Criteria for transition is that the rate of entrainment thus computed exceed that computed by the initial stage theory and is applicable when environmental turbulence in the inertial subrange dominates mixing. This predicts a leveling off to an asymptotic rise which Briggs takes as the final rise height. Csanady introduces a third stage in which the eddy diffusivity is taken as constant and a linear rate of rise is predicted. In both these models the initial region of momentum dominated rise is neglected as insignificant in contributing to the final rise height.

Hoult, Fay and Forney (14) introduced a continuous model for the rise of a buoyant plume in a laminar uniform crosswind. Utilizing the Morton et al. assumptions of self similarity and conservation of mass and momentum and employing entrainment constants for velocity differences parallel and perpendicular to the flow direction, the model predicts a momentum-dominated jet behavior close to the stack with a $1/2$ power parabola trajectory. It subsequently suggests a buoyancy dominated plume with a $2/3$ power parabola trajectory far from the stack similar to the initial stages of the Briggs and Csanady models. For a bent-over jet in a laminar crosswind all of the above models predict a $1/3$ power parabola a trajectory.

Several investigators (16), (24), (30) have observed and recorded the internal and surrounding flows associated with jets and plumes injected into a cross flow. The plume emerges as a jet from the stack exit, traveling upward much like a typical momentum jet. The cross-wind effect soon becomes dominant bending the plume over and convecting it downstream with a lateral velocity essentially equal to the cross-wind.

It has been further noted that as the plume rises, its cross-sectional shape changes from circular to "kidney-shaped" (30), and finally as it is bent over, the outside shear layer which envelopes the plume tends to roll up behind the core and from two line vortices of equal strength but opposite sign.

Noting this fact, Tulin and Schwartz (28) conducted investigations into the rise and growth of a two-dimensional vortex pair passing through neutral and stably stratified surroundings. As the plume falls or rises in stably stratified surroundings a lateral spreading and deviation from circular cross section was noted.

In all of the above cited models the Boussinesq approximation is made, i.e. that the density in the inertial terms of the equations of motion is approximately equal to ambient density, or more properly, that potential density is equal to ambient potential density.

1.3 Moist Plumes

Morton (20) considered the case of a moist plume released vertically into a quiescent atmosphere using entrainment theory and conservation of mass, volume, momentum and specific humidity. Assuming a linear variation in atmospheric humidity, he obtained an expression for the plume specific humidity as a function of height.

Csanady (10) and Slawson and Wigley (33) extended this analysis and formulated a model for the dynamic behavior of a bent-over plume containing both free water and water vapor. The model considers evaporation and condensation along with the resulting effects on the buoyancy flux. Wigley and Slawson (32) applied this analysis to the rise of a saturated plume.

1.4 Velocity and Concentration Distributions

Prandtl's mixing length theory applied to circular turbulent jets predicts a constant eddy viscosity and diffusivity (25) which in turn predicts Gaussian distributions of velocity and effluent concentration along with a decay rate of maximum values of these quantities that is inversely proportional to downstream distance. Experimental measurements have confirmed this theory.

Albertson et al. (1) measured velocity distributions in a simple momentum jet. The profiles were determined to be Gaussian and the rate of decay of maximum velocity inversely proportional to downstream distance following the zone of flow establishment. Becker (2) et al. measured concentrations in a jet and found them to be Gaussian also, but flatter in profile than the velocity distributions measured by Albertson. The decay rate of maximum concentration was found to be inversely proportional to downstream distance, but decaying at a faster rate than the velocity.

Rouse et al. (22) measured velocities and temperatures above a point source of heat and obtained Gaussian profiles for both, though slightly sharper in profile for those obtained for jets. Maximum velocities and temperatures were observed to decay according to $-1/3$ and $-5/3$ powers of downstream distance respectively. Hewett (13)

measured temperature distributions in heated plumes injected into a laminar cross flow in a wind tunnel for neutral and stratified cases and found the distributions to be qualitatively Gaussian, although he proposed no model and did not report a decay rate with downstream distance. It was noted that concentration gradients were much steeper on the bottom than the top indicating the influence of buoyancy on the local diffusion.

For turbulent diffusion phenomena in the lower atmosphere, Sutton's equations have been widely used to estimate concentration distributions for a point source, but the application is restricted because of many ideal assumptions. Also, they are not sensitive to atmospheric stratification situations. In an attempt to improve sensitivity to real conditions Pasquill-Gifford's semi-empirical formulas have become popular. A set of transverse and vertical standard deviations of the dispersion are plotted as functions of downstream distance. A "stability category" which classifies six different kinds of possible atmospheric stratifications, relates the various plume dispersions to different meteorological conditions.

Wind tunnel studies of diffusion over topographic models in turbulent boundary layers indicate good correlation with Pasquill-Gifford prediction techniques (18). In addition wind tunnel diffusion studies have been conducted for idealized source conditions. Davar (11) studied diffusion from a horizontal point source in a neutral turbulent boundary layer. Malhotra (17) performed similar experiments under unstable conditions, while Chaudhry (7) studied diffusion in a stably stratified boundary layer. Shih (26) evaluated the effects of

the growth of boundary layer thickness and free stream turbulent intensity upon diffusion.

Yang and Meroney (35) studied the diffusion in the wake of a cubical structure placed in a turbulent boundary layer. They found that the critical conditions, such that the plume will not be trapped in the building cavity region are:

$$R \geq 1, h_s/h_b \geq 2$$

where R is the velocity ratio and h_s and h_b are the stack and building heights as measured from the ground.

SECTION II

PLUME RISE EQUATIONS

2.1 Vertical Plumes in a Quiescent Medium

Smoke pictures of negatively buoyant plume rise in a quiescent medium indicate that the behavior is such that the plume exists in a jet with approximately linear growth of radius with vertical distance to between 1/3 and 1/4 plume rise height. The plume width then grows in a highly non-linear fashion, becoming quite large in the upper regions. Although simple entrainment theory can not be expected to give a complete description of this motion, especially as entrainment occurs in a complex manner along the top of the plume and the bottom of the plume "crown", it may serve as an aid to dimensional analysis in predicting the relationship between pertinent parameters. Clearly, some accounting for the entrainment is necessary since the assumption of a frictionless plume with no entrainment leads to

$$H/D_o = F_R^2/2$$

General Equations of Conservation:

If the effects of the descending fluid on the exterior of the plume are neglected due to their much smaller density and velocities, the equations of conservation (after Morton et al.) become:

Buoyancy:

$$\frac{d}{dZ} \int_0^\infty \rho U 2\pi r dr = \rho_A \frac{d}{dZ} \int_0^\infty U 2\pi r dr$$

Assuming ρ_A to be a function of Z alone.

$$\frac{d}{dZ} \int_0^\infty (\rho_A - \rho) U 2\pi r dr = \left[\int_0^\infty U 2\pi r dr \right] \frac{d\rho_A}{dZ}$$

For $\frac{d\rho_A}{dZ} = 0$ (neutral atmosphere)

$$\int_0^{\infty} (\rho_A - \rho) U 2\pi r dr = b_o^2 U_o (\rho_A - \rho_o) 2\pi \quad (2.1)$$

One may define the average density $\bar{\rho} = \frac{\int_0^{\infty} \rho U 2\pi r dr}{\int_0^{\infty} U 2\pi r dr}$ as:

$$\bar{\rho} = \rho_A \left[1 + \frac{(b_o^2 U_o) (SG-1)}{\int_0^{\infty} U 2\pi r dr} \right] \quad (2.2)$$

Momentum:

$$\frac{d}{dZ} \int_0^{\infty} \rho U^2 2\pi r dr = \int_0^{\infty} (\rho_A - \rho) g 2\pi r dr$$

Equations of Conservation (Top Hat Profile):

If a "top hat" profile and the Morton et al. entrainment hypothesis are employed $\int_0^{\infty} U 2\pi r dr = b^2 U$

Volume:

$$\frac{d}{dZ} (b^2 U) = 2\alpha b U \quad (2.3)$$

where α is an entrainment constant of proportionality relating inflow velocity of outside air to plume velocity. Similarly

Buoyancy:

$$(\rho_A - \rho) b^2 U = \rho_A (1 - SG) b_o^2 U_o \quad (2.4)$$

where $SG = \rho_o / \rho_A$. Also:

$$\rho = \rho_A \left[1 + \frac{b_o^2 U_o (SG-1)}{b^2 U} \right] \quad (2.5)$$

Momentum:

$$\frac{d}{dz} (\rho b^2 U^2) = (\rho_A - \rho) b^2 g \quad (2.6)$$

Maximum Rise Time (Top Hat Profile):

Combining equations (2.4), (2.6), and the relationship $dz/dt = U$ one may obtain

$$\frac{d}{dt} (\rho b^2 U^2) = \rho_A (1-SG) b_o^2 U_o^2 g$$

or

$$\rho b^2 U^2 = \rho_A (1-SG) b_o^2 U_o^2 g t + \rho_o b_o^2 U_o^2$$

And since at maximum rise $\rho b^2 U^2 = 0$, the time of rise can be calculated as

$$T = \frac{\rho_o U_o}{(\rho_o - \rho_A) g} \quad (\text{Time of Maximum Rise}) \quad (2.7)$$

If a Gaussian distribution is assumed and if the ratio of α for the two cases is adjusted so that the conservation of mass is consistent at stack exit, the same expression for maximum rise results.

Equations of Conservation (Gaussian):

If a Gaussian distribution is assumed such that b is a characteristic length (different from the value of b in the top hat model), following Morton, Taylor and Turner, and:

$$\rho - \rho_A = (\rho_m - \rho_A) e^{-r^2/b^2 \gamma}$$

$$U = U_m e^{-r^2/b^2}$$

γ = Ratio of characteristic lengths for density and velocity

b_o = Initial Radius

Subscript m = Centerline Values

The equations of conservation become:

$$\frac{d}{dz} [b^2 U_m] = 2\alpha b U_m \quad (2.3a)$$

$$(\rho_A - \rho_m) \frac{\gamma b^2 U_m}{1+\gamma} = \rho_A (1-SG) b_o^2 U_o \quad (2.4a)$$

$$\frac{d}{dz} \left[\int_0^\infty \rho U^2 2\pi r dr \right] = (\rho_A - \rho_m) b^2 \gamma g \quad (2.6a)$$

Maximum Rise Time (Gaussian):

If Z is measured along the plume centerline. $dZ/dt = U_m$, so that:

$$\frac{d}{dt} \left[\int_0^\infty \rho U^2 2\pi r dr \right] = (\rho_A - \rho_m) U_m b^2 \gamma g$$

If γ is taken as unity to simplify the equations and initial conditions are made to match, using (2.4a) we obtain:

$$\frac{d}{dt} \left[\int_0^\infty \rho U^2 2\pi r dr \right] = 2\rho_A (1-SG) b_o^2 U_o g$$

and

$$\int_0^\infty \rho U^2 2\pi r dr = 2\rho_A (1-SG) b_o^2 U_o g t + \rho_o b_o^2 U_o^2 \quad (A)$$

At maximum rise height the integral on the left hand side is zero and an expression for time of maximum rise results as:

$$T = \frac{\rho_o U_o}{2(\rho_o - \rho_A)g} \quad (2.7a)$$

Maximum Rise Height (Gaussian):

The assumption of nearly constant density i.e. in equation (A), yields:

$$\rho U_m^2 b^2 = 4\rho_A (1-SG) b_o^2 U_o g t + 2\rho_o b_o^2 U_o^2$$

So that:

$$b_m^2 U_m^2 = \frac{4\rho_A(1-SG)b_o^2 U_o g t + 2\rho_o b_o^2 U_o^2}{\rho}$$

If it is assumed that $\rho \approx \rho_o$ then equation (2.8) becomes

$$b_m^2 U_m^2 = 4 \frac{(1-SG)}{SG} b_o^2 U_o g t + 2b_o^2 U_o^2 \quad (2.6b)$$

The conservation of volume expression is taken to be the same here as for top hat velocity profiles with the understanding that the value of α thus defined will in general be different from the top hat value, and since $dZ = U_m dt$:

$$\frac{d}{dt} [b_m^2 U_m] = 2\alpha b U_m^2 \quad (2.3b)$$

Matching the fluxes of volume and momentum to stack exit quantities:

$$U_{mo} = 2U_o$$

$$b_{mo} = b_o / \sqrt{2}$$

The velocity and radius may be non-dimensionalized with their initial values such that:

$$b_* = b/b_o \approx b/\sqrt{2} b_{mo}$$

$$U_* = U/U_o \approx 2U/U_{mo}$$

$$t_* = t/T$$

$$Z_* = Z/U_o T$$

Thus utilizing the above and the definition of maximum rise time equation (2.7a):

$$\frac{d}{dt_*} (b_*^2 U_{m*}) = 2\alpha b_* U_{m*}^2 \left(\frac{U_o T}{b_o} \right) \quad (2.3c)$$

$$(1 - \rho_m/\rho_A) b_*^2 U_{m*} = 2(1-SG) \quad (2.4c)$$

$$b_*^2 U_{m*}^2 = 2(1-t_*) \quad (2.6c)$$

One can now eliminate b_* from equation (2.3c) by utilizing equation (2.6c) to obtain a differential equation in U_{m*} alone.

$$\frac{d}{dt*} \left(\frac{(1-t*)}{U_{m*}} \right) = \sqrt{2} \alpha F_R^2 U_{m*} \sqrt{1-t*}$$

thus may be integrated to yield

$$U_{m*} = \frac{2(1-t*)}{\sqrt{\frac{16\alpha\sqrt{2}F_R^2}{5} \{1-(1-t*)^{5/2}\} + 1}}$$

Information is now available to calculate the maximum rise height H , defined as $H = U_o T \int_0^1 U_{m*} dt*$. The result is

$$\begin{aligned} \frac{H}{D_o} &= \frac{2F_R^2}{5} \frac{N^{3/10}}{M^{4/5}} \int_0^{\frac{M}{N}} \frac{dR}{R^{1/5}(1-R)^{1/2}} \\ &= 2 \frac{F_R^2}{5} \left(\frac{N}{M} \right)^{3/10} \frac{1}{M^{1/2}} \left\{ B(4/5, 1/2) - \int_{\frac{M}{N}}^1 \frac{dR}{R^{1/5}(1-R)^{1/2}} \right\} \end{aligned}$$

where

$$P = (1-t_*)^{5/2}, \quad M = \frac{16\alpha\sqrt{2} F_R^2}{5}, \quad \text{and } N = 1+M.$$

Note $R = \frac{MP}{N}$ and B is the Beta Function. The second integral on the right can be evaluated by a series expansion as:

$$\left\{ \frac{5}{4} R^{4/5} + \sum_{n=1}^{\infty} \frac{\Gamma(\frac{n}{2})}{\Gamma(n+1)} R^{\frac{5n+4}{5}} \left(\frac{5}{5n+4} \right) \right\} \frac{1}{M/N}$$

The series can be shown to be convergent if Stirling's Formula for $\Gamma(n)$ as n gets large is assumed. For most Froude numbers, however, $M/N \approx 1$ and

$$\frac{H}{D_o} \approx \frac{2}{5} \frac{F_R^2 B(1/2, 4/5)}{\sqrt{\frac{16\sqrt{2}}{5} \alpha F_R^2}} = \frac{2.30 F_R}{(2)^{5/4} (5)^{1/2} \sqrt{\alpha}}, \quad \text{or}$$

$$\frac{H}{D_o} = \frac{0.43 F_R}{\sqrt{\alpha_{\text{Gaussian}}}}$$

If α for the Gaussian and top hat cases are adjusted to make equation (2.4) equivalent at stack exit for both top hat and Gaussian assumptions:

$$\alpha_{\text{top hat}} = \sqrt{2} \alpha_{\text{Gaussian}}$$

and

$$H/D_o = \frac{0.515 F_R}{\sqrt{\alpha_{\text{top hat}}}} \quad (2.8a)$$

And if it is assumed $\rho \approx \rho_A$:

$$H/D_o = \frac{0.515 SG^{1/4} F_R}{\sqrt{\alpha_{\text{top hat}}}} \quad (2.8b)$$

These expressions are identical to those obtained with the same constant density assumptions and a top hat profile of plume quantities if the top hat rise time is used.

In the above F_R is the densimetric Froude number based on stack exit velocity, density and density difference rather than the one obtained using the Boussinesq approximation and is defined as:

$$F_R = \frac{U_o}{\sqrt{\frac{(\rho_o - \rho_A)}{g D_o \rho_o}}}$$

Expressions (2.8) represent the rise computed by neglecting the entrainment resulting from lateral velocities due to radial growth at the top and bottom of the plume "crown" and predicts an infinite radius at maximum rise height.

Estimation of Entrainment Constant:

Equations (2.8) cannot be utilized experimentally to give a precise estimate for the actual value of α . Good correlation with the Froude number or Froude number and specific gravity is a valid expectation, however.

A method of evaluating α results from considering motion in the jet region immediately downstream from the stack. The conservation of momentum leads to:

$$\rho b^2 U^2 = -(\rho_o - \rho_A) b_o^2 U_o g t + \rho_o b_o^2 U_o^2$$

In the jet region t is small and $\bar{\rho} b^2 U^2 \approx \rho_o b_o^2 U_o^2$

$$\text{From (2.5) } \bar{\rho} = \rho_A \left[1 + \frac{b_o^2 U_o^2 (SG-1)}{b^2 U} \right]$$

This leads to:

$$b^2 U = \frac{-b_o^2 U_o (SG-1) + \sqrt{[b_o^2 U_o (SG-1)]^2 + 4SG b_o^2 U_o^2 b^2}}{2}$$

Substituting in (2.4) and integrating results in an expression for α for a top hat profile which should be approximated close to the stack.

$$\alpha = \frac{1}{Z} \left[\frac{b-b_o}{2} + \frac{b_o (SG-1)}{4\sqrt{SG}} \ln \left\{ \frac{\sqrt{[b_o^2 U_o (SG-1)]^2 + 4SG b_o^2 U_o^2 b^2} + 2\sqrt{SG} b_o U_o b}{\sqrt{[b_o^2 U_o (SG-1)]^2 + 4SG b_o^4 U_o^2} + 2\sqrt{SG} b_o^2 U_o} \right\} \right] \quad (2.9)$$

It should be noted here that the value of α computed in this manner is of the order of half the value of α as computed for a point source of buoyancy where α is taken as db/dZ . The jet assumption is

subject to the limitations of assuming that the buoyancy forces are small in the jet region, while the point source is subject to the limitations of ignoring finite momentum flux and the assumption of a point source for a finite diameter. Briggs (5) gives an estimate for the point source of $\alpha = 0.075$.

2.2 Bent Over Negatively Buoyant Plume In a Laminar Crosswind

The effect of negative buoyance on plume behavior and resulting downwind concentrations will be greatest when crosswinds are light, and turbulence intensities are low. The sinking velocity of the plume relative to the horizontal convective velocity will be much higher than under "normal" conditions. In such cases, the entrainment of outside air into the plume and the resulting diffusion is a function of this interaction between the plume and the crosswind, and approaches the behavior of a turbulent plume injected into a laminar crosswind.

General Equations of Conservation (Top Hat Profiles):

Assuming a crosswind of constant velocity, a "top hat" profile, and the Hoult et al. model for the entrainment of outside air into the plume, where entrainment due to "parallel" and "perpendicular" velocity differences are assumed to superimpose, the equations of motion become:

(a) Conservation of "Volume"

$$\frac{d}{ds} (b^2 U) = 2\alpha b (U - V \cos \theta) + 2\beta b V |\sin \theta|; \quad (2.10)$$

(b) Conservation of Horizontal Momentum:

$$\frac{d}{ds} (\rho b^2 U^2 \cos \theta) = \rho_A V \frac{d}{ds} (b^2 U) \quad (2.11)$$

(c) Conservation of Vertical Momentum:

$$\frac{d}{ds} (\rho b^2 U W) = (\rho_A - \rho) b^2 g \quad (2.12)$$

(d) Conservation of Mass

$$\frac{d}{ds} (\rho b^2 U) = \rho_A \frac{d}{ds} (b^2 U) \quad (2.13)$$

which leads to the buoyancy flux relation:

$$\frac{d}{ds} (\rho_A - \rho) b^2 U g = b^2 U g \frac{d\rho_A}{dz} \sin\theta \quad (2.14)$$

where:

s = Distance measured along plume axis

U = Axial velocity = ds/dt

W = Vertical component of velocity

θ = Angle of plume axis with the horizontal

Trajectory Near Stack:

In the case of a neutral atmosphere equation (2.12) still leads to equation (2.7) for the time of maximum rise. Examining the case of the plume as it initially leaves the stack, where the trajectory is approximately vertical, $\cos\theta \approx 0$, $\sin\theta \approx 1$, $U \approx W$.

Equation (2.13) integrates to

$$\rho b^2 W^2 = (\rho_A - \rho_o) b_o^2 g U_o t + \rho_o b_o^2 U_o^2$$

And since t is still small:

$$\rho b^2 W^2 \approx \rho_o b_o^2 U_o^2 \quad (B)$$

Noting that $\cos\theta = \frac{dx}{ds} = \frac{1}{(1 + (\frac{dz}{dx})^2)^{1/2}}$, equation 2.11 becomes:

$$\frac{\rho b^2 W^2}{(1 + Z'^2)^{1/2}} = \rho_A V(b^2 W - b_o^2 U_o)$$

or rearranging and utilizing equation (B) above,

$$b^2 W \approx \frac{R(SG)}{Z'} + 1 - b_o^2 U_o$$

This may be substituted directly into equation (2.10).

$$\frac{d}{dZ} (b^2 W) = b_o^2 U_o \frac{d}{dZ} \frac{R(SG)}{Z'} = 2\alpha b W + 2\beta b V$$

One may replace the right hand terms by:

$$\begin{aligned} bW &= \frac{\sqrt{\rho_o} b_o U_o}{\sqrt{\rho}} = \frac{\sqrt{\rho_o} b_o U_o}{\sqrt{\rho_A \left(1 + \frac{b_o^2 U_o (SG-1)}{b^2 W}\right)}} = \frac{\sqrt{SG} b_o U_o \sqrt{R(SG)+Z'}}{\sqrt{SG} \sqrt{R+Z'}} \\ &= b_o U_o \frac{\sqrt{R(SG)+Z'}}{R+Z'} \end{aligned}$$

$$bV = \frac{b^2 W V}{bW} = b_o U_o \left(\frac{R(SG)+Z'}{Z'} \right) \sqrt{\frac{R+Z'}{R(SG)+Z'}}$$

If $\sqrt{\frac{R+Z'}{R(SG)+Z'}}$ can be taken as ≈ 1 the new continuity of volume expression is:

$$\frac{d}{dZ} \left[\frac{R(SG)}{Z'} \right] - \frac{2\beta}{Rb_o} \frac{R(SG)}{Z'} = \frac{2\alpha}{b_o} + \frac{2\beta}{b_o R}$$

Integrating this differential expression results in:

$$\begin{aligned} R(SG)/Z' &= \left(1 + \frac{\alpha}{\beta} R\right) \left(e^{\frac{2\beta Z}{Rb_o}} - 1\right) = \left(1 + \frac{\alpha R}{\beta}\right) \left(0 + \frac{2\beta Z}{Rb_o} + \frac{2\beta^2}{R^2 b_o^2} Z^2 + \dots\right) \\ X &= \frac{1}{R(SG)} \left[\frac{(\alpha R + \beta) Z^2}{Rb_o} + \frac{2\beta}{3Rb_o} \left(\frac{(\alpha R + \beta) Z^3}{Rb_o} \right) + \dots \right] \end{aligned}$$

$$Z = R \sqrt{\frac{(SG)b_o X}{\alpha R + \beta}}$$
 for values of Z/b_o sufficiently small that higher order terms will not be significant. This is identical to the expression denoted by Hoult, Fay and Forney except for the specific gravity term.

Evaluating $\rho b^2 U$ from this expression:

$$\rho b^2 U \approx \rho b^2 W = \rho_A \left[\frac{4(\alpha R + \beta)}{R} \frac{Z}{D_o} + SG \right] b_o^2 U_o$$

Subsequent Trajectory:

For the bent over case where $\cos\theta \approx 1$, $\sin\theta \approx Z'$, $\rho \approx \rho_A$, $U \approx V$, the assumption of Gaussian profiles in vertical component of velocity and concentration (density difference) yields expressions that are identical to those resulting from the "top hat" case with the exception that b is now the radial distance at which the quantities described by the Gaussian expression assume values equal to $\frac{1}{e}$ of the centerline values. In this case the entrainment hypothesis is equivalent to the assumption of a mixing length proportional to the width of the plume, such that a linear rate of growth of radius with Z and Gaussian profiles of vertical velocity and density difference are predicted.

The new conservation of volume expression will be:

$$\frac{d}{dt} (b^2 V) = 2bV \frac{db}{dt} \approx 2bV W_m$$

or since $dZ \sim W_m dt$

$$\frac{d(b^2 V)}{dZ} \sim 2bV$$

If the constant of proportionality is taken as β , then

$$\frac{db}{dZ} = \beta, \text{ and } b = \beta Z + C$$

If it is assumed that C can be taken as zero without large error and if $d\rho_A/dZ = 0$ in equation (2.14) then equation (2.12) becomes:

$$\frac{d}{dX} \int_0^\infty V W_m e^{-r^2/b^2} 2\pi r dr = \frac{(\rho_A - \rho_o) b_o^2 U_o g \pi}{\rho_A V}$$

or

$$b^2 V W_m \approx \beta^2 Z^2 V^2 Z' = \frac{F}{V^3} \frac{(\bar{X} - X)}{\rho_A}$$

or

$$Z = \left[H^3 - \frac{3F(\bar{X} - X)}{2V^3 \beta^2 \rho_A} \right]^{1/3}$$

Which is a slight variation on the well known expression for positively buoyant plumes. In the above F the buoyancy flux has been substituted for $(\rho_o - \rho_A) b_o^2 U_o g$, \bar{X} is the horizontal distance to the point of maximum rise, and H is maximum plume rise. For this case

$$b^2 U = b^2 V = b_o^2 U_o \left[\frac{4\beta^2}{R} \left(\frac{Z}{D_o} \right)^2 + 1 \right].$$

Expression for Maximum Plume Rise:

Using equation (2.12) in time derivative form:

$$\rho b^2 U W = -Ft + \rho_o b_o^2 U_o^2$$

and

$$W = \frac{-Ft + \rho_o b_o^2 U_o^2}{\rho b^2 U}$$

The previously evaluated expressions for $b^2 U$ for the asymptotic cases of the plume close to the stack and of the bent over plume indicates $b^2 U = b_o^2 U_o f(R, Z/d_o)$ if the Boussinesq approximation is

made for the density on the grounds that it is valid over most of the rise. If the original density is retained in the time calculations the result is:

$$W = \frac{-Ft + \rho_o b_o^2 U_o^2}{\rho_A f(R, ZD_o) b_o^2 U_o^2}$$

where R is constant.

Therefore maximum plume rise is in general:

$$\int_0^H \frac{f(Z/D_o, R)}{D_o} dZ = \int_0^T \left(\frac{-Ft + \rho_o b_o^2 U_o^2}{D_o \rho_A b_o^2 U_o^2} \right) dt = \frac{(SG) F_R^2}{2}$$

or

$$H/D_o = \phi(R, (SG) (F_R^2)) \quad (2.15)$$

The jet region equations apply only when time is small and $R(SG)/Z' \ll 1$, however for purposes of comparison (2.15) can be calculated for this assumption over the entire plume rise resulting in:

$$H/D_o = \frac{R(SG)}{4(\alpha R + \beta)} \left\{ \sqrt{1 + \frac{16(\alpha R + \beta)}{R(SG)} F_R^2} - 1 \right\} \quad (2.16a)$$

For bent over plumes (if considered for the whole rise) (2.15) becomes:

$$H/D_o = \left[\frac{3R(SG) F_R^2}{8\beta^2} \right]^{1/3} \quad (2.16b)$$

This predicts values of H/D_o which vary a maximum of ≈ 10 percent in the range of specific gravities from 1.25 to 5 if the exit and crosswind velocities are held constant. The minimum predicted rise is at a specific gravity of two. This agrees qualitatively with the

observations of Bodurtha who stated that the rise of plumes he observed with roughly this range in specific gravities was independent of specific gravity.

Trajectory During Descent:

For the descending portion of the plume equation (2.10) can be transformed, noting that $\cos\theta = \frac{dx}{ds} = \frac{1}{(1+Z'^2)^{1/2}}$, to

$$\frac{d}{dx} [b^2 V (1+Z'^2)^{1/2}] = 2abZ'^2 V + 2\beta b |Z'| V$$

For values of $Z' < 0.3$, then $1. \leq (1+Z'^2)^{1/2} \leq 1.05$. Since measurements discussed by Briggs (5) indicate $\beta \approx (6 \text{ to } 8)\alpha$ for these conditions, the bent over plume expressions will still apply approximately. Hence,

$$b \approx \beta (H+H-Z)$$

and

$$\rho_A \beta^2 (2H-Z)^2 \left(\frac{d(H-Z)}{d(X-\bar{X})} \right) = + \frac{F}{V^3} (X-\bar{X})$$

which integrates to produce:

$$\frac{X-\bar{X}}{D_o} = \left[\frac{8\beta^2}{3} \frac{\{(2H-Z)^3 - H^3\}}{D_o^3} \right]^{1/2} \frac{F_{RH}}{\sqrt{R}}$$

Where F_{RH} is the "horizontal" Froude Number $\frac{\sqrt{\rho_A} V}{\sqrt{(\rho_o - \rho_A) g D_o}}$ and \bar{X} is

the horizontal location of maximum plume rise. At ground level

$Z = -h_s$, the stack height. Then

$$\frac{X_D - \bar{X}}{D_o} = \left[\frac{8\beta^2}{3} \left(\frac{H}{D_o} \right)^3 \left\{ \left(2 + \frac{h_s}{H} \right)^3 - 1 \right\} \right]^{1/2} \frac{F_{RH}}{\sqrt{R}} \quad (2.17)$$

Where X_D is the horizontal point of plume touchdown. The position of \bar{X} can be estimated from the time of rise by assuming that the plume is convected horizontally with crosswind velocity V . Thus

$$\frac{\bar{X}}{D_o} = \frac{VT}{D_o} = \frac{V \rho_o U_o}{\Delta \rho g D_o} = \frac{F_R^2}{R} \quad (2.18)$$

It should be noted that entrainment theory is not expected to provide a completely accurate description of negatively buoyant motion due to the low velocity differences in the region of maximum rise. However, it is a useful tool in developing relationships between parameters for experimental measurement.

SECTION III

CONCENTRATION DETERMINATIONS

3.1 Plumes in a Laminar Crosswind

Rouse, Yih, and Humphries showed theoretically and experimentally that the decay of maximum concentration in a vertical positively buoyant plume is $\sim X^{-5/3}$. Morton et al. obtained the same results using entrainment theory. In that particular case mixing length theories are consistent with the entrainment hypothesis and both predict a linear rate of growth of radius with vertical distance, and Gaussian profiles of velocity and concentration. If the same approach is taken and it is noted that:

$$\rho = \rho_A \left[1 + \frac{\chi(SG-1)}{\chi_o} \right]$$

where χ is the concentration at any point and ρ is the corresponding density. If Gaussian profiles are assumed, equation (2.4a) becomes:

$$\int_0^{\infty} (\rho_m - \rho_A) U_m e^{-(1+\gamma)r^2/b^2} 2\pi r dr =$$

$$\int_0^{\infty} U_m \rho_A \frac{\chi_m}{\chi_o} (SG-1) e^{-(1+\gamma)r^2/b^2} 2\pi r dr =$$

$$\frac{b^2}{1+\gamma} (\rho_o - \rho_A) U_m \frac{\chi_m}{\chi_o} = (\rho_o - \rho_A) U_o b_o^2 = \text{constant}$$

so that

$$\frac{\chi_m}{\chi_o} \sim \frac{b_o^2 U_o}{b^2 U_m}$$

Vertical Plumes:

For a negatively buoyant vertical plume, this predicts at maximum rise height:

$$\chi_m/\chi_o \sim (H/D_o)^{-1} \text{ or, } \frac{\chi_m U_o D_o^2}{Q} \sim (H/D_o)^{-1}$$

Bent Over Plumes:

For plumes in a crosswind the concentration delay can be examined in the asymptotic regions. Close to the stack, in the jet region,

$$b^2 U = b_o^2 U_o \left[\frac{4(\alpha R + \beta)}{R} \frac{Z}{D_o} + 1 \right]$$

$$\frac{\chi_m}{\chi_o} \sim \frac{1}{\left[4 \frac{(\alpha R + \beta) Z}{R D_o} + 1 \right]} \sim \left(\frac{Z}{D_o} \right)^{-1}$$

For the bent over region of the plume

$$b^2 U \approx \rho^2 V \approx b_o^2 U_o \left[\frac{4\beta^2 Z^2}{R D_o^2} + 1 \right] \approx b_o^2 U_o \left[\frac{4\beta^2 Z^2}{R D_o^2} \right]$$

since $(Z/D_o)^2 \gg R$ over most of the rise and

$$\frac{\chi_m}{\chi_o} \sim \frac{R}{\left[\left(\frac{Z}{D_o} \right)^2 \right]}, \quad \text{or} \quad \frac{\chi_m V D_o^2}{Q} \sim \left(\frac{Z}{D_o} \right)^{-2}$$

so that the bounds on concentration are

$$\left(\frac{H}{D_o} \right)^{-2} \leq \frac{\chi_m V D_o^2}{Q} \leq \left(\frac{H}{D_o} \right)^{-1}$$

For the descending plume region

$$\frac{\chi}{\chi_o} \sim (b^2 V)^{-1} \sim (2H - Z)^{-2}$$

which at large distances downstream approaches proportionality with

$$\frac{\sqrt{R}}{F_{RH}} (X-\bar{X})^{-4/3}$$

$$\frac{\chi V D_o^2}{Q} \sim \frac{F_{RH}^{4/3}}{R^{5/3}} (X-\bar{X})^{-4/3}$$

Implicit in the above is the assumption of a mixing length proportional to the characteristic length b , similarity in the form of diffusivities of mass and momentum, and similarity in profiles of velocity and concentration at all cross sections.

3.2 Dense Ground Source in a Turbulent Boundary Layer

3.2.1 Eulerian Diffusion Formulation

In a field of small scale turbulence the diffusion may be considered through the concept of an "eddy diffusivity" as analogous to molecular diffusion. A coefficient k , the "diffusivity", is taken as proportional to $U'\ell$. U' is the turbulent fluctuation velocity. ℓ can be interpreted in terms of a proportionality coefficient between the average turbulent flux of a given substance $\overline{C'U'}$ and the gradient of average concentration $\nabla\bar{C}$,

$$\overline{U'C'} = -K\nabla\bar{C}.$$

When the diffusion is considered in three dimensions, the concept is generalized by introducing three such coefficients, k_x , k_y , k_z which are assumed to be functions of position. Application of the conservation principle yields:

$$\frac{\partial c}{\partial t} + U \frac{\partial c}{\partial x} + V \frac{\partial c}{\partial y} + W \frac{\partial c}{\partial z} = \frac{\partial}{\partial x} \left[k_x \frac{\partial c}{\partial x} \right] + \frac{\partial}{\partial y} \left[k_y \frac{\partial c}{\partial y} \right] + \frac{\partial}{\partial z} \left[k_z \frac{\partial c}{\partial z} \right]$$

If the boundary layer assumption of $W=V=0$ is combined with neglect of the longitudinal dispersion term, the following equation results:

$$\frac{\partial c}{\partial t} + U \frac{\partial c}{\partial x} = \frac{\partial}{\partial y} \left[k_y \frac{\partial c}{\partial y} \right] + \frac{\partial}{\partial z} \left[k_z \frac{\partial c}{\partial z} \right]$$

The assumption of constant diffusivity $k_y = k_z = k$ as formulated by Roberts leads to a Gaussian distribution in the radial direction and a longitudinal decay rate inversely proportional to X . The predictions of this analysis unfortunately do not agree with observations. The observed decay rate of maximum concentration is much greater than that predicted by this model. Several investigators (see (29)) were able to obtain closed form solutions for the two dimensional version of (3.4) for an infinite line source in a crosswind by use of Schmidt's conjugate power.

Other dispersion predictions have been proposed for power law profiles and constant flux atmospheres such that:

$$U = U_1 (Z/Z_1)^m, \quad K_m \frac{du}{dz} = \text{constant}$$

which require $K_m = K_1 (Z/Z_1)^{1-m}$ where U_1 and K_1 are the velocity and diffusivity at the reference height Z_1 . The solutions obtained predict a power law decay rate in maximum concentration with X .

Several other investigations have obtained closed form solutions for the three dimensional problem of ground and elevated point sources by the assumption of variable lateral diffusivity combined with the conjugate power laws. These proposals have varying degrees of success in predicting the decay rate of maximum concentration and lateral dispersion. (7, 27, 29)

3.2.2 Lagrangian Formulations

Lagrangian formulation of diffusion assumes one follows the motions of a specific particle in time. Taylor (27) considered the motion of a fluid element with the assumptions of homogeneous, isotropic, stationary turbulence and obtained:

$$\overline{Y_i^2(t)} = \overline{U'^2} \int_0^t \int_0^{t_1} R_L(\tau) d\tau dt_1$$

where $\overline{Y_i^2(t)}$ is the variance in one dimensional motion, and $\overline{U'^2}$ is the RMS value of the turbulent velocity fluctuation in that direction. The velocity correlation, $R_L(\tau)$ is defined by.

$$R_L(\tau) = \frac{\overline{U'(t)U'(t+\tau)}}{\overline{U'^2}}$$

when t is small $R_L(\tau) \approx 1$ and $\overline{Y_i^2} = \overline{U'^2} t^2$. As $t \rightarrow \infty$, $R_L(\tau) \rightarrow 0$ and $\int_0^\infty R_L(\tau) d\tau = \text{const.}$ Then $\overline{Y_i^2(t)} = \text{Const} \times \overline{U'^2}$.

Sutton (29) on dimensional grounds proposed an empirical form for $R_L(\tau)$

$$R_L(\tau) = \frac{v}{(v + \overline{U'^2} \tau)^n}$$

with n as an adjustable constant. This led to the following solution for a continuous point source:

$$C(x, y, z) = \frac{2Q}{\pi C_y C_z \overline{U_x}^{2-n}} e^{-x^{n-2} \left(\frac{y^2}{C_y^2} + \frac{z^2}{C_z^2} \right)}$$

where C_y and C_z are generalized coefficients of diffusion in their respective directions. Sutton's formula has been widely used in

practice even though it was developed under the assumption of homogeneous isotropic turbulence. In use it is typically applied to the shear flow of the lower atmosphere.

The principle of Lagrangian similarity has recently been utilized by several investigators to provide a more rational approach to shear flow diffusion, i.e. without postulating a diffusivity in advance. Reasoning dimensionally Batchelor and Ellison related the time rate of change of the vertical mean position of a particle to the shear velocity and a universal function of \bar{z}/L , where L is the stability length. Assuming a probability density distribution about the mean position and noting that for a ground source in neutral flow this function as applied to maximum ground concentration is essentially the dirac delta function, they obtained relations for the decay of maximum concentrations for continuous point and line sources. Concentrations from point sources were predicted to decay as $\bar{\chi}^{-1.8}$ - $\bar{\chi}^{-1.9}$, while line sources decay $\bar{\chi}^{-1}$. Gifford, Cermak, and Chaudhry (7) extended this principle to diffusion in a stably stratified atmosphere.

The results of Lagrangian theory are usually incorporated into statistical models in terms of the calculated first, second, or higher moments. For a continuous ground source the expression obtained is:

$$\frac{\bar{\chi}U}{Q} = \frac{1}{\pi\sigma_y\sigma_z} \text{Exp} \left[-\left(\frac{y^2}{2\sigma_y^2} + \frac{z^2}{2\sigma_z^2} \right) \right]$$

Where:

Q is the flow rate in units of concentration per second

$\sigma_y(x)$ and $\sigma_z(x)$ are distribution moments found by the

Lagrangian theory

$\bar{\chi}$ is the average concentration

3.2.3 Wind Tunnel Simulation of Diffusion

Cermak et al. (6) point out that for small scale diffusion, in which there is no variation in the mean wind direction, and non-neutral stratification, dynamic similarity of flows with geometrically similar boundary conditions, is determined by three dimensionless parameters:

$$VL/\nu \quad (\text{Reynolds Number})$$

$$\frac{k}{C_p \mu} \quad (\text{Prandtl Number})$$

$$\frac{gL\Delta T}{T_o V^2} \quad (\text{Richardson Number})$$

If the tunnel flow consists of air, Prandtl Number similarity is assumed. If only micro scale eddy motion is considered, such that there is no variation in the mean wind direction, experience has shown that for shear flows of high Reynolds Number, that viscosity has no effect on the scale components of the motion which contains nearly all the energy which might effectively contribute to turbulent diffusion. Plate and Lin, Chuang and Cermak, Malhotra and Cermak, Arya and Chaudhry have all demonstrated the reliability of the use of wind tunnel shear layers for modeling atmospheric flows, even though a ratio in Reynolds Numbers between model and prototype is of the order of 10^3 .

For flow of this sort, the gradient form of the Richardson Number must be used i.e.

$$Ri = \frac{g}{T_o} \frac{\left(\frac{dT}{dZ}\right)}{\left(\frac{dU}{dZ}\right)^2}$$

If power law relationships in Z for profiles of temperature and velocity are obtained such that:

$$\frac{U}{U_1} = \left(\frac{Z}{Z_1}\right)^n, \quad \left(\frac{T-T_r}{T_1-T_r}\right) = \left(\frac{Z}{Z_1}\right)^m$$

$$Ri = \frac{g}{T_o} \frac{m}{n^2} \left(\frac{Z}{Z_1}\right)^{m-2n+1} (Z_1) \left(\frac{T_1-T_r}{U_1^2}\right)$$

Since $Ri = \frac{\text{Buoyancy force}}{\text{Inertial force}}$, therefore

<0 Unstable stratification

$Ri = 0$ Neutral stratification

>0 Stable stratification

SECTION IV

EXPERIMENTAL MEASUREMENTS

4.1 Plume Rise

Experiments on negatively buoyant plumes were conducted to check previous and present theories for plume rise characteristics and to obtain reliable data on the nature of the descending plume. Vertical plume rise experiments with no crosswind were conducted in the Industrial Aerodynamics wind tunnel in the Fluid Dynamics and Diffusion Laboratory at Colorado State University. The 6x6 ft area of the test section (which was closed at each end for this experiment to limit corrective currents) provided a very still environment for the experiment. The experiments with bent over plumes were performed in the thermal tunnel in the Fluid Dynamics and Diffusion Laboratory. The tunnel has a 24x24 inch cross section. Turbulent plumes were injected into both laminar and turbulent crosswinds. Plumes were also injected into a low-speed turbulent crosswind in the Industrial Aerodynamics wind tunnel. These plumes were of large specific gravity and descended quickly to the tunnel floor, where the longitudinal decay rate was measured.

Additional details of the wind tunnels are described in Section 5.

The pertinent parameters regarding plume rise appeared in the equations in Section 2. Values of these parameters applicable to actual conditions can be duplicated in the wind tunnel. Implicit in the assumptions was the existence of a Reynolds Number sufficiently large to justify the assumptions of turbulent entrainment. The Reynolds Numbers based on pipe flow calculations did not meet this criteria for all cases studied so that the turbulence was artificially

generated. A sharp edged orifice was placed in the stacks 8 diameters upstream from the exit. Hewett (13) has shown that plume rise is independent of Reynolds Number if the plume is turbulent at exit.

The range in parameters was as follows. For the vertical plumes, specific gravities ranged from 1.08 to 3.0 and exit velocities from ≈ 9 to 75. Stack diameters of 1/8 inch and 1/4 inch were used.

For the plumes in a laminar crosswind, velocity ratios ranged from 2.5 to 25, specific gravities from 1.10 to 4.16 and Froude Numbers from ≈ 5.2 to 75. Two diameters, 1/4 inch and 1/8 inch were used and two crosswind velocities ≈ 0.75 and ≈ 1.5 ft per second were employed. Stack heights of 3 inch and 6 inch were employed at various points, both to provide variations in this parameter and to avoid hitting the tunnel roof with plumes of high exit velocity. The specific gravities were obtained by mixing Freon 12 with Air in appropriate proportions. Freon 12 has a molecular weight of 121. Densities at appropriate pressures and temperatures were obtained from applicable Mollier Charts.

The experiments were conducted as follows. Tunnel and stack flow rates were set. The effluent was bubbled through TiCl_4 to produce smoke. Extended time exposure photographs were taken against a blackboard divided into marked horizontal and vertical increments. Measurements were then corrected for the parallax resulting from the fact that this plume was in the center of the tunnel and the blackboard at the tunnel wall. Several photographs are shown in Fig. 11.

In addition a $4\frac{1}{2}$ inches x $4\frac{1}{2}$ inches x $4\frac{1}{2}$ inches cubical structure with a stack exiting in the center was installed in the Colorado State University thermal tunnel in a turbulent shear flow. Velocity at this top of the building was set at 6.75 ft per second for a Reynolds Number

of $\approx 13,500$. Smoke photographs were taken for specific gravities of 1, 1.5 and 2.5; velocity ratios of 1 and 2; and stack height to building height ratios of 1, 1.5 and 2.

4.2 Concentration Measurements

4.2.1 Plumes in a Laminar Crosswind

Concentration measurements at the maximum rise height were made of 18 plumes injected into the laminar crosswind. Concentrations at the points where these plumes touched the floor was also taken. These plumes were from 1/4 inch and 1/8 inch diameter stacks with specific gravities of 1.5, 2 and 3 respectively.

Detailed cross-sectional concentration measurements taken in roughly equal longitudinal increments between the point of maximum rise height and plume touchdown were made for six plumes of specific gravities 2 and 3; and exit ratios of ≈ 5 , 10, and 15 from a 1/8 inch diameter stack. The cross-sectional measurements were made so that the plane of measurement was at right angles to the plume motion as determined from the smoke pictures.

4.2.2 Dense Ground Source in a Turbulent Boundary Layer

Concentration measurements were taken in a turbulent boundary layer of negatively buoyant ground sources. Specific gravities of 1.0 (Air), 1.10, 1.25, 1.50, 2.0 and 3.0 were employed. Measurements were made in neutral and inversion stratifications. Free stream velocity was 6 ft per second and the boundary layer thickness was approximately 6 inches. Velocity of discharge from the source was set equal to tunnel velocity at the height of the source centerline. The turbulent boundary layer was artificially generated in the Colorado State

University thermal tunnel by the use of vortex generators after the method of Counihan (9). An approximate $1/7$ law velocity profile was obtained. Using the thermal stratification capabilities of the tunnel, an approximate $1/7$ law temperature profile was also generated. The vortex generator arrangement is described in Section 5.

Finally, five plumes were examined in the Colorado State University Industrial Aerodynamics Tunnel (briefly described in Section 5) with a free stream velocity of approximately 2.5 ft per second and a boundary layer thickness of approximately 12 inches. These plumes were emitted from $1/4$ inch stacks with velocity ratios ranging from 5 to 25 and specific gravity of 3 and thus tended to intercept the tunnel floor at relatively short distances from the stack. The decay rate of maximum concentration downstream from point of touchdown was then determined to provide information supplementing that of the plumes injected into the laminar crosswind. This provided data concerning dispersion of heavy plumes due to background turbulence as opposed to plumes which entrain fluid as a result of their own vertical motion.

SECTION V

APPARATUS AND INSTRUMENTATION

5.1 Wind Tunnels

The thermal wind tunnel (Fig. 1) at the Fluid Dynamics and Diffusion Laboratory, Colorado State University, was designed to provide a low speed wind tunnel with vertical thermal gradient capability. The section is 15 ft long with a two ft square cross section. A bank of metal plates with electrical resistance heaters placed in the tunnel inlet allows an initial thermal gradient to be established. Water cooled panels on the tunnel floor and electrical resistance heaters on the tunnel roof subsequently maintain the gradient along the test section. In addition, the longitudinal pressure gradient along the test section can be controlled by the tunnel roof which can be adjusted vertically. The fan speed can be adjusted, thus controlling the air speed in the tunnel. Maximum air velocity obtainable is ≈ 10 ft per second.

The Colorado State University Industrial Aerodynamics tunnel has a six ft square cross section and a test section which is 30 ft in length. An adjustable pitch fan allows wind speeds up to 60 ft per second. The boundary layer thickness ranges from ≈ 3 inches at the start of the test section to ≈ 16 inches at the end.

5.2 Velocity and Temperature Measurements

Extremely low velocities were measured utilizing the vortex shedding properties of circular cylinders and known relationships between shedding frequency and approach velocity in the form of the Strouhal Number of cylinder Reynolds Number. The device is similar to one

described by Hewett (13), and requires a "hot wire" probe positioned in the cylinder wake to measure the eddy shedding frequency. The trace of the signal was observed on an oscilloscope and the probe position adjusted so that only frequency of vortex shedding from the bottom of the cylinder was counted. The signal appeared in wave form and thus was counted on a digital counter. Velocity was determined from Roshko's data relating Strouhal Number to Reynolds Number. This method of velocity measurement was checked with a smoke wire.** The measurements are good within three percent.

Velocities of higher magnitude were measured with a pitot-static tube and a Transonic pressure meter, with the exception that velocity and turbulence intensity profiles in boundary layers were measured with a hot wire anemometer.

Measurements of temperature were made using a movable bank of eight copper constant and thermocouples mounted vertically. Their voltage output was measured by a sensitive millivolt potentiometer.

5.3 Gas Mixing and Smoke Visualization

The dense gas was formed by mixing air and Freon 12 in a flow tee in the desired proportions. The air and Freon flow rates were measured by Fisher and Porter "flowrators" which were calibrated for each gas. Smoke was generated by impinging the mixture in jet form on the surface of titanium tetrachloride in a container. The smoke thus formed was then transported to the stack inside the tunnel where it was released. A schematic of this arrangement is shown in Fig. 2.

** See Orgill, M. M. et al., "Laboratory Simulation and Field Estimates of Atmospheric Transport-Dispersion Over Mountainous Terrain," FDDL Dept. CER70-71MMO-JEC-LOG40, 1971.

5.4 Vortex Generators

Since concentrations from a negatively buoyant ground source were measured in the thermal tunnel to utilize the thermal inversion capability, it was necessary to generate a turbulent boundary layer. This was done using the method of Counihan by constructing eight "elliptic wedge" vortex generators with the shape of a quarter ellipse with minor axis equal to one-half major axis and a wedge angle of six degrees. The generators were six inches high and three inches long at the base. A serrated barrier was located six inches upstream from the generators. A metal honeycomb section was placed immediately downstream of the heaters but upstream of the serrated barrier. It was found that best results were obtained when the barrier was placed at a 60 degree angle with the tunnel floor such that the top of the barrier was placed adjacent to the downstream metal "Honeycomb" section. The barrier was $1 \frac{1}{8}$ inches high at the serrations and $\frac{7}{8}$ inches high elsewhere. Downstream from the generators a three inch wide plate with $\frac{3}{16}$ inch steel shot placed in staggered rows on the surface was installed. Downstream from the shot-covered plate a four-inch wide layer of $\frac{3}{8}$ inch gravel was placed on the tunnel floor. A sketch of the arrangement with details of the vortex generators and serrated barrier is shown in Fig. 3. Velocity profiles produced closely approximated a $1/7$ power law profile. The "Boundary Layer" was developed within twenty-five inches downstream from the generators. Velocity, turbulence intensity and temperature profiles in the boundary layer are shown in Fig. 5 to 9.

5.5 Concentration Measurements

5.5.1 Measuring Apparatus

Concentration measurements were made using Krypton-85. Krypton-85 is a radioactive noble gas produced by nuclear fission. With the atomic number 36, atomic mass unit 85, and the maximum energy of 0.67 M.E.V., Kr-85 has been widely used as an effective tracer gas in recent years because of its long half life (10.3 years) and its pure Beta emitting property. The Beta particles emitted by K_R -85 ionize gas molecules as it passes through them. With these ionization properties gas concentrations can be detected by Geiger Mueller counters. The counter tube consists of two electrodes, a fine metal wire, the anode, surrounded by a hollow conducting cylinder, the cathode. Gas samples were removed from the test section by a rake of sampling probes and flushed through the tube jackets for a period of three minutes. Sampling ceased, and the samples isolated by valves. Concentrations were then determined by counting the tube pulses. The tubes used were Halogen-Quenched, stainless steel, thin-walled G-M tubes (Tracer-lab 1108).

5.5.2 Tube and Gas Calibration

G-M tubes and radioactive source gas were calibrated by using the following procedure. A reference G-M tube was calibrated using the scalar counter and a radioactive source of known strength. This source was placed inside a lead-shielded safe containing the reference G-M tube. The reference tube is then calibrated in counts per minute vs. source strength in curies. The radioactive strength of either a calibrating or a source gas was then determined by passing the gas through a plastic container with a Mylar cover at the same position in

the lead safe as the reference source. Using the known volume of the container, concentrations of the gases was determined in $\mu\text{Ci/cc}$. A calibrating gas may then be passed through the test G-M tubes which permits final calibration in counts per minute vs. concentration.

5.5.3 Concentration Calculations and Counting Statistics

Gas concentrations were determined by first eliminating the "background" count corresponding to the naturally occurring radiation. This was done by subtracting the background counts per minute from the sample plus background count, and multiplying this by the "tube constant" previously determined for each tube. The tube constant was determined by passing the calibrating gas through the tube jacket, subtracting the background (obtained by counting ambient air samples) and correcting for "dead time", which is the time required for the positive space charge to move far enough from the anode for further pulses to occur. The result is then a tube constant in $\text{CPM}/\mu\mu\text{Ci/cc}$. The details are shown below:

$$\text{CPM}_1 = \text{CPM} - \text{Background}$$

$$\text{CPM}_2 = \frac{\text{CPM}_1}{1 - (2 \times 10^{-6}) \text{CPM}_1} \quad (\text{dead time correction})$$

$$\text{Tube constant} = \frac{\text{CPM}_2}{\text{Source strength } (\mu\mu\text{Ci/cc})}$$

The standard deviation in the net counting rate (sample plus background) σ_{R_s} for a sample is

$$\sigma_{R_s} = \left(\frac{R_s + b}{t_s} + \frac{R_b}{t_v} \right)^{1/2}$$

where R_{s+b} is the observed sample-plus-background count, R_b is the background count and t_s and t_b are the sample and background counting times respectively. Since R_b is of this order of 20 CPM and was determined with 15 minute counts for each tube, the background contribution is constant and small. If R_{s+b} is large, t_s does not have to be large to obtain a small value of σ_{R_s} in terms of percentage of R_{s+b} . As R_{s+b} goes down however, t_s must be increased. In these experiments the following procedure for counting was used.

$$R_{s+b} \geq 1000, t_s = 1 \text{ minute}, \sigma_{R_s} \leq 3.2 \text{ percent}$$

$$100 \leq R_{s+b} < 1000, t_s = 2 \text{ minutes}, \sigma_{R_s} \leq 7.2 \text{ percent}$$

$$R_{s+b} < 100, t_s = 3 \text{ minutes}$$

SECTION VI

RESULTS OF EXPERIMENTS

6.1 Plume Rise

6.1.1 Vertical Plumes

The vertical plumes emitted into a quiescent atmosphere were observed to rise initially in a jet with almost linear growth of radius with vertical distance. This jet region appeared to encompass from $\sim 1/4$ to $\sim 1/3$ the total rise height. Measurements of the point of maximum rise of the top of the plume indicated better correlation with Froude Number than with Froude Number multiplied by the one-fourth power of specific gravity. Actual least squares correlation indicated a proportionality to $SG^{.08}F_R$. This indicates the assumption $\rho \approx \rho_O$ produces better results than $\rho \approx \rho_A$. This at first seems completely unreasonable, particularly since it is later shown that for bent over plumes, $\rho \approx \rho_A$ produces good results. There are, however, important physical differences between two situations. Measurements indicate that the entrainment constant perpendicular to the flow direction is greater than the one for the parallel flow by a factor of from six to eight; thus the presence of a crosswind greatly increases the entrainment. The negatively buoyant vertical plume may also reentrain some of the falling dense fluid, so that the flux of negative buoyancy increases with distance, rather than being constant. This would have the effect of reducing rise time. Since correlation with specific gravity yields such a small power, the correlation was made with Froude Number. The least squares value of the proportionality constant was determined to be 2.96. So that (See Fig. 12):

$$H/D_o = 2.96 F_R \quad (6.1)$$

This value is close to that indicated by Turner which appears to yield a relationship of

$$H/D_o \approx 3.1 F_R$$

The value of the entrainment constant, α , was determined for the "top hat" region immediately downstream from the stack exit. Matching radial and height measurements from the smoke photographs to equation (2.09) suggests that:

$$\alpha \approx 0.045.$$

When this value of α is used in equation (2.8a) to calculate plume rise one predicts:

$$H/D_o = 2.43 F_R$$

This relation somewhat underestimates rise height. Apparently, in the upper regions of the plume where velocities are low, the proportional entrainment theory over-predicts entrainment.

6.1.2 Plumes in a Laminar Crosswind

Bodurtha noted that over a given range in specific gravities, the plume rise is independent of specific gravity. This was also found in the present experiments for plume rise in a laminar crosswind. Rise height was obtained by measuring the maximum centerline plume height from the smoke pictures. Froude Number dependence was determined by comparing rise heights from 1/4 inch and 1/8 inch diameter stacks of equal specific gravity and velocity ratio. Dimensionless rise height was determined to be proportional to (diameter ratio)⁻ⁿ, with least squares value of n as 0.35. Velocity ratio dependence was determined by comparing rise heights for equal Froude Numbers and

specific gravities but differing velocity ratios i.e. $H \propto R^m$. The least squares value of m was found to be 0.32. Thus correlation appears to follow the expression suggested by equation (2.16). H/D_0 is plotted vs. $R^{1/3} SG^{1/3} F_R^{2/3}$ in Fig. 13. The least squares value for the constant of proportionality is 1.32 so that:

$$H/D_0 = 1.32 R^{1/3} SG^{1/3} F_R^{2/3} \quad (6.2)$$

The correlation with this equation is good except for the lowest Froude Numbers, where the rise is moderately less than predicted. Apparently the rise time is low enough that the net entrainment is rather low; hence the Boussinesq approximation is not valid over a sufficient range of the height.

The fact that plumes correlate well with this equation is fortuitous, since a significant portion of plume rise over the range of variables examined takes place in a near-vertical configuration, whereas equation (2.16) was obtained under assumptions of a near horizontal plume. The fact that rise heights of plumes with specific gravities from 1.5 to 3 would not significantly differ seems strange since in the jet region plume rise is predicted as \sqrt{SG} .

Measurements also indicate that equation (2.18) gives a good estimate for the horizontal position of the point of maximum rise.

For plumes such that the point where the lower edge of the plume touched the floor could be determined with reasonable certainty (diffusion of the smoke downstream made some plumes visually indeterminate at larger distances) the results indicate that strong correlation of touchdown distance with the "horizontal" Froude Number occurs for plumes of equal diameter, velocity ratio and rise height, but

differing specific gravities. Linear proportionality was noted. Correlation with equation (2.17) was noted but with a fair amount of scatter. The correlation of variables of equation (2.17) is plotted in Fig. 14. A least squares value of the constant of proportionality of 0.56, was found, so that:

$$\frac{x_D - \bar{X}}{D_o} = 0.56 \left\{ \left(\frac{H}{D_o} \right)^3 \left[\left(2 + \frac{h_s}{H} \right)^3 - 1 \right] \right\}^{1/2} \frac{F_{RH}}{\sqrt{R}} \quad (6.3)$$

where x_D is the horizontal distance from the stack to the point where the lower edge of the plume touches the tunnel floor.

6.1.3 Plume Rise in the Presence of a Cubical Structure

The plumes emitted from the center of a cubical structure exhibited no variation with specific gravity as far as avoiding entrainment into the cavity immediately behind the building. All plumes were found to obey the criteria of Meroney and Yang that for $R \geq 1$ and $h_s/h_b \geq 2$ entrainment in this region will be avoided. Farther downstream, the negatively buoyant plumes were observed to fall into the wake region of the building at distances beyond \bar{X} as calculated from (2.18), but in this region subsequent entrainment into the building will not occur as it does in the cavity region. The criteria to avoid such entrainment into the cavity region for negatively buoyant plumes, in addition to that of Yang and Meroney, appears to be that (from equation 2.18)

$$\bar{X} = D_o \frac{F_R^2}{R} \geq 3h_b$$

For a cubical structure $3h_b$ is the downstream extent of the cavity region as found by Halitsky (12).

6.2 Concentrations

6.2.1 Plumes in a Laminar Crosswind

The plumes injected into a laminar crosswind exhibited the following behavior regarding diffusion. The plume cross section isopleths at the maximum rise height (See Fig. 15) indicate a semi-elliptic cross section at this point. The concentration gradients are much steeper at the top of the plume than at the bottom, which would be expected since a condition analogous to diffusion in unstable stratification exists at the lower plume boundary. The negative buoyancy of individual plume particles contributes to diffusion in this direction since if a particle is displaced from the center of the plume in a downward direction, it tends to continue due to the increased density over that of the surrounding fluid. During the rise period, this trend is accentuated since the direction of greatest diffusion is opposite to the mean plume motion, thus increasing the relative displacement. As the plume descends, the cross sections become more nearly circular and the vertical distribution of concentration becomes more symmetrical with the skew decreasing. The longitudinal rate of decay of the "non-dimensional" concentration $\frac{xVD_0^2}{Q}$ approaches proportionality with $(x-\bar{x})^{-4/3}$ as the plume approaches x_D (See Figs. 16-18). Plots of maximum values of non-dimensional concentration at the plume high point and at the point where plume centerline touches the tunnel floor vs. H/D_0 indicate approximate proportionality with $(H/D_0)^{-2}$. Thus simple mixing length theory predicts good approximations for the decay in maximum concentrations for the "worst case" of negatively buoyant

plumes injected into light winds such that the diffusion is essentially controlled by plume turbulence. The proportionality constants indicated are:

$$\frac{\chi V D_o^2}{Q} = 2.15 (H/D_o)^{-1.85} \text{ at point of maximum rise} \quad (6.4)$$

$$\frac{\chi V D_o^2}{Q} = 3.10 \left(\frac{2H+h}{D_o} \right)^{-1.95} \text{ at point of plume "touchdown"} \quad (6.5)$$

6.2.2 Dense Ground Source in a Turbulent Boundary Layer

Density differences were observed to have a significant effect on the downstream diffusion pattern of a ground source. This effect was primarily multiplicative, however, rather than a change in the power law of decay with downstream distance as is normally observed with an inversion stratification. Fig. 21 and 22 show the rate of decay of maximum values of the quantity of $\bar{\chi}U/Q$. With downstream distances from the source U in this case is taken as the velocity at the source centerline. In this case U was taken as 3.5 ft per second. Decay rates of maximum concentration with downstream distance for a specific gravity of one were observed to be proportional to power laws of -1.68 and -1.45 for the neutral and inversion cases respectively, which is in good agreement with previously observed values (7, 27). The maximum concentrations of the denser gases decay at a slightly greater rate when the concentrations slowly approach those of air since the density effects are attenuated by diffusion. Over the range of downstream distances examined, a specific gravity of two, for example, increases maximum ground concentrations by a factor of approximately 30 percent in both neutral and inversion stratifications.

The lateral and vertical plume dimensions for the 50 and 10 percent levels reveal the following behavior (See Figs. 23-30). As the dense plumes leave the source, the radial density gradients inhibit vertical diffusion and accelerate lateral spread, so that initially the lateral values of the spread rate are greater while the vertical values are smaller. As the plume proceeds downstream, the 50 percent concentration plume dimension becomes larger for the less dense gases as the concentration distributions for the denser gases exhibit sharper "peaks. See Fig. 31. Apparently a "core" of dense gas resistant to vertical diffusion is formed as the density differences in the outer lateral regions of the plume are attenuated by diffusion. The lighter gases thus arrive at heights where they are transported laterally faster by diffusion than the heavier gases can move laterally at ground level solely due to gravitational effects. The vertical spread of the 50 and 10 percent concentration levels is shown to be less for the dense gases over the distance studied, but they approach that of air as the plume proceeds downstream.

6.2.3 Decay of Concentration in Buoyancy Dominated Plumes After Touchdown

The plumes injected into the turbulent boundary layer with free stream velocity of 2.5 ft per second exhibited the following behavior. An extremely large lateral spreading occurred immediately after touchdown. The concentration profiles in the lateral direction were quite flat. The initial decay rate is approximately proportional to $x^{-0.65}$ (See Fig. 32), which is similar to the behavior noted by Holly and Grace with salt water plumes in an open channel. The decay rate appears to approach ground source behavior as all plumes approach a -1.7 power law decay rate. (Values of velocity in the $\overline{x}\overline{U}z_0^2/Q$ are

free stream velocity.) Such behavior is expected to occur only in those plumes where as a result of high densities and/or low exit velocities and crosswinds, the plume touches down a short distance from the stack.

SECTION VII

CONCLUSIONS

1. The rise height of a negatively buoyant plume is increased by increasing the discharge velocity. For a given flow rate, this can be accomplished by decreasing the stack or relief valve diameter. For a constant flow rate, rise height is proportional to $D_o^{-3/2}$ for vertical plumes in a quiescent atmosphere and to $D_o^{-4/3}$ for plumes in a cross-wind. The horizontal position of plume descent to the ground will also be increased by decreasing the stack diameter for a given flow rate and stack height. This horizontal distance is proportional to D_o^{-2} , and is of course increased with increased stack height being approximately proportional to $(2+h_s/H)^{3/2}$ for significant values of h_s/H .

2. For plumes of relatively high density exhausted into light winds, such that the density difference and resulting vertical motion dominates diffusion, the ground concentration will be approximately proportional to $(2H+h_s)^{-2}$. The downstream decay rate from this point is $\frac{\bar{X}U}{Q} = \left(\frac{\bar{X}U}{Q}\right)_D \left(\frac{X}{X_D}\right)^{-.65}$ where D is the point of plume touchdown. The -.65 power law decay rate can be extended to the intersection with the ground source decay rate and that rate assumed from that point on.

3. The effect of negative buoyancy on the behavior of ground source is primarily multiplicative as the decay relationship is not changed in form. Large specific gravities produce only moderate percentage increases in downstream concentration values rather than order of magnitude changes. Negative buoyance causes larger lateral and smaller vertical plume dimensions than are observed in cases of neutral buoyancy.

BIBLIOGRAPHY

- (1) Albertson, M. L., Dai, Y. B., Jenson, R. A., and Rouse, H., "Diffusion of Submerged Jets," ASCE Transactions, 115, pp. 639-697 (1950).
- (2) Becker, H. A., Hottel, H. C., and Williams, G.C., "The Nozzle-Fluid Concentration Field of the Round Turbulent Free Jet," Journal of Fluid Mechanics, 30, pp. 285-304 (1968).
- (3) Bodurtha, F. T. "The Behavior of Dense Stack Gases," J. Air Pollution Control Assoc., 11, 431-437 (1961).
- (4) Briggs, G. A., "A Simple Model for Bent Over Plume Rise," Ph.D. Dissertation, Pennsylvania State University, (1970).
- (5) Briggs, G. A., Plume Rise, Atomic Energy Commission Critical Review Series, Division of Technical Information, TID-25075, (1969).
- (6) Cermak, J. E. et al., "Simulation of Atmospheric Motion by Wind Tunnel Flows," Colorado State University, Report No. CER66-67 JEC-VAS-EJP-GJB-HC-RNM-SI-17, (1966).
- (7) Chaudhry, F. H. and Meroney, R. N., "Turbulent Diffusion in a Stably Stratified Shear Layer," FDDL Report CER69-70FHC-RMN12 (U.S. Army Electronics Command Technical Report C-0423-5), (1969).
- (8) Chesler, S. and Jesser, B. W., "Some Aspects of Design and Economic Problems Involved in Safe Disposal of Inflammable Vapors from Safety Relief Valves," Transactions of the ASME, pp. 229-246 (Feb. 1952).
- (9) Counihan, J., "An Improved Method of Simulating an Atmospheric Boundary Layer in a Wind Tunnel," Atmospheric Environment, Vol. 3, pp. 197-214 (1969).
- (10) Csanady, G. T., "Bent Over Vapor Plumes," Journal of Applied Meteorology, 10, pp. 36-42 (1970).
- (11) Davar, K. S., "Diffusion from a Point Source Within a Turbulent Boundary Layer," Ph.D. Dissertation, Colorado State University, (1961).
- (12) Halitsky, J., "Gas Diffusion Near Buildings," Meteorology and Atomic Energy, pp. 221-225 (1968).
- (13) Hewett, T. A., "Model Experiments of Smokestack Plumes in a Stable Atmosphere," Ph.D. Dissertation, M.I.T., (1971).
- (14) Hoult, D. P., Fay, J. A., and Forney, L. J., "A Theory of Plume Rise Compared with Field Observations," Paper No. 68-77, Air Pollution Control Association, Pittsburgh, (1968).

- (15) Holly, F. M. and Grace, J. L., "Model Study of Dense Jets in Flowing Fluid," Proceedings of the Hydraulics Division No. 9365, ASCE, (1972).
- (16) Keefer, J. F. and Baines, W. A., "The Round Turbulent Jet in a Crosswind," Journal of Fluid Mechanics, 15, pp. 481-496 (1963).
- (17) Malhotra, R. C., "Diffusion From a Point Source of Buoyancy in a Turbulent Boundary Layer with Unstable Density Stratification," Ph.D. Dissertation, Colorado State University, (1962).
- (18) Meroney, R. N. and Chaudhry, F. H., "Wind Tunnel Analysis of Dow Chemical Facility at Rocky Flats, Colorado," Colorado State University Report No. CER71-72 RNM-FC-45 (1972).
- (19) Morton, B. R., Taylor, G. I., and Turner, J. S., "Turbulent Gravitational Convection from Maintained and Instantaneous Sources," Proc. Royal Society A23, pp. 1-23 (1956).
- (20) Morton, B. R., "Buoyant Plumes in a Moist Atmosphere," Journal of Fluid Mechanics, 2, pp. 127-143 (1957).
- (21) Plate, E. J. and Lin, C. W., "Investigations of the Thermally Stratified Boundary Layer," Fluid Mechanics Paper No. 5, Colorado State University, (1966).
- (22) Rouse, H., Yih, C. S. and Humphries, H. W., "Gravitational Convection from a Boundary Source," Tellus, 4, p. 201ff. (1952).
- (23) Scorer, R. S., "The Behavior of Chimney Plumes," Int. J. Air Pollution, 1, pp. 198-220 (1959).
- (24) Scorer, R. S., "Experiments on Convection of Isolated Masses of Buoyant Fluid," Journal of Fluid Mechanics, 2, pp. 583-594 (1957).
- (25) Schlichting, H., Boundary Layer Theory, McGraw-Hill, New York, 6th Edition (1966).
- (26) Shih, C. C., "Continuous Point Source Diffusion in a Turbulent Shear Layer," M.S. Thesis, Colorado State University, (1966).
- (27) Slade, D. H., Editor, Meteorology and Atomic Energy, U.S. Atomic Energy Commission, Division of Technical Information, (1968).
- (28) Slawson, P. R. and Csanady, G. T., "On the Mean Path of Buoyant Bent Over Chimney Plumes," Journal of Fluid Mechanics, 28, Part 2, pp. 311-312 (1967).
- (29) Sutton, O. G., Micrometeorology, McGraw-Hill Book Co., Inc., New York (1953).
- (30) Tulin, M. P. and Schwartz, J., "Chimney Plumes in Neutral and Stable Surroundings," Journal of Atmospheric Environment, Vol 6 (1), pp. 19-35 (1972).

- (31) Turner, J. S., "Plumes with Negative or Reversing Buoyancy," Journal of Fluid Mechanics, 26, pp. 779-792 (1966).
- (32) Wigley, T. M. L. and Slawson, P. R., "A Comparison of Wet and Dry Bent Over Plumes," Journal of Applied Meteorology, 11, No. 2, pp. 335-340 (1972).
- (33) Wigley, T. M. L. and Slawson, P. R., "On the Condensation of Buoyant Moist Bent Over Plumes," Journal of Applied Meteorology, 10, (1971).
- (34) Yang, B. T. and Meroney, R. N., "Gaseous Dispersion Into Stratified Building Wakes," Colorado State University Report No. CER70-71 BTY-RNM-8, (1970).
- (35) Yang, B. T. and Meroney, R. N., "Wind Tunnel Study on Gaseous Mixing due to Various Stack Heights and Injection rates above an Isolated Structure," FDDL Report, CER71-72 RNM-BTY 16, (1971).

TABLE I
VERTICAL PLUMES
SMOKE VISUALIZATION DATA

Stack Exit Velocity Ft. Per Second	Stack Diameter Inches	Specific Gravity	Rise Height Inches
5.44	.250	1.50	8.29
5.44	.250	2.00	6.39
5.62	.250	1.24	11.95
7.39	.250	1.25	19.33
8.13	.250	1.52	14.00
8.03	.250	1.97	9.05
7.50	.125	1.09	13.70
7.50	.125	1.25	13.00
7.50	.125	1.50	10.86
3.70	.125	1.09	8.10
7.39	.125	2.00	6.53
14.61	.125	1.96	13.00
22.07	.125	2.00	20.23
15.19	.125	1.49	16.43
22.34	.125	1.50	23.55
20.10	.125	1.42	23.96
22.08	.125	1.42	25.44
7.38	.125	1.35	8.89
14.85	.125	1.35	18.28
20.30	.125	1.35	26.10
22.18	.125	1.35	27.30
14.80	.125	3.00	11.35

TABLE II
PLUMES IN A LAMINAR CROSSWIND
SMOKE VISUALIZATION DATA

Stack Exit Velocity Ft/Sec	Velocity Ratio	Specific Gravity	Stack Diameter Inches	Stack Height Inches	Rise Height Inches	Horizontal Distance From Stack to "Touchdown" Inches
3.712	5.10	1.077	0.250	3.0	3.70	-
7.467	10.22	1.096	0.250	3.0	6.90	-
11.137	15.24	1.102	0.250	3.0	10.18	-
14.395	20.50	1.096	0.250	3.0	14.12	-
3.755	5.18	1.572	0.250	3.0	3.05	19.50
7.511	10.36	1.572	0.250	3.0	5.21	28.20
11.266	15.54	1.572	0.250	3.0	8.15	44.20
15.022	20.72	1.572	0.250	3.0	10.80	56.00
3.712	5.10	2.158	0.250	3.0	2.71	12.64
7.424	10.20	2.158	0.250	3.0	5.22	23.75
11.137	15.30	2.158	0.250	3.0	7.78	28.20
15.022	20.72	2.126	0.250	3.0	10.82	38.80
15.022	20.72	2.174	0.250	3.0	10.30	32.60
3.712	5.10	3.316	0.250	3.0	2.37	8.64
7.424	10.20	3.278	0.250	3.0	5.24	13.35
11.137	15.24	3.290	0.250	3.0	8.18	19.60
3.712	5.10	4.160	0.250	3.0	2.36	4.85
7.511	10.32	4.160	0.250	3.0	5.12	9.68
3.712	5.21	1.077	0.250	6.0	3.43	-

TABLE II (continued)

Stack Exit Velocity Ft/Sec	Velocity Ratio	Specific Gravity	Stack Diameter Inches	Stack Height Inches	Rise Height Inches	Horizontal Distance From Stack to "Touchdown" Inches
7.467	10.45	1.096	0.250	6.0	6.90	-
3.755	5.15	1.572	0.250	6.0	2.30	23.40
7.511	10.30	1.572	0.250	6.0	5.42	37.40
3.712	5.21	2.158	0.250	6.0	2.81	19.60
7.424	10.42	2.158	0.250	6.0	5.00	28.70
3.712	4.96	3.316	0.250	6.0	2.07	9.68
7.424	9.92	3.278	0.250	6.0	5.00	18.00
3.712	4.96	4.160	0.250	6.0	2.24	8.84
7.511	10.06	4.160	0.250	6.0	5.14	13.80
14.935	20.30*	1.096	0.250	0.0	14.11	-
18.820	25.20*	1.122	0.250	0.0	16.85	-
15.022	21.30*	1.572	0.250	0.0	9.68	37.20
18.820	26.20*	1.572	0.250	0.0	12.45	45.20
15.022	21.20*	2.126	0.250	0.0	10.13	26.30
18.820	26.00*	2.126	0.250	0.0	12.00	32.20
15.022	21.00*	2.714	0.250	0.0	10.58	21.60
18.820	25.60*	2.690	0.250	0.0	13.82	25.60
7.597	10.10	1.608	0.125	3.0	3.22	31.50
10.750	14.60	1.523	0.125	3.0	4.48	44.12
3.799	5.05	2.217	0.125	3.0	1.38	21.23
7.597	10.10	2.217	0.125	3.0	3.20	22.20

TABLE II (continued)

Stack Exit Velocity Ft/Sec	Velocity Ratio	Specific Gravity	Stack Diameter Inches	Stack Height Inches	Rise Height Inches	Horizontal Distance From Stack to "Touchdown" Inches
10.750	14.60	2.254	0.125	3.0	4.62	28.15
3.799	5.05	3.281	0.125	3.0	1.49	10.30
6.216	8.80	3.044	0.125	3.0	2.88	14.05
6.560	9.25	3.465	0.125	3.0	3.03	15.13
3.750	5.05	1.500	0.125	3.0	1.12	17.35
3.750	5.05	2.001	0.125	3.0	1.13	11.35
3.750	5.05	3.008	0.125	3.0	1.32	10.16
7.500	10.20	1.503	0.125	3.0	3.35	35.80
7.500	10.20	2.001	0.125	3.0	2.96	17.70
7.500	10.20	3.008	0.125	3.0	3.35	15.95
11.250	15.45	1.502	0.125	3.0	4.99	43.20
11.250	15.45	2.001	0.125	3.0	4.90	26.60
11.250	15.45	3.006	0.125	3.0	4.72	23.45
3.750	5.05	2.001	0.125	6.0	1.26	15.85
3.750	5.05	3.008	0.125	6.0	1.35	16.95
7.500	10.20	2.001	0.125	6.0	3.03	29.75
7.500	10.20	3.008	0.125	6.0	3.05	20.35
11.250	15.45	2.001	0.125	6.0	4.85	34.30
11.250	15.45	3.006	0.125	6.0	4.86	25.80
3.750	5.10	1.500	0.250	6.0	2.94	24.60
3.750	5.10	2.001	0.250	6.0	2.64	15.15
3.750	5.10	3.006	0.250	6.0	2.39	10.65
7.500	10.40	1.503	0.250	6.0	4.86	30.20

TABLE II (continued)

Stack Exit Velocity Ft/Sec	Velocity Ratio	Specific Gravity	Stack Diameter Inches	Stack Height Inches	Rise Height Inches	Horizontal Distance From Stack to "Touchdown" Inches
7.500	10.40	2.001	0.250	6.0	4.66	20.20
7.500	10.40	3.008	0.250	6.0	4.93	14.62
11.250	15.65	1.502	0.250	6.0	7.89	38.90
11.250	15.65	2.001	0.250	6.0	7.71	25.50
11.250	15.65	3.006	0.250	6.0	7.91	21.15
7.500	5.10	2.001	0.125	6.0	2.62	-
7.500	5.10	3.008	0.125	6.0	2.38	-
11.250	10.20	1.502	0.125	6.0	4.02	-
11.250	10.20	2.001	0.125	6.0	3.80	-
11.250	10.20	3.006	0.125	6.0	3.98	-
3.750	2.55	1.503	0.250	6.0	2.10	-
3.750	2.55	2.001	0.250	6.0	1.88	-
3.750	2.55	3.008	0.250	6.0	1.85	-
7.500	5.10	1.503	0.250	6.0	3.85	-
7.500	5.10	3.008	0.250	6.0	4.02	-
11.250	7.65	1.503	0.250	6.0	6.40	-
11.250	7.65	2.001	0.250	6.0	6.22	-
11.250	7.65	3.008	0.250	6.0	6.40	-

* Represents Velocity Ratio Averaged Over Rise Height.

- Exact Position Where Lower Edge of Plume Touches Floor Indeterminate Due to Downstream Diffusion.

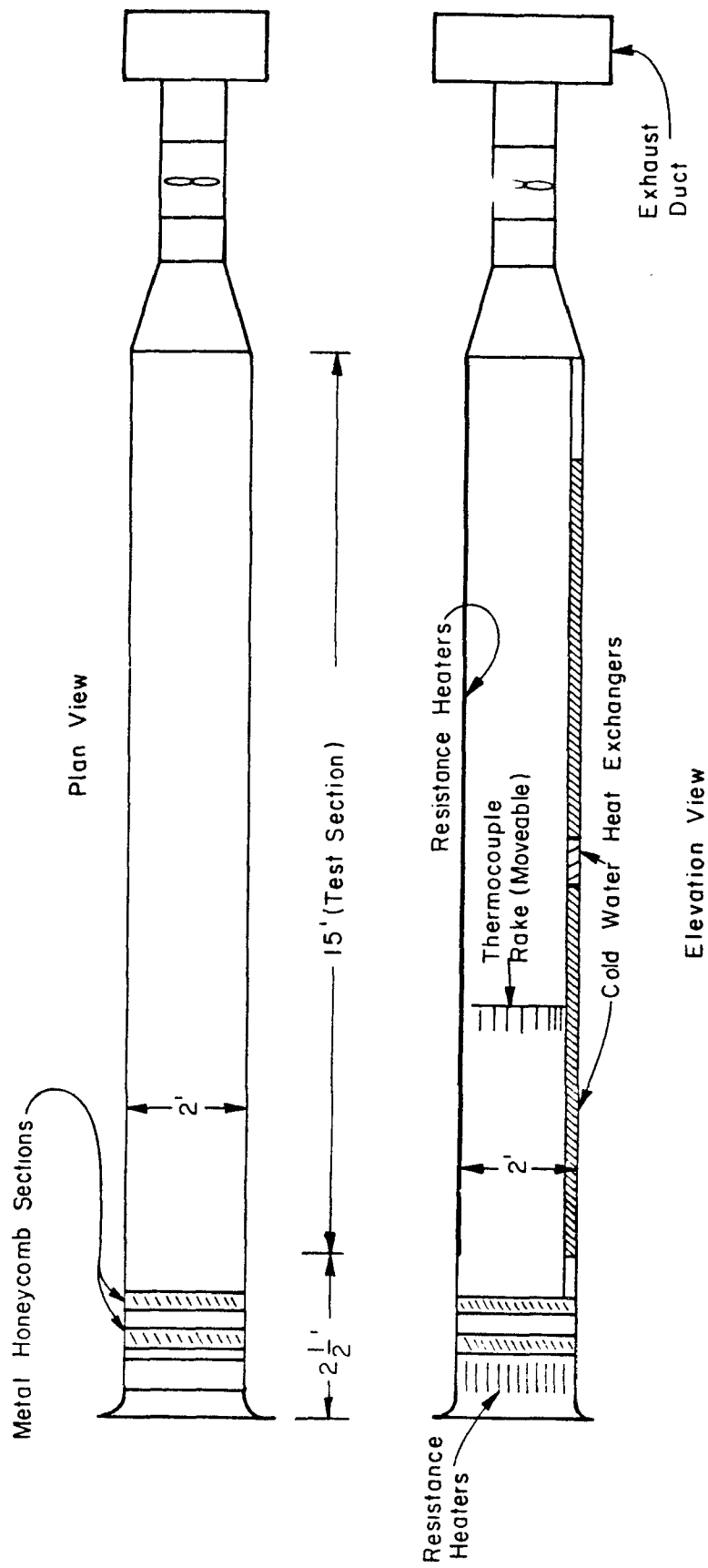


Fig. 1. CSU Thermal Wind Tunnel

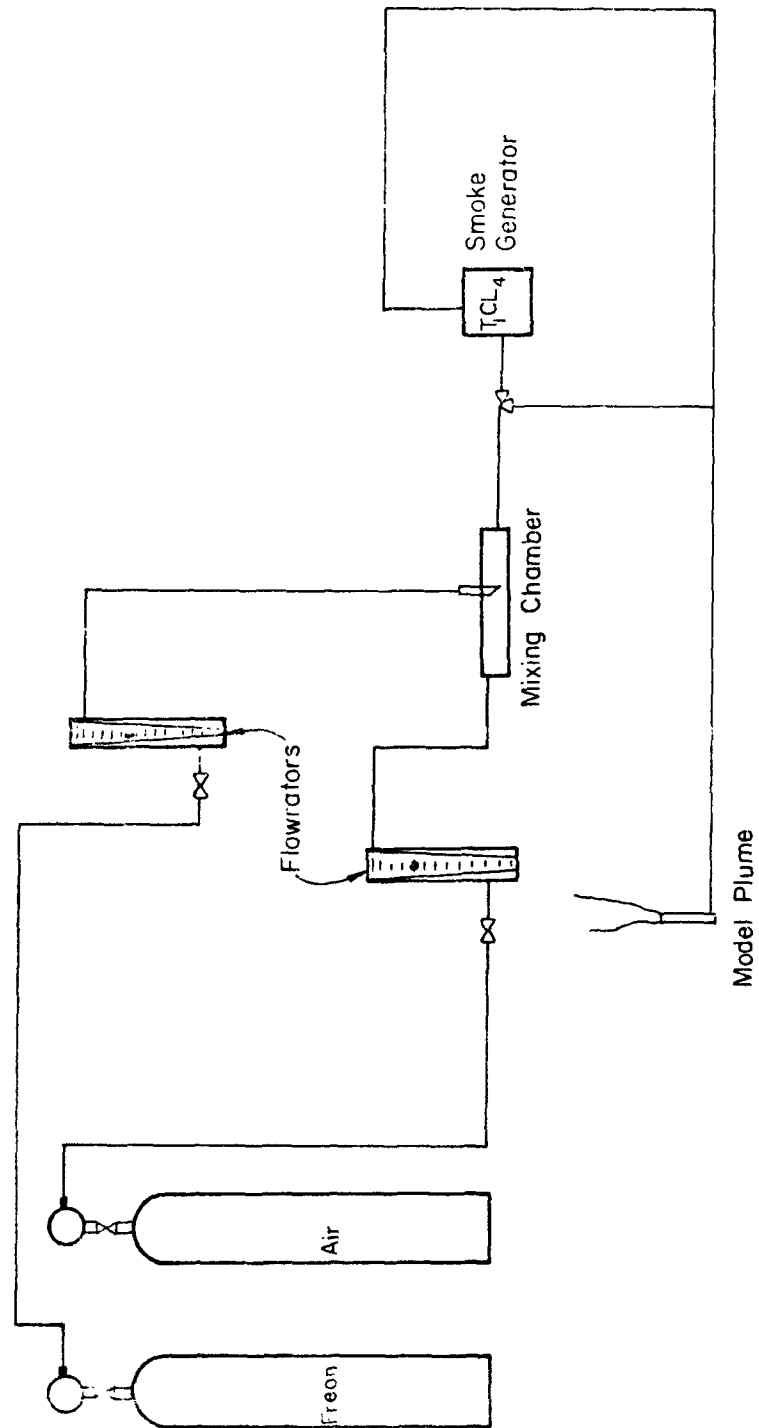


Fig. 2. Flow Mixing and Visualization System

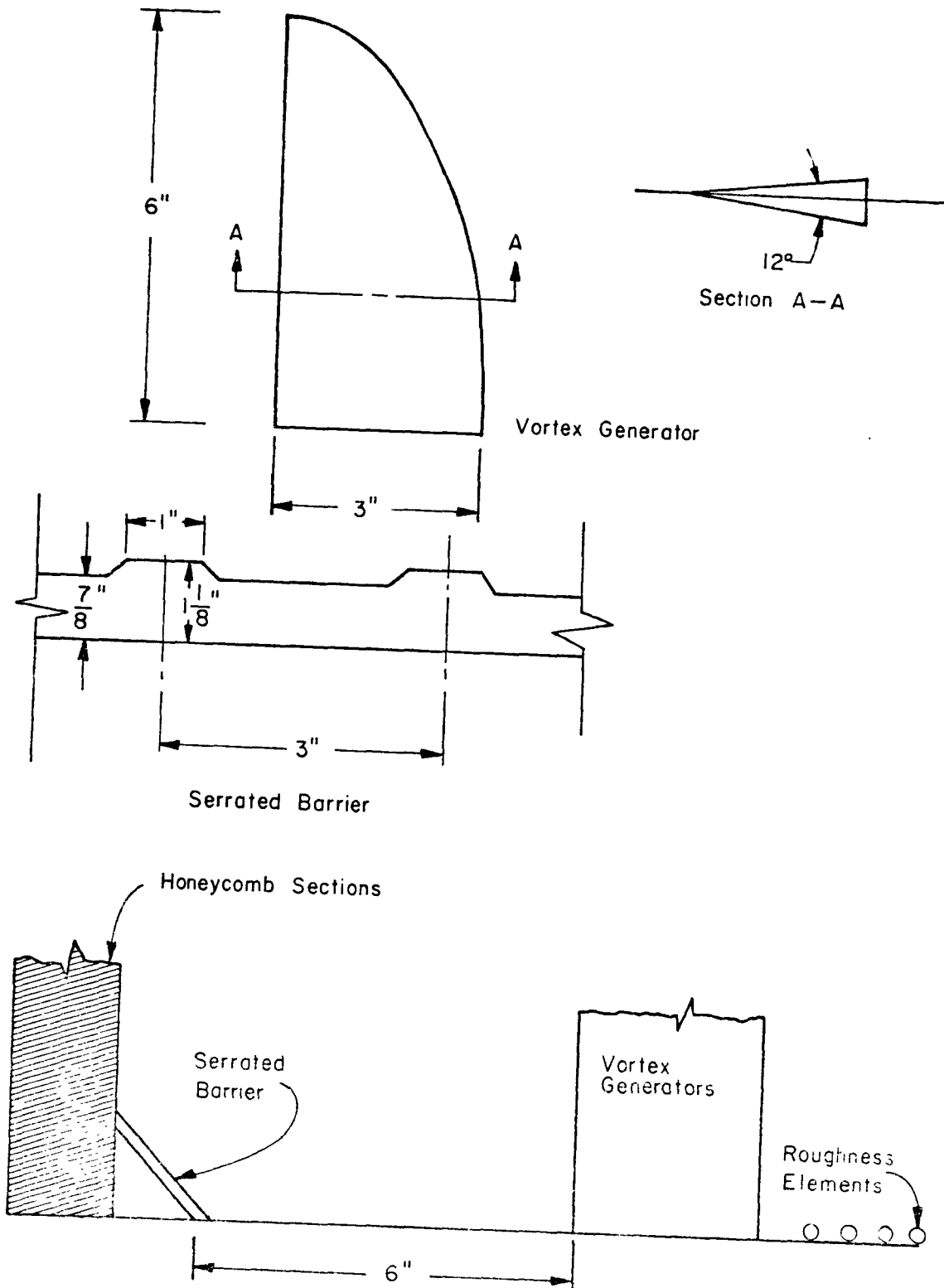


Fig. 3. Vortex Generator Details

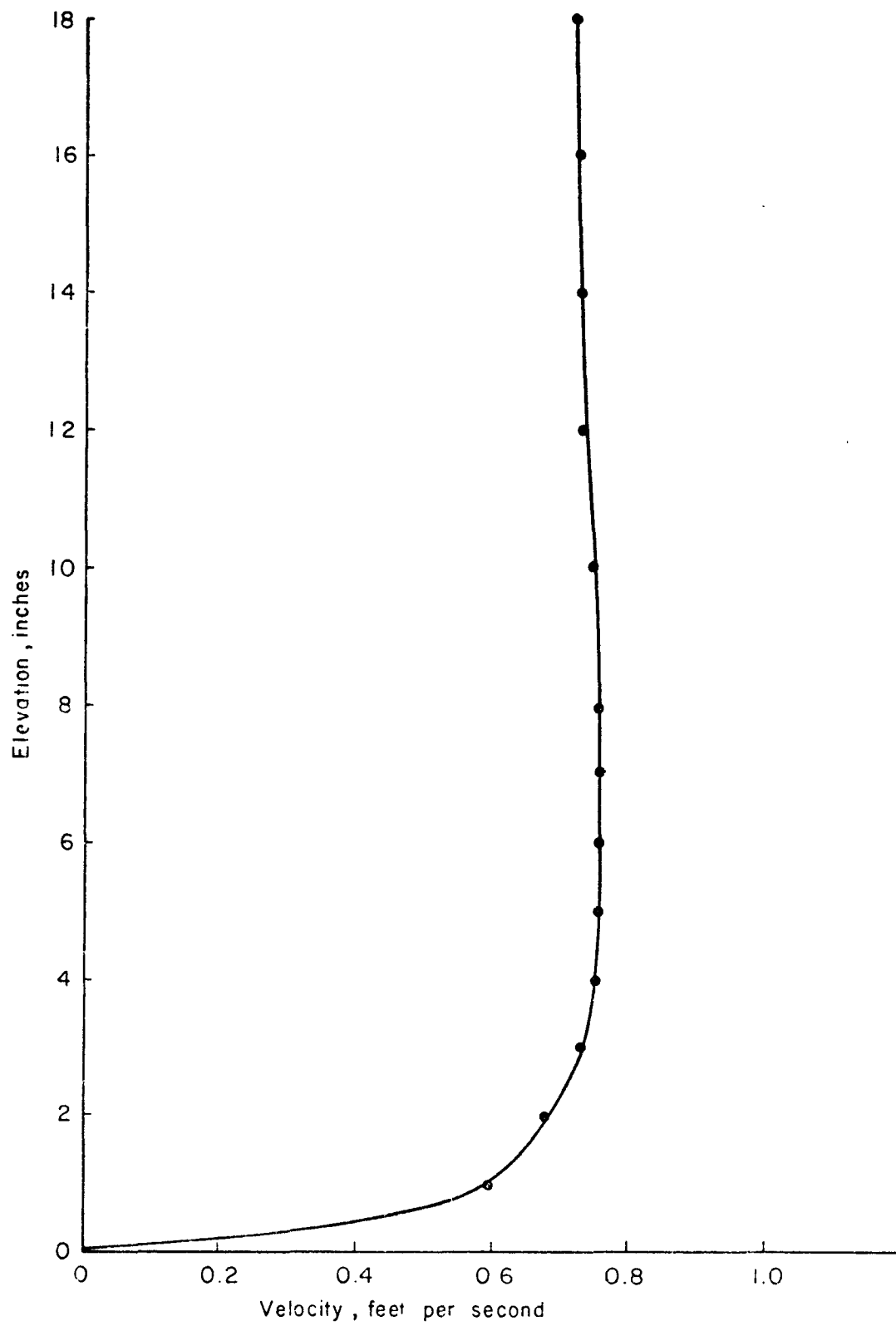


Fig. 4. Velocity Profile Laminar Flow

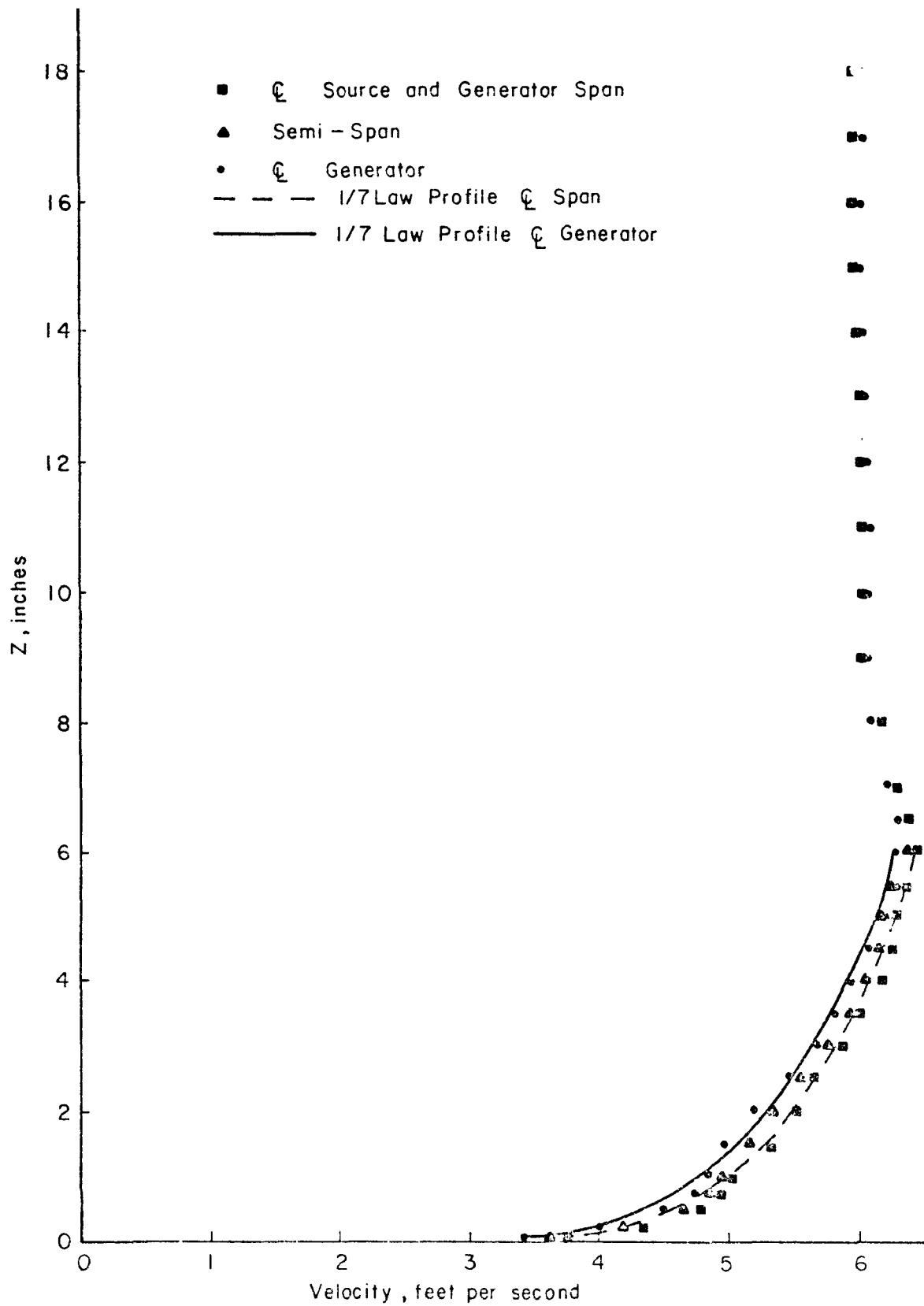


Fig. 5. Velocity Profile at Source, Turbulent Boundary Layer

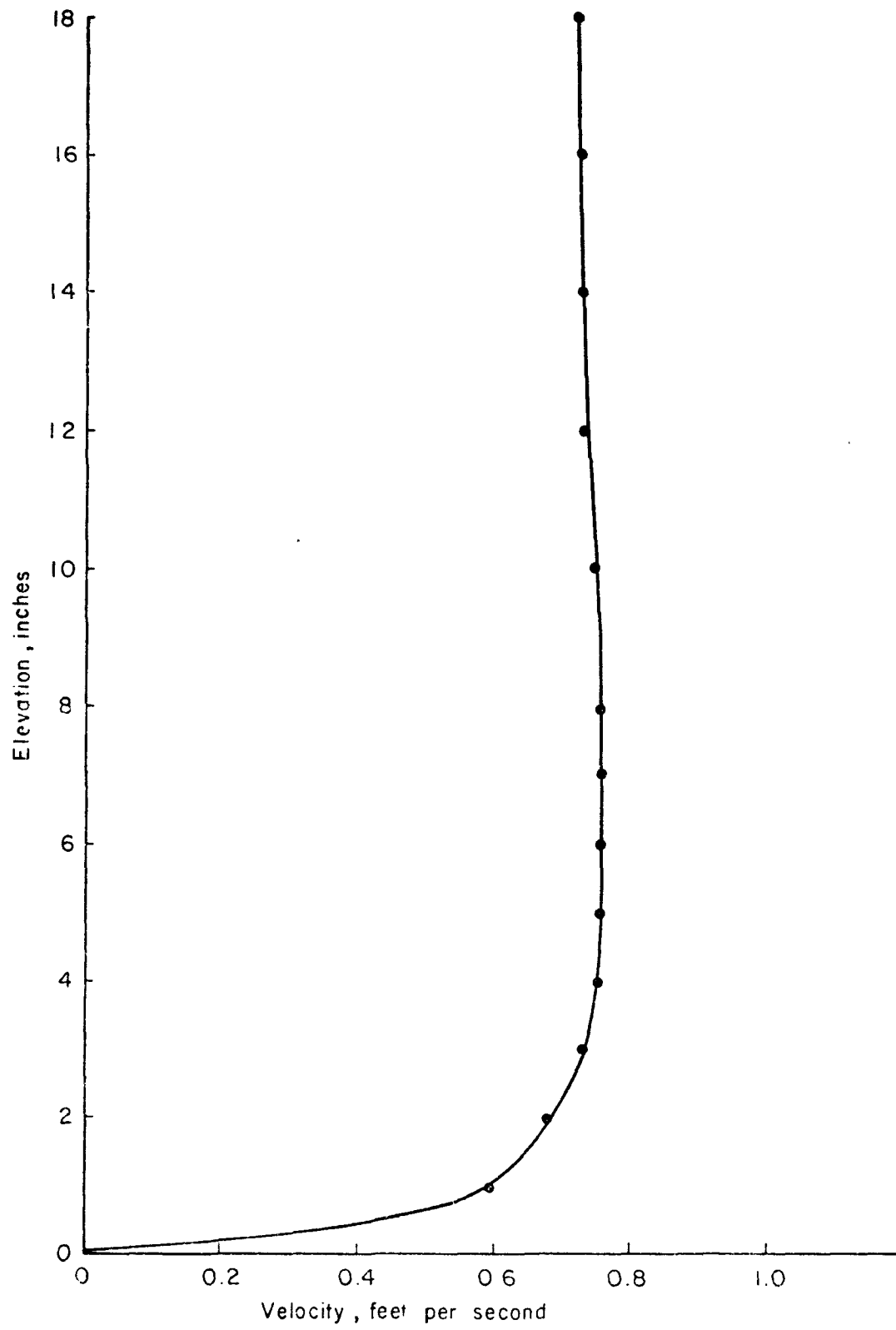


Fig. 4. Velocity Profile Laminar Flow

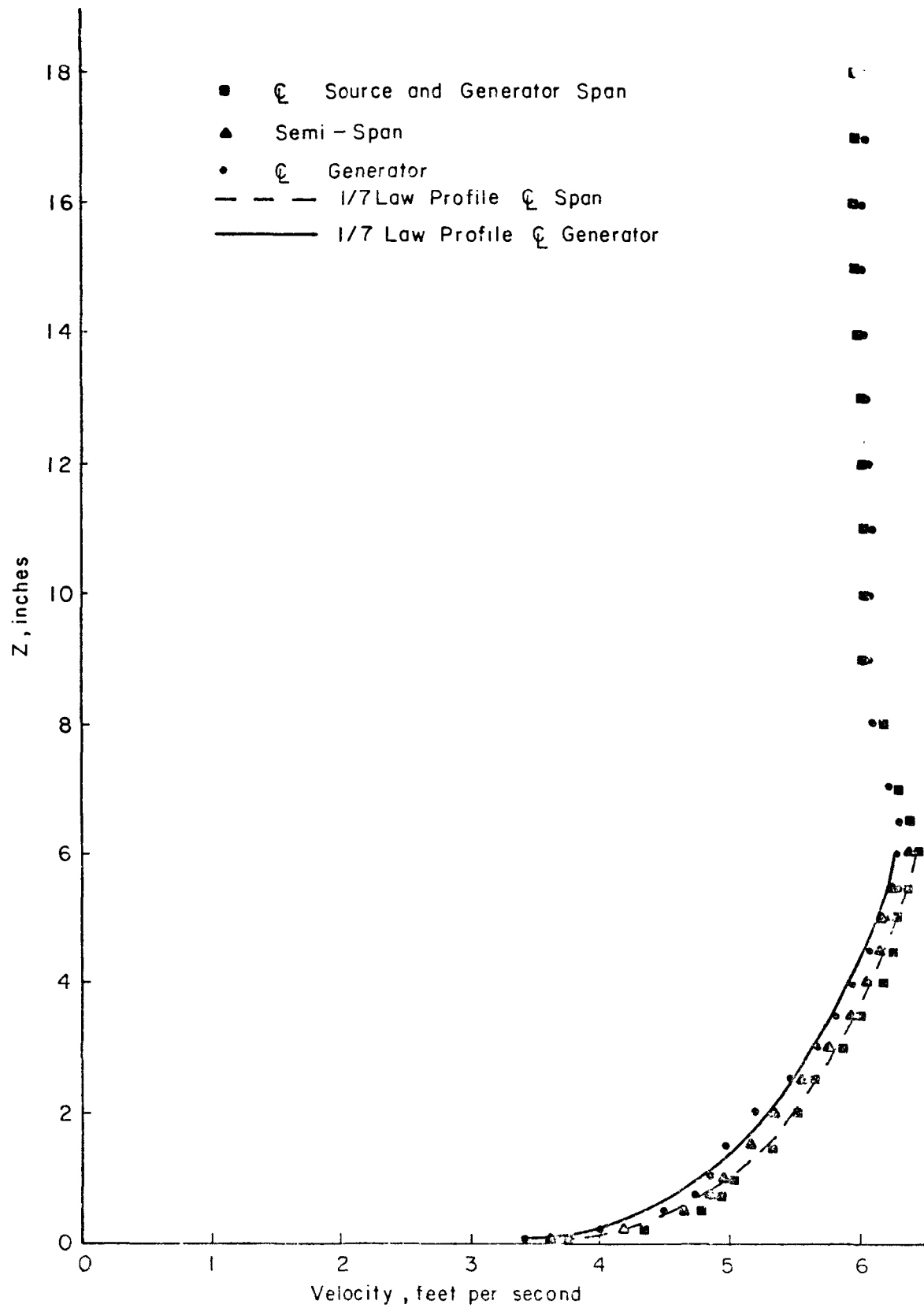


Fig. 5. Velocity Profile at Source, Turbulent Boundary Layer

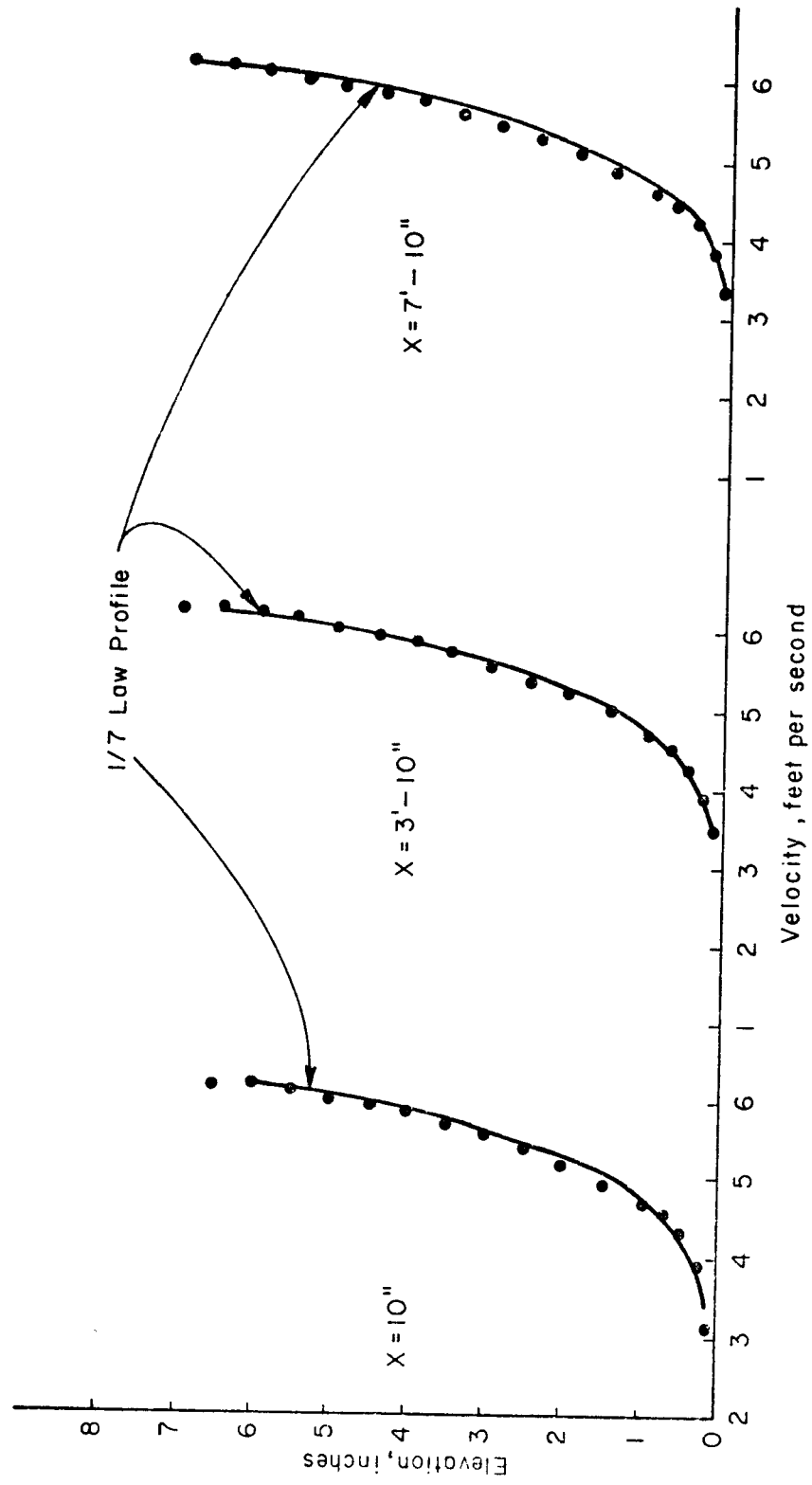


Fig. 6. Velocity Profiles, Tunnel Centerline, Turbulent Boundary Layer

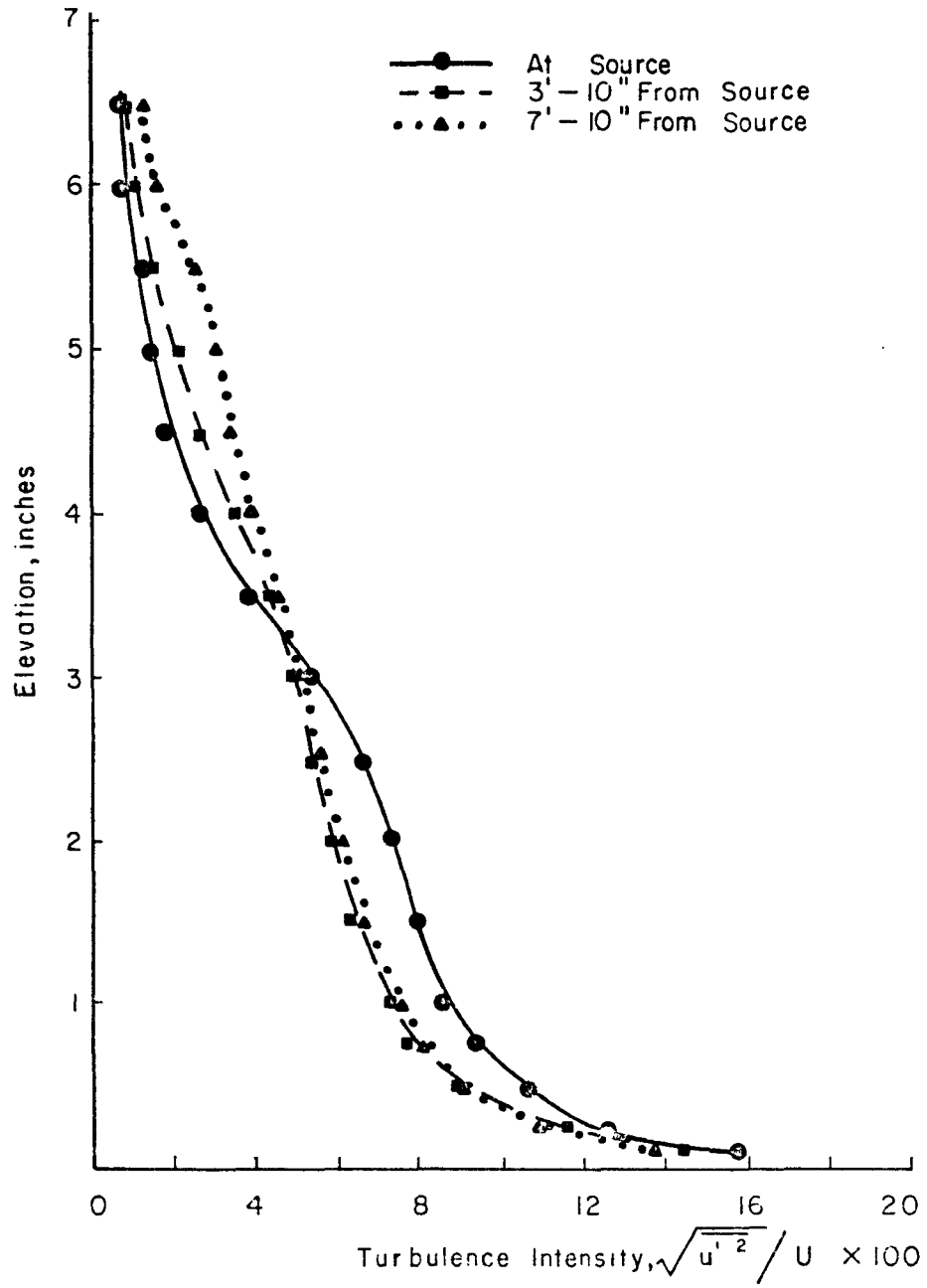


Fig. 7. Turbulence Intensities, Tunnel Centerline

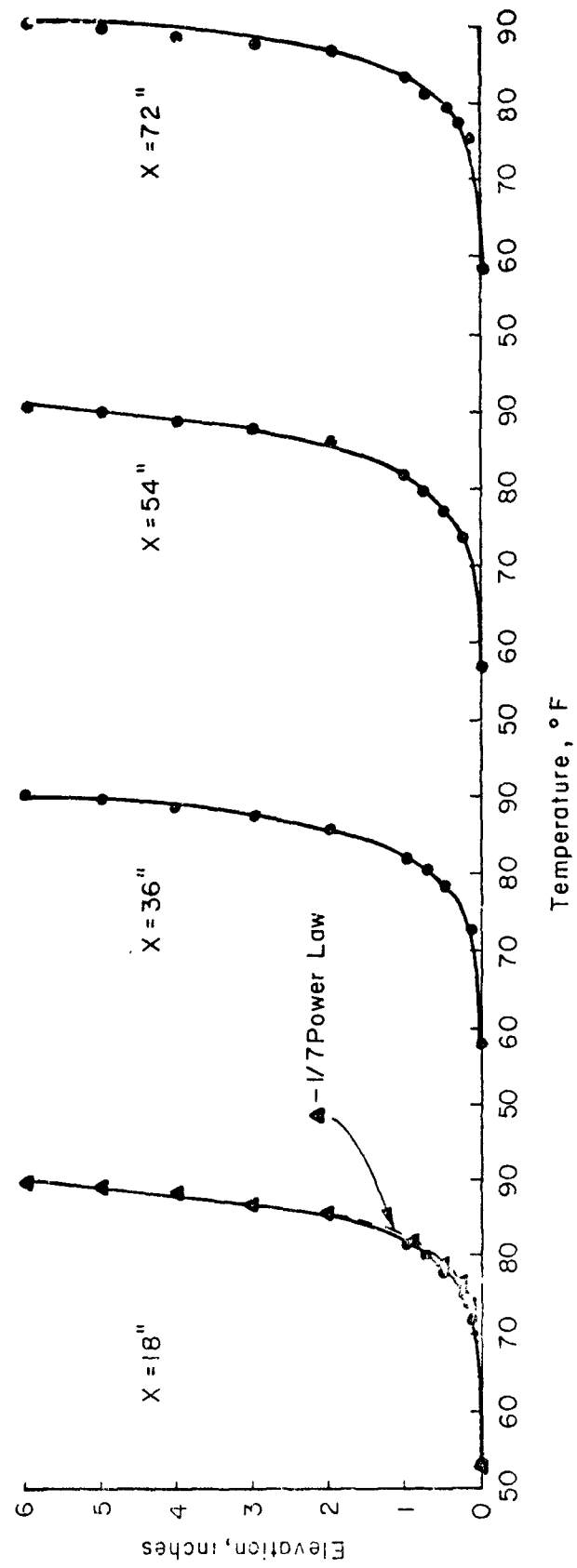


Fig. 8. Temperature Profiles, Thermal Stratification

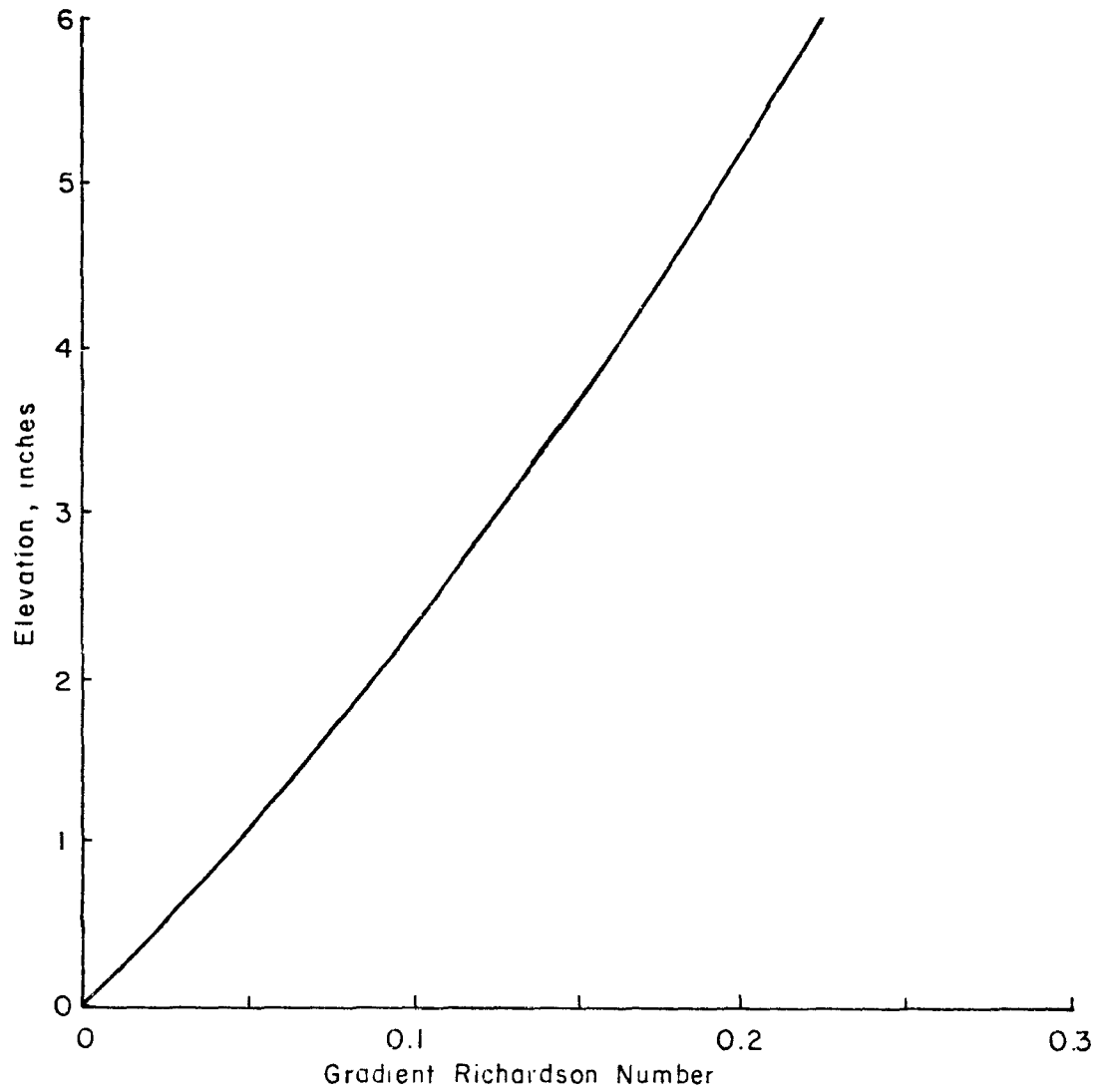


Fig. 9. Gradient Richardson Number, Thermal Stratification

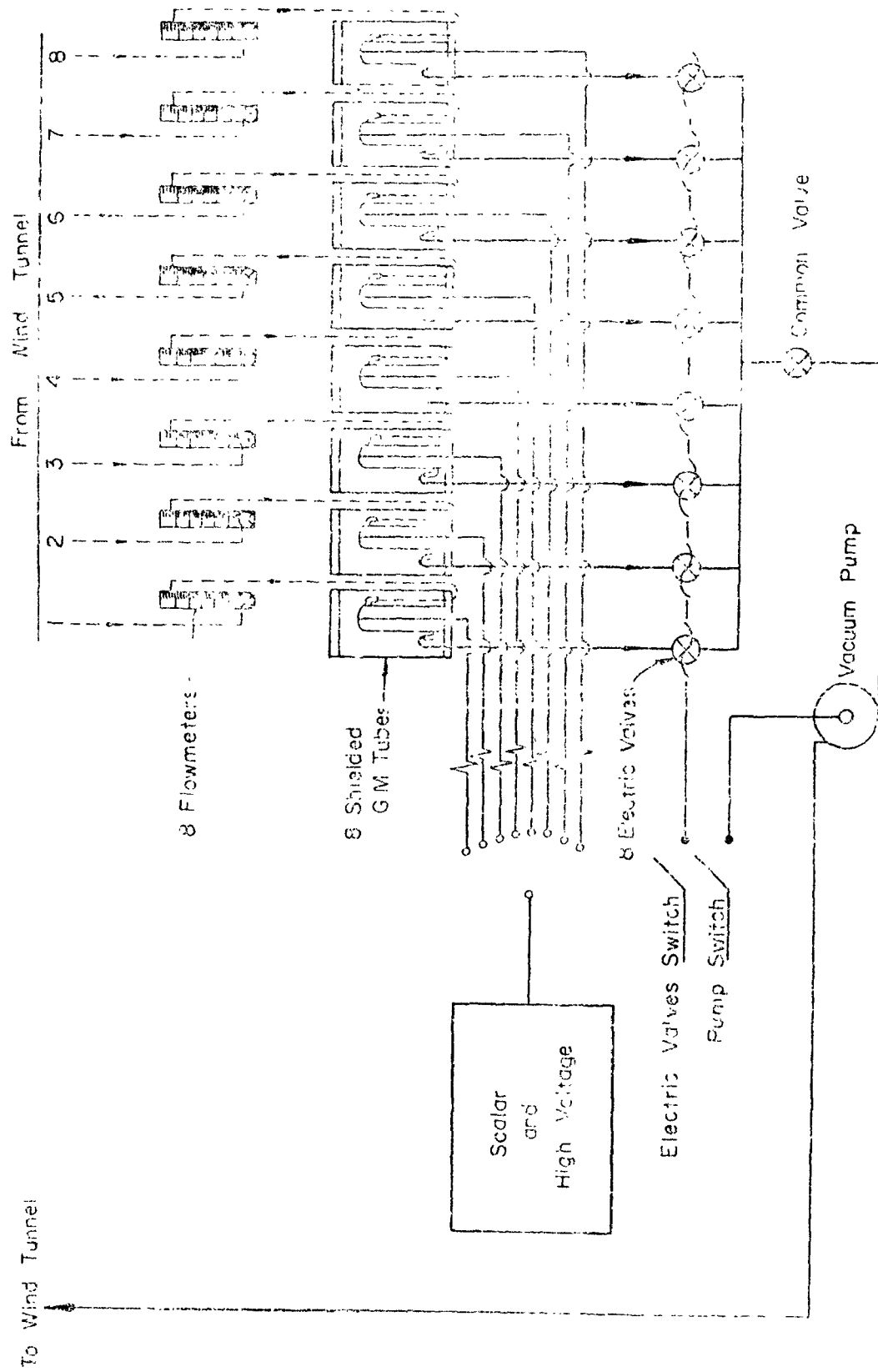
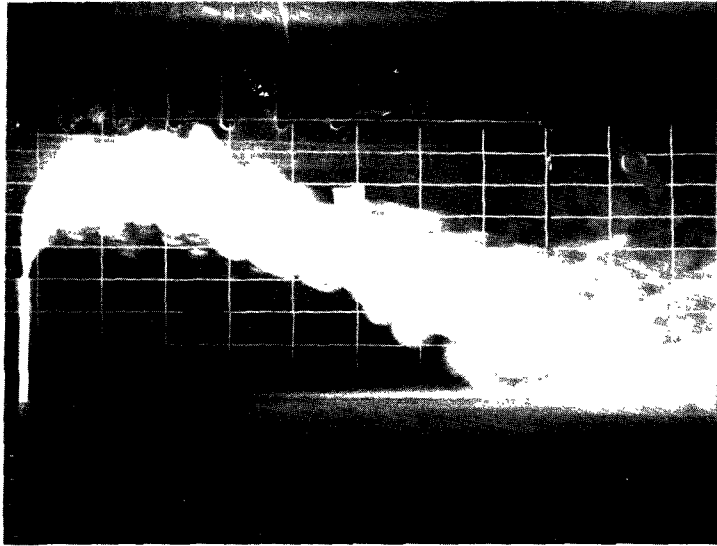
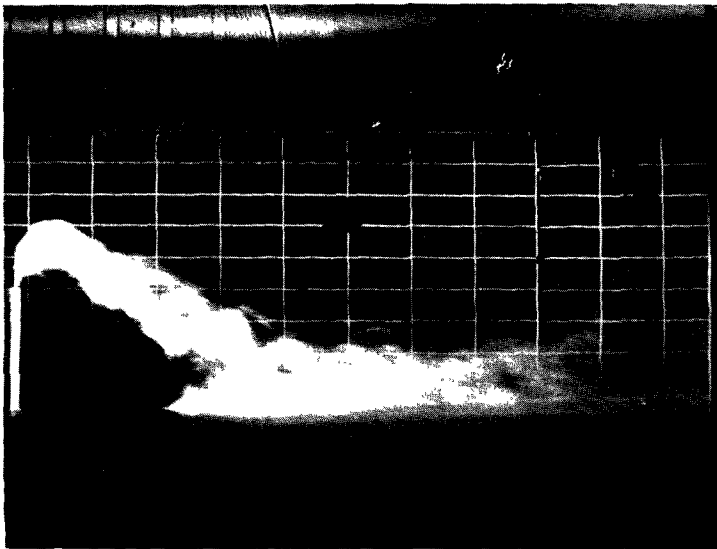


Fig. 10. Radiation Detection System



$R=10.44$, $F_R=12.95$, $SG=2$, $U_O=7.50$ ft/sec

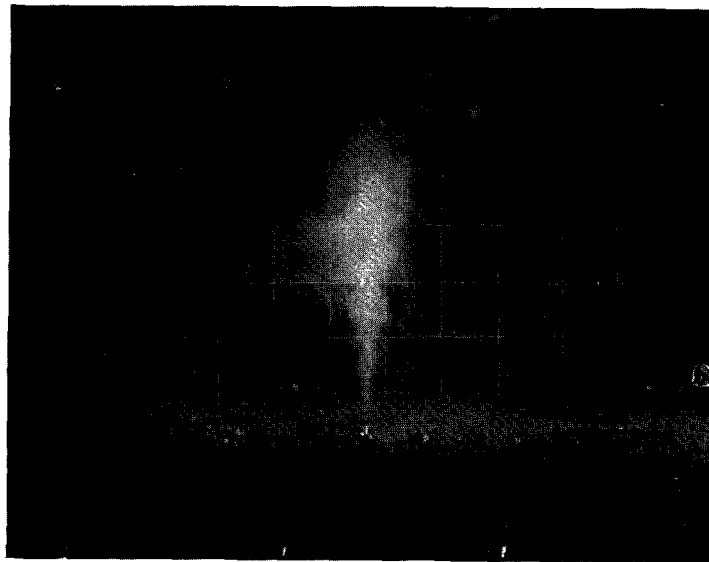


$R=5.14$, $F_R=5.60$, $SG=3$, $U_O=3.75$ ft/sec

Fig. 11. Smoke Photographs



$$F_R = 54, SG = 2.0, D_O = 1/8''$$



$$F_R = 75, SG = 1.36, D_O = 1/8''$$

Fig. 11. (Cont.) Smoke Photographs

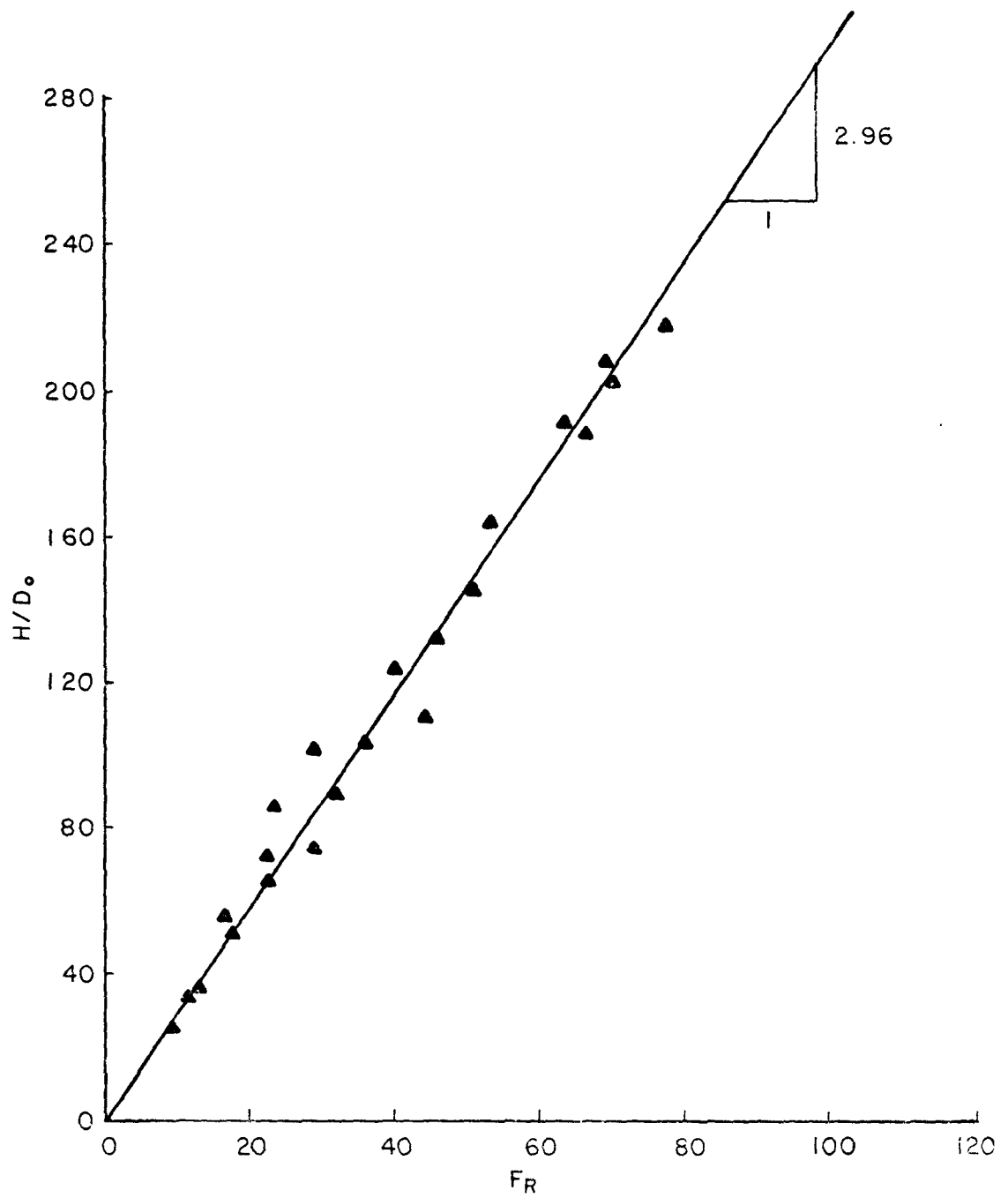


Fig. 12. Dimensionless Rise Height vs. Froude Number-
Vertical Plumes

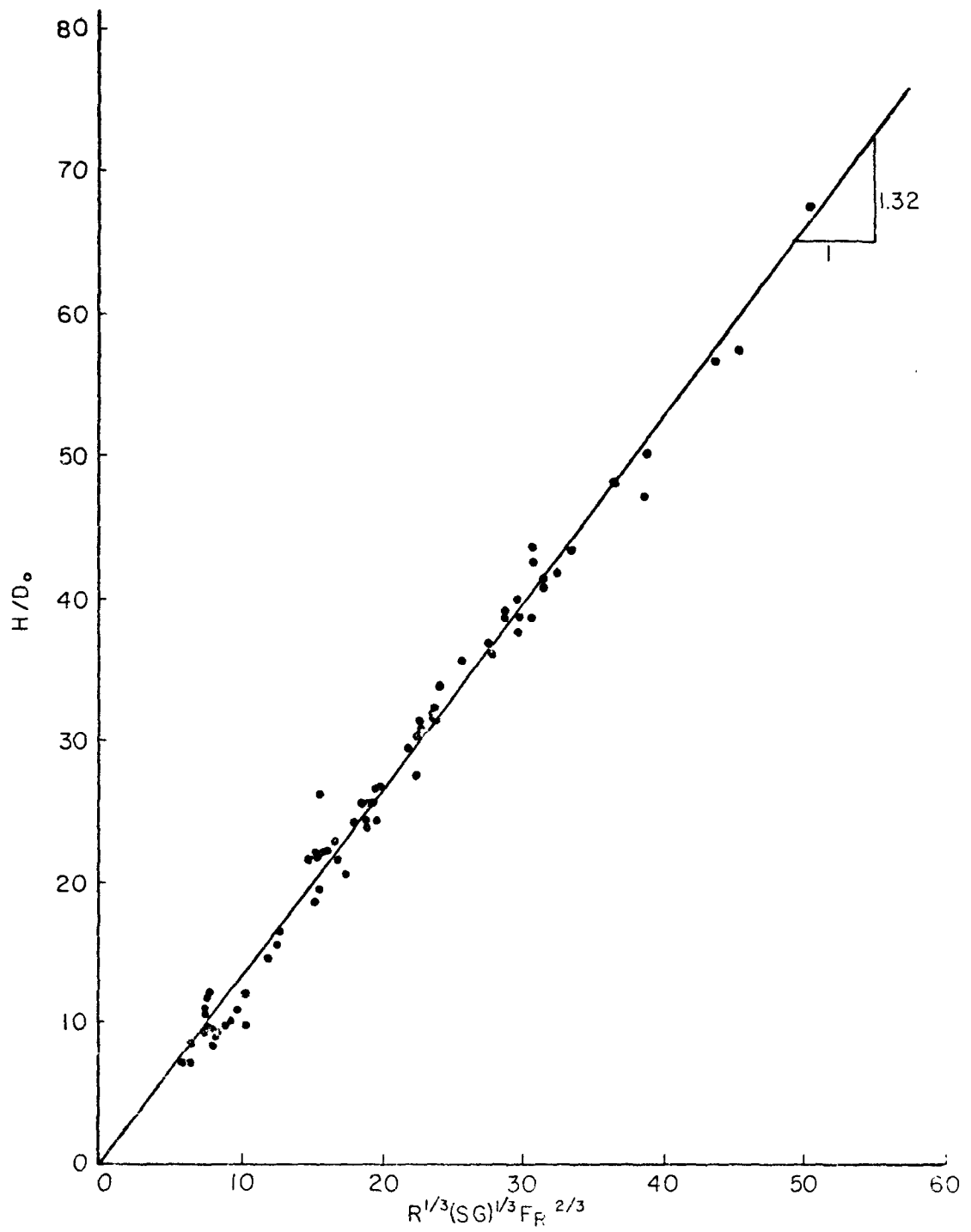


Fig. 13. Dimensionless Rise Height vs. Rise Height Parameter

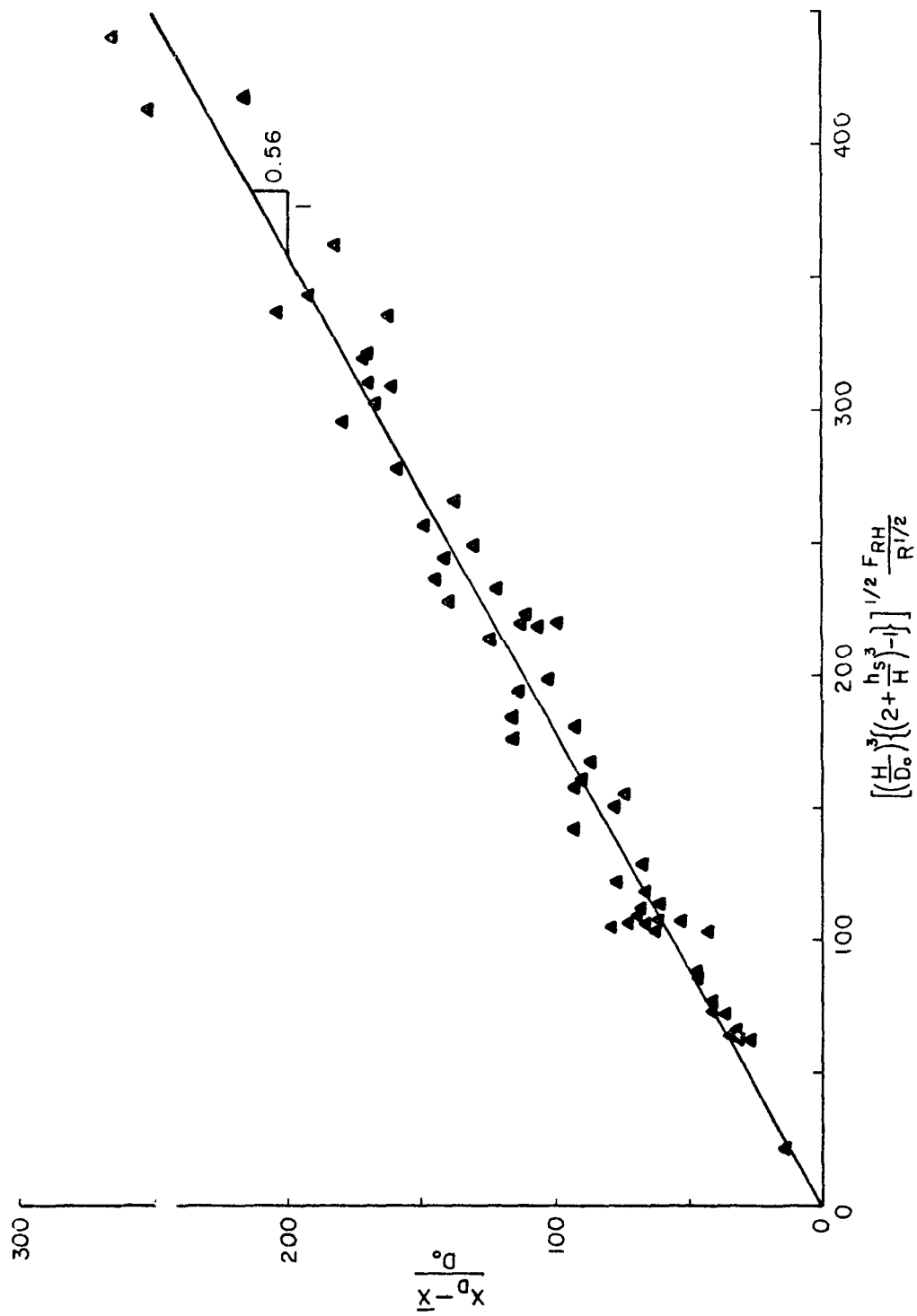
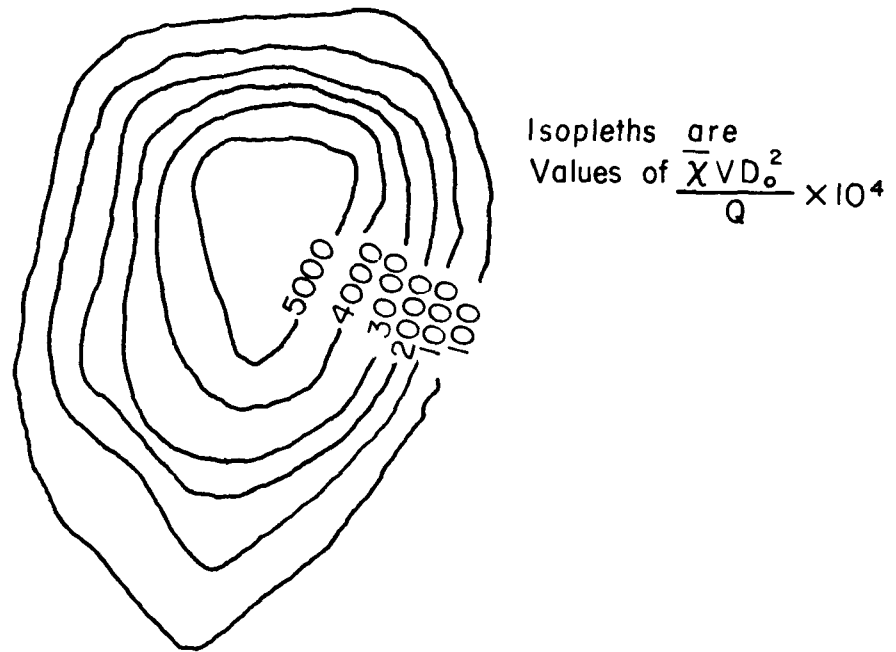
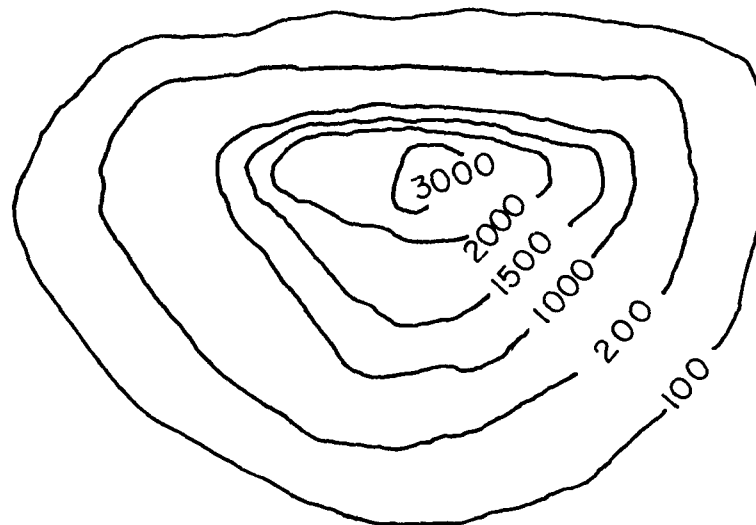


Fig. 14. Dimensionless "Touchdown" Distance vs. "Touchdown Parameter"

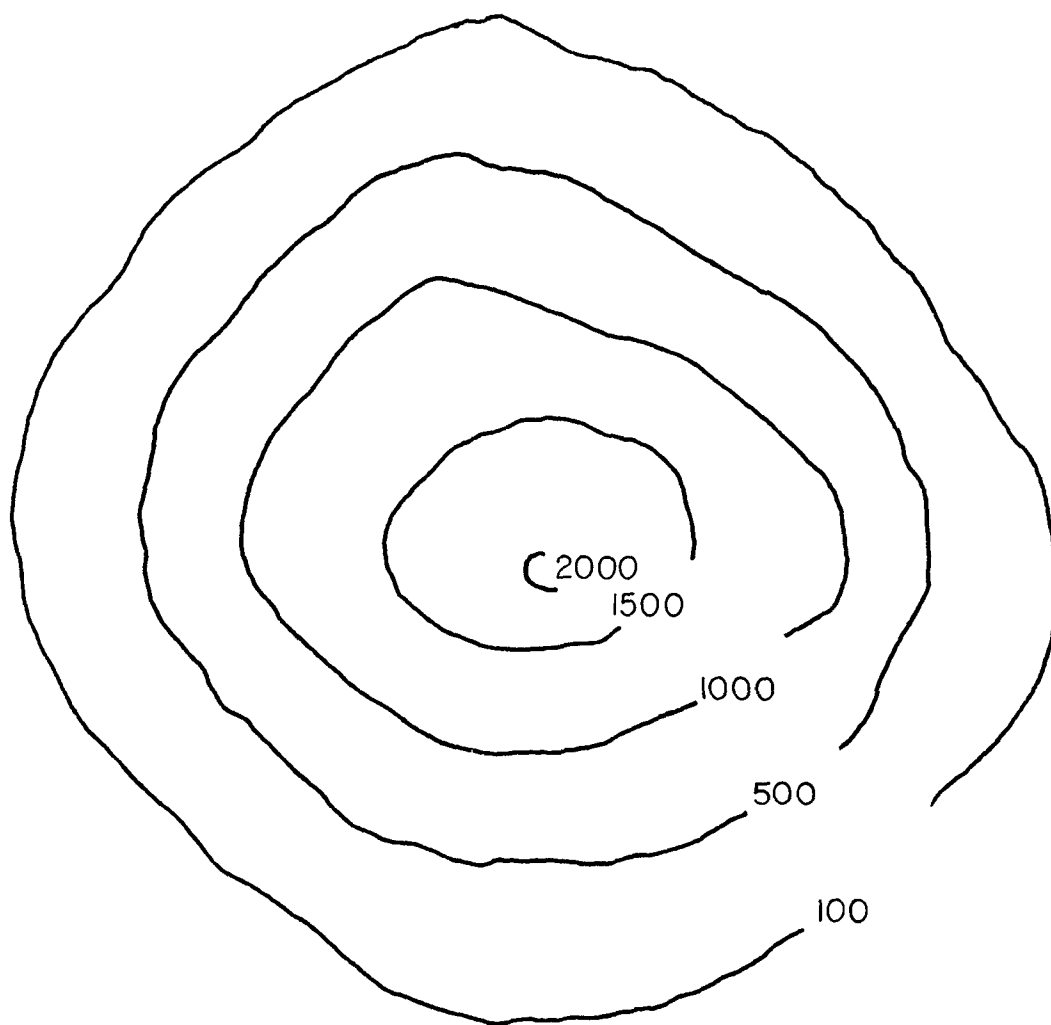


a) At Maximum Rise Height



b) Downstream in Near Horizontal Region

Fig. 15. Isopleths of Plume in Laminar Crosswind



c) Downstream in Rapidly Sinking Region

Fig. 15. (Cont.) Isopleths of Plume in Laminar Crosswind

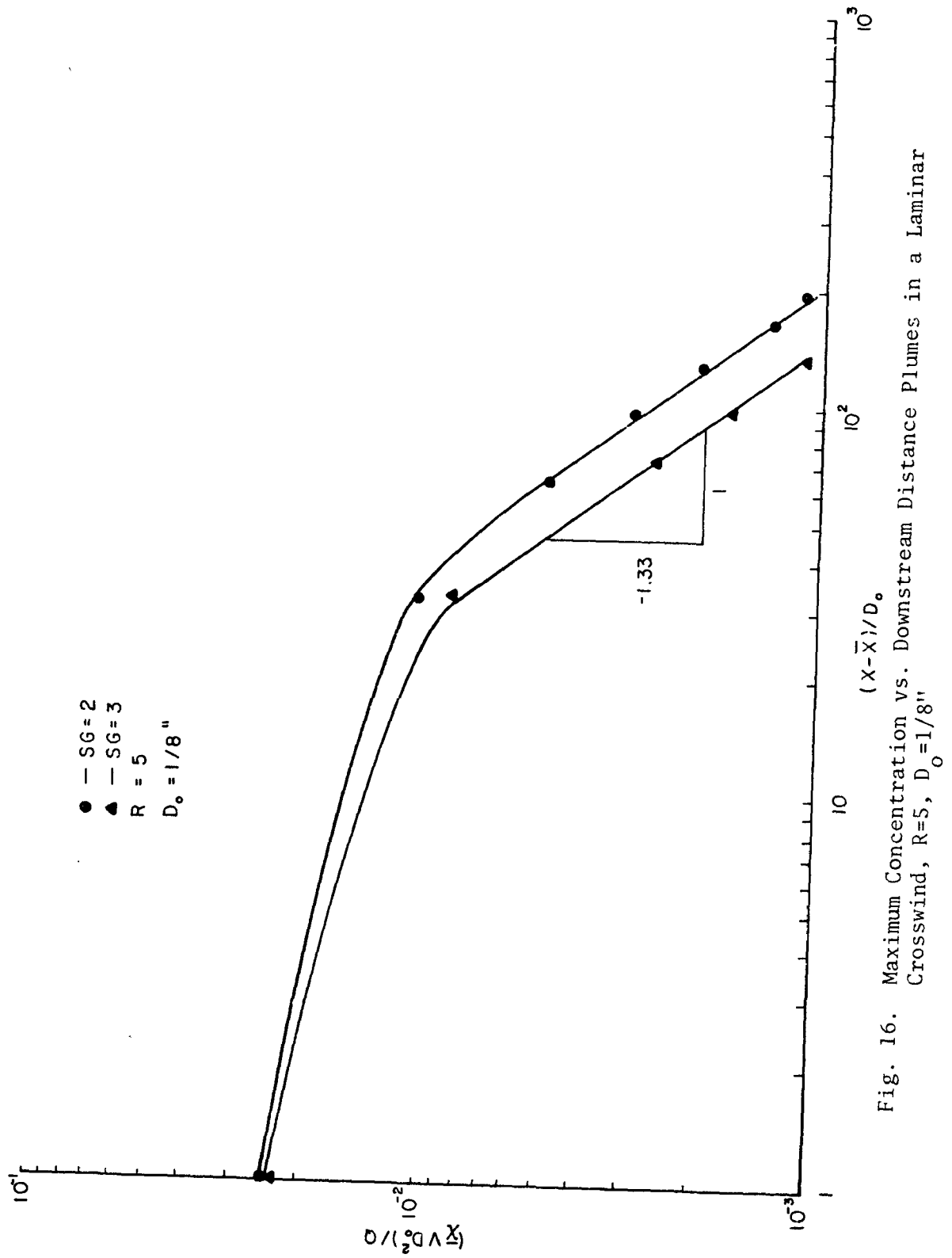


Fig. 16. Maximum Concentration vs. Downstream Distance Plumes in a Laminar Crosswind, $R=5$, $D_0=1/8"$

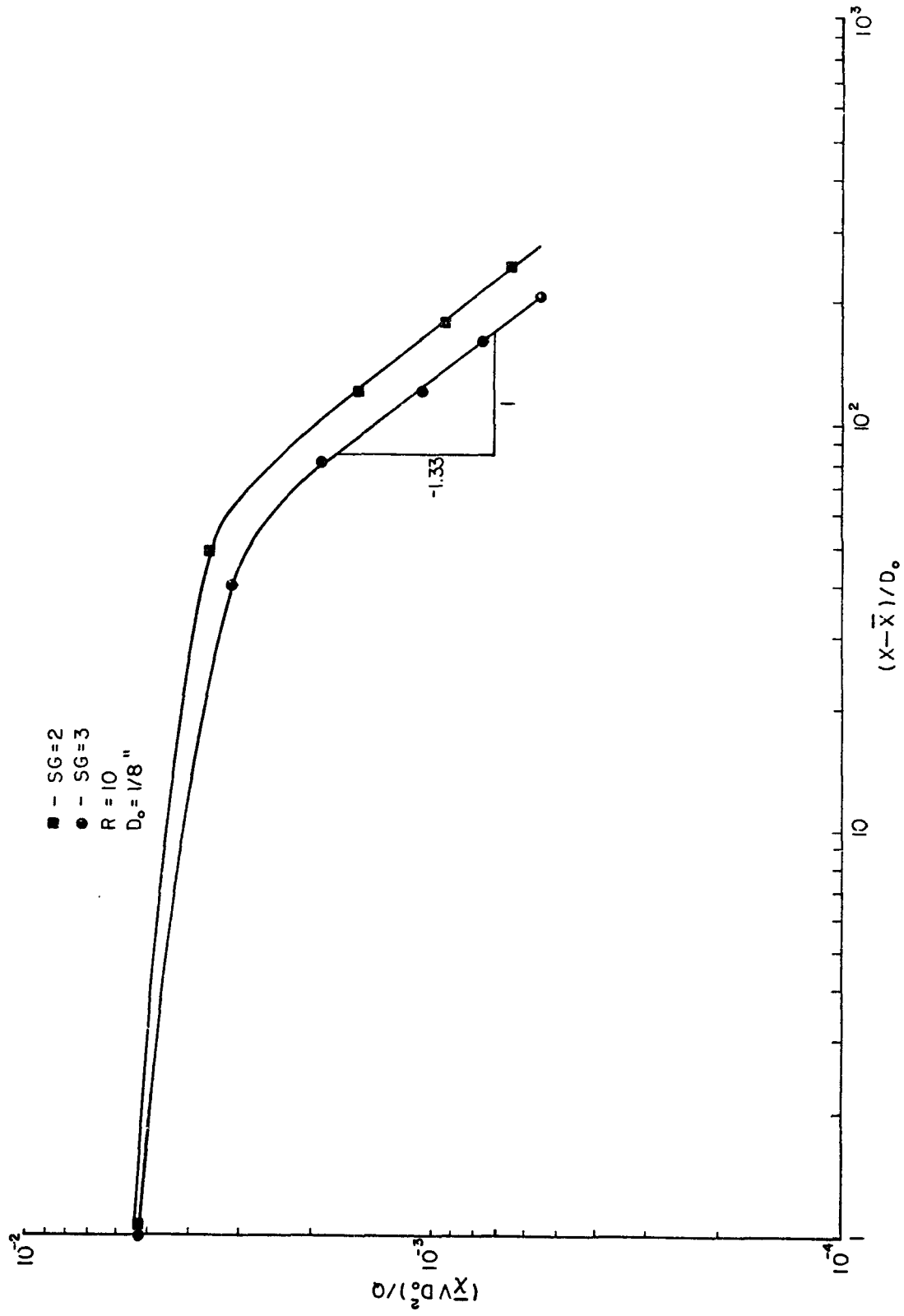


Fig. 17. Maximum Concentration vs. Downstream Distance, Plumes in a Laminar Crosswind, $R=10$, $D_o=1/8$ "

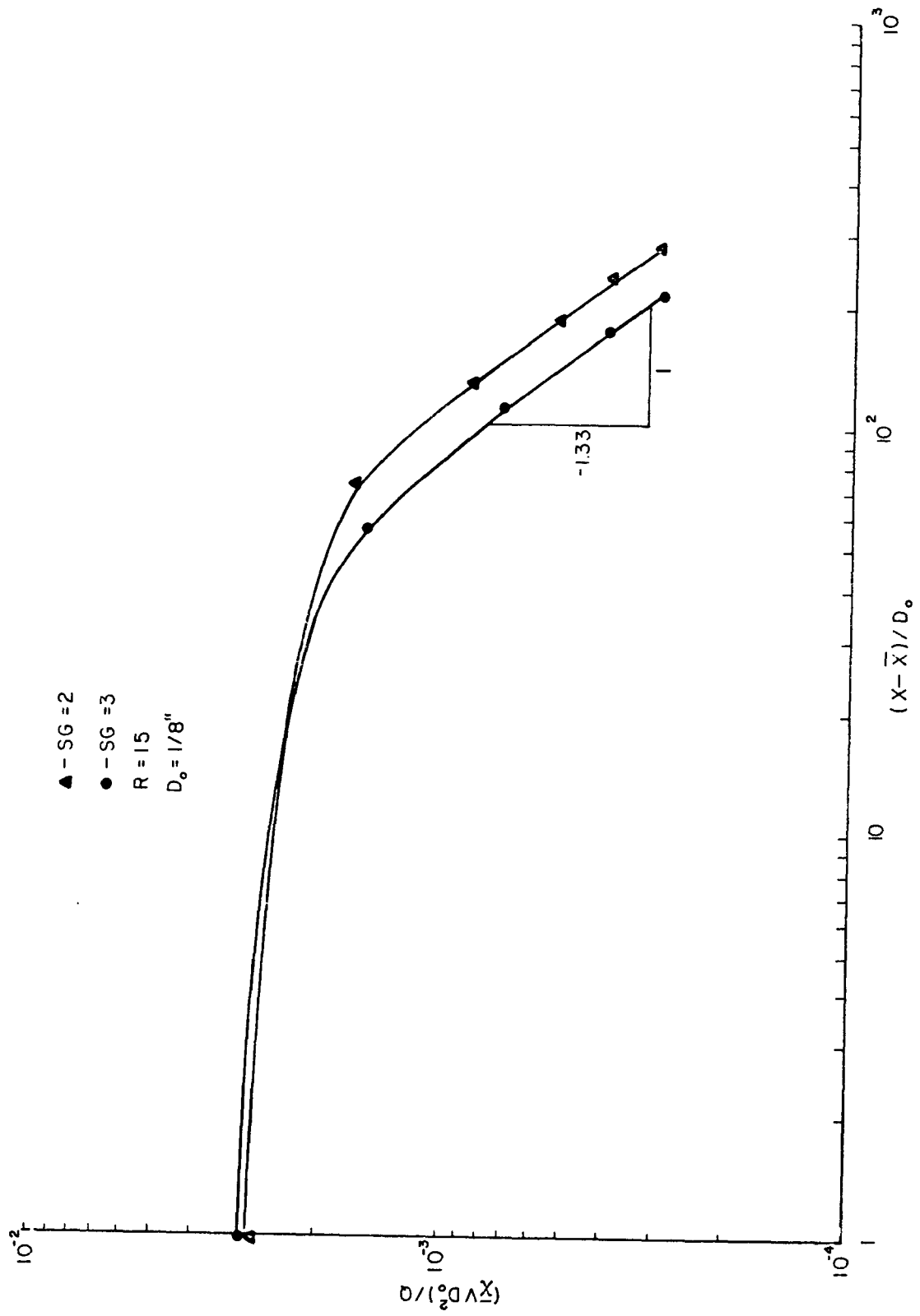


Fig. 18. Maximum Concentration vs. Downstream Distance, Plumes in a Laminar Crosswind, R=15, D₀=1/8"

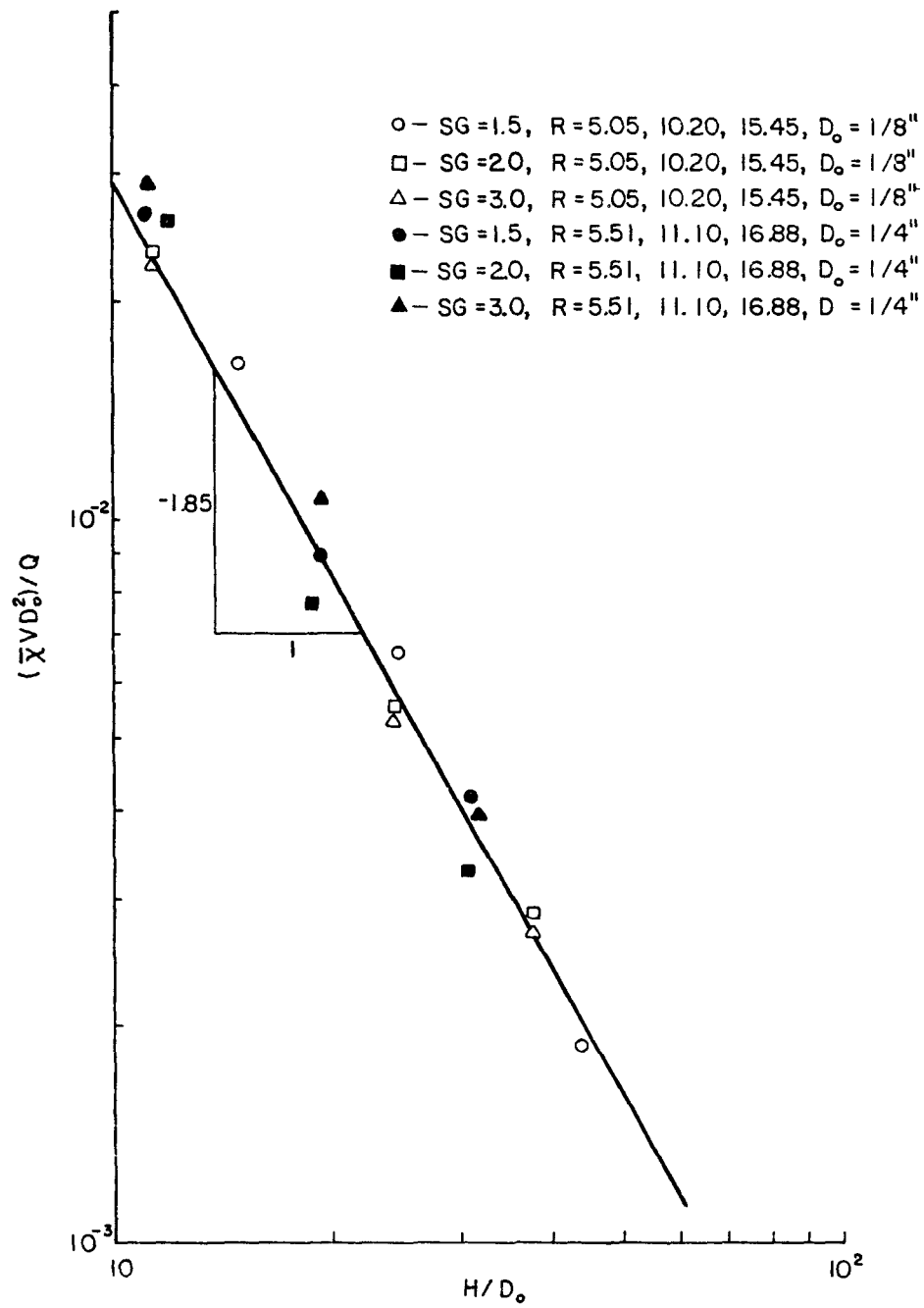


Fig. 19. Maximum Concentration at Plume High Point vs. H/D_o

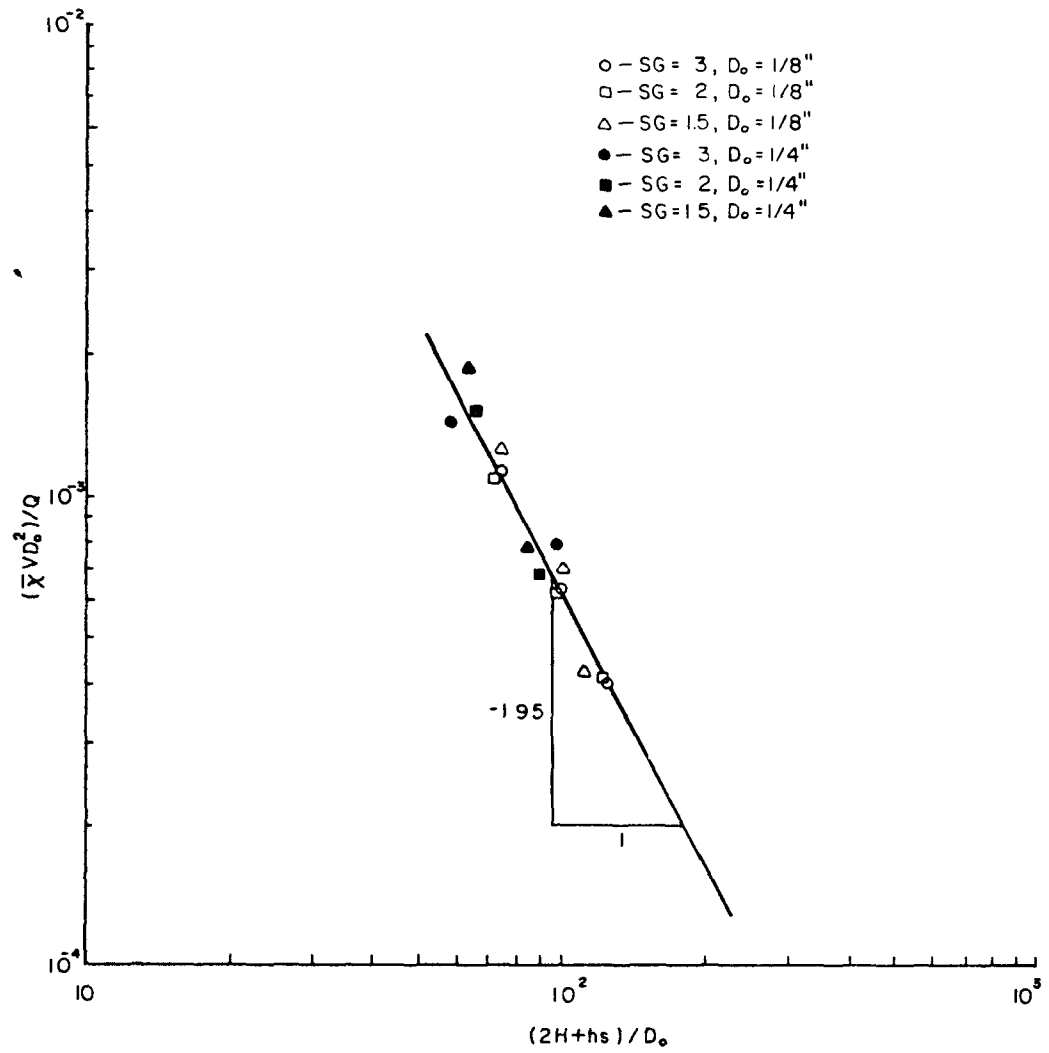


Fig. 20. Maximum Concentration at Plume Touchdown
vs. Fall Parameter

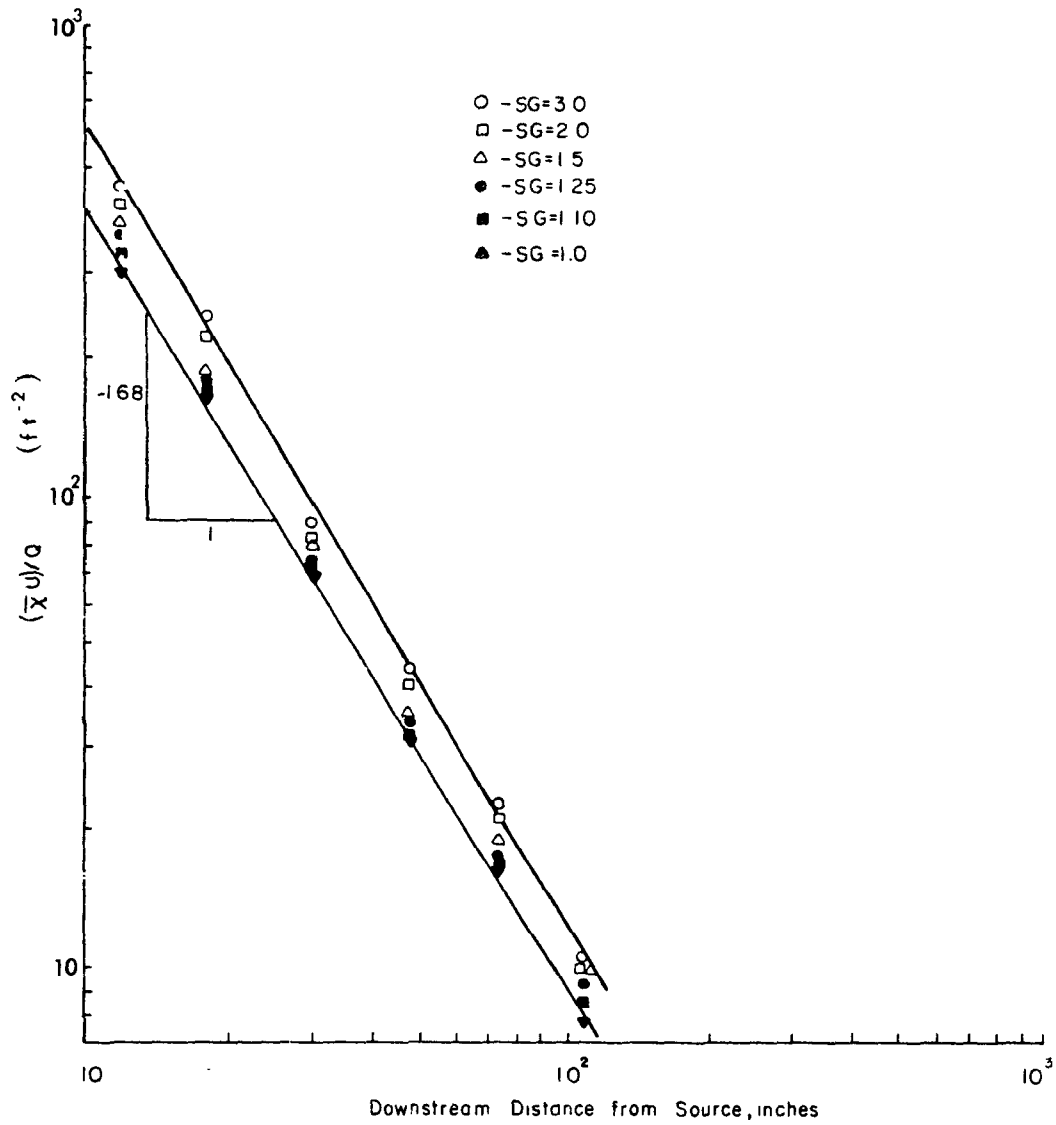


Fig. 21. Maximum Concentrations vs. Downstream Distance, Negatively Buoyant Ground Source, Neutral Stratification.

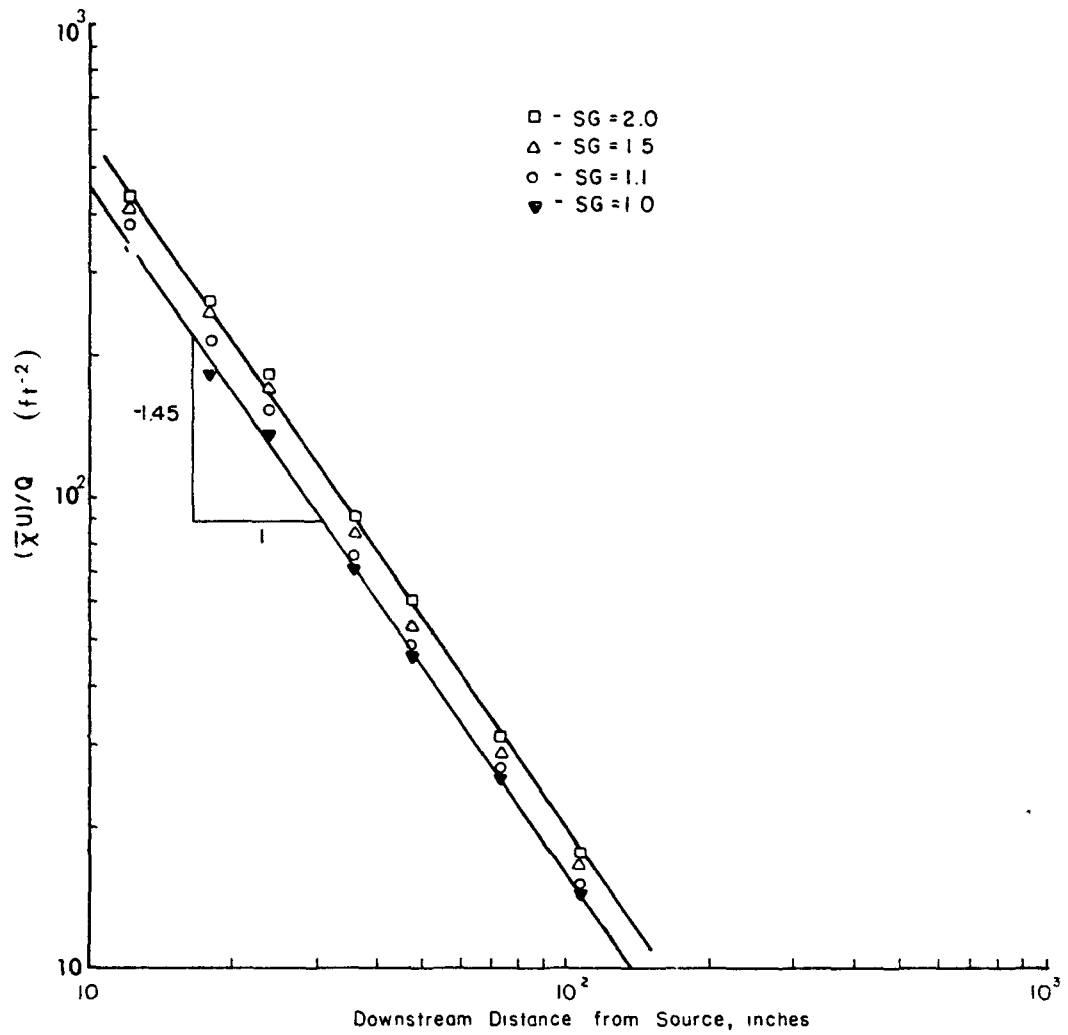


Fig. 22. Maximum Concentrations vs. Downstream Distance, Negatively Buoyant Ground Source, Inversion Stratification

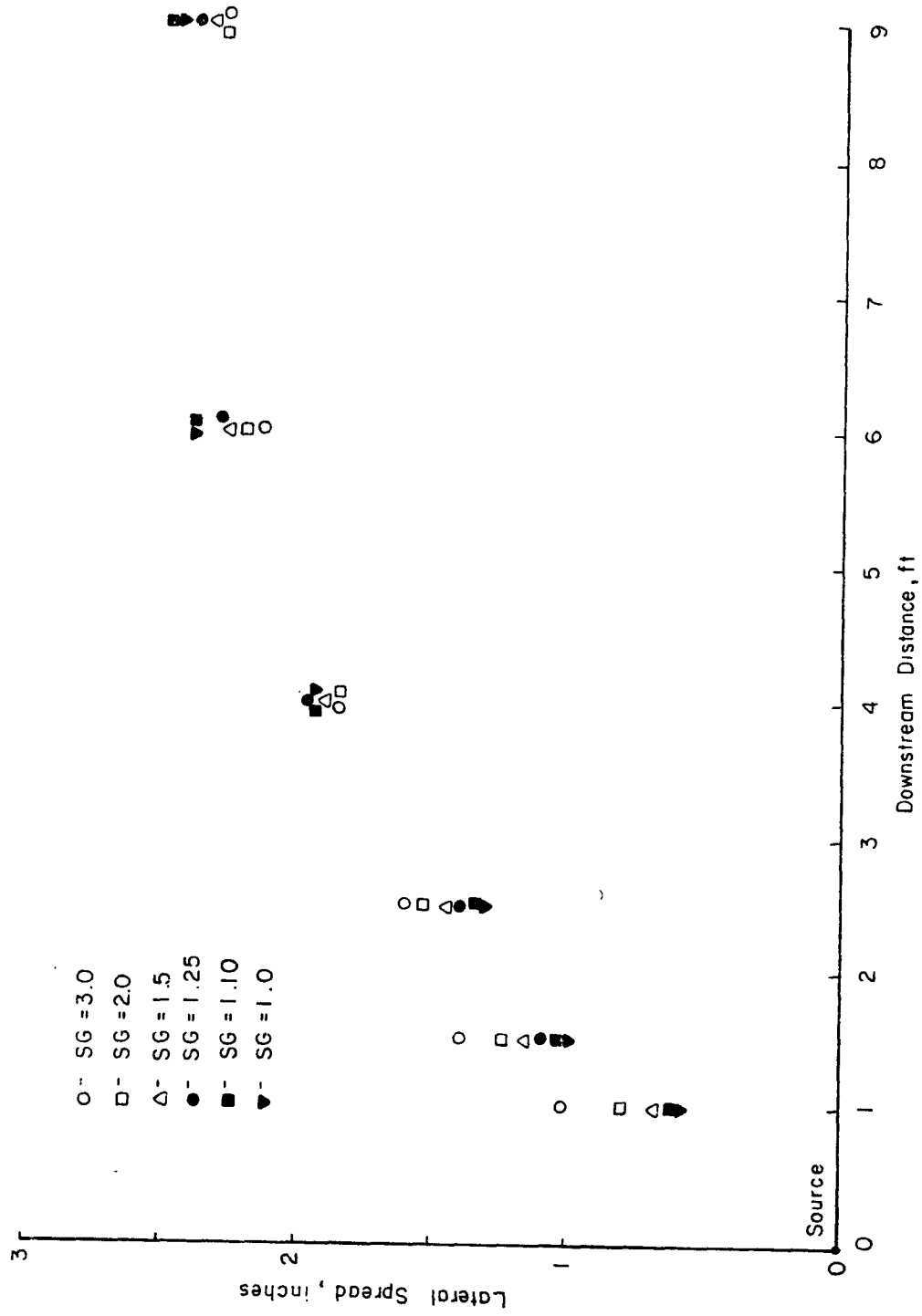


Fig. 23. Lateral Spread 50 Percent Concentration Neutral Stratification

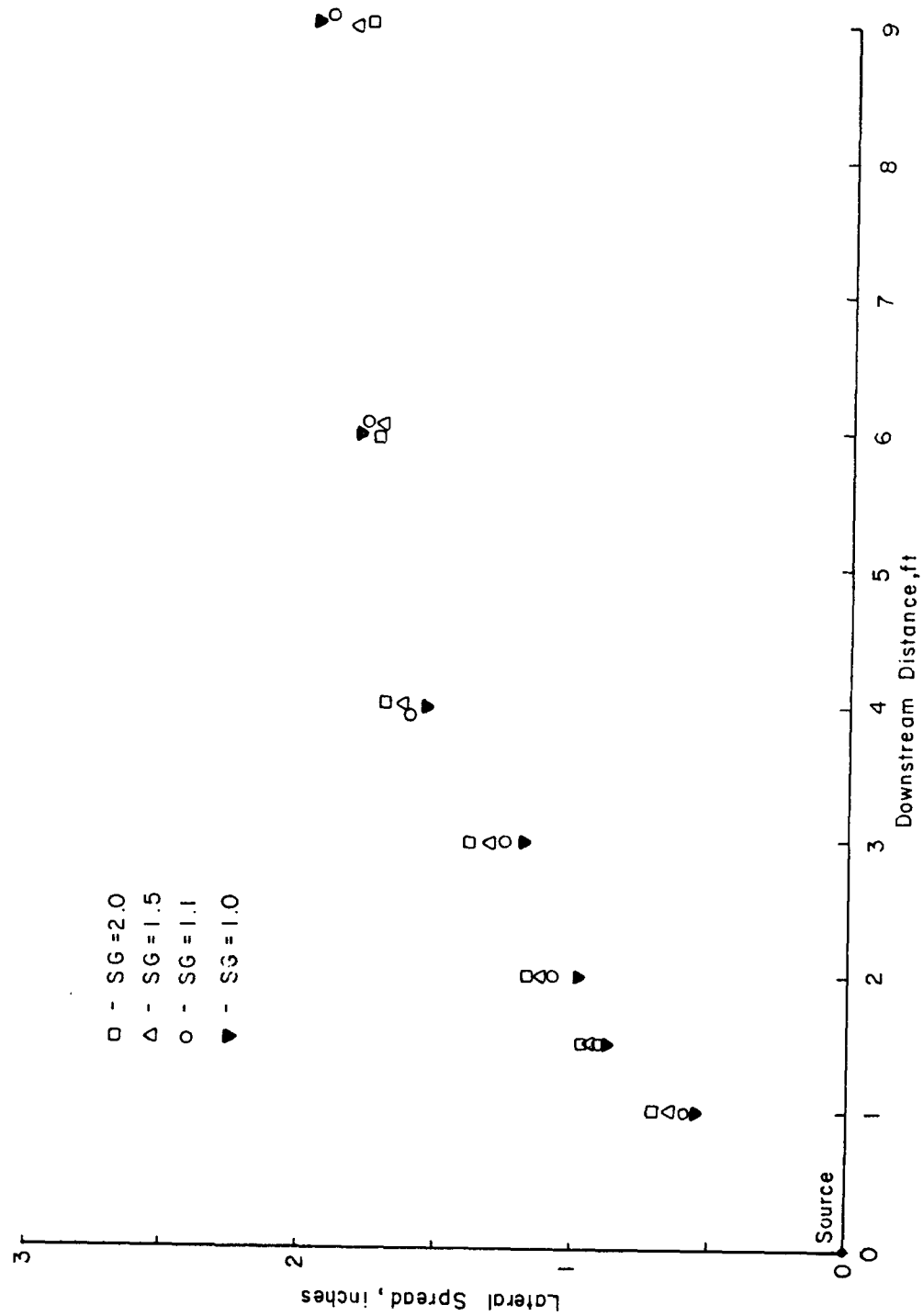


Fig. 24. Lateral Spread 50 Percent Concentration Inversion Stratification

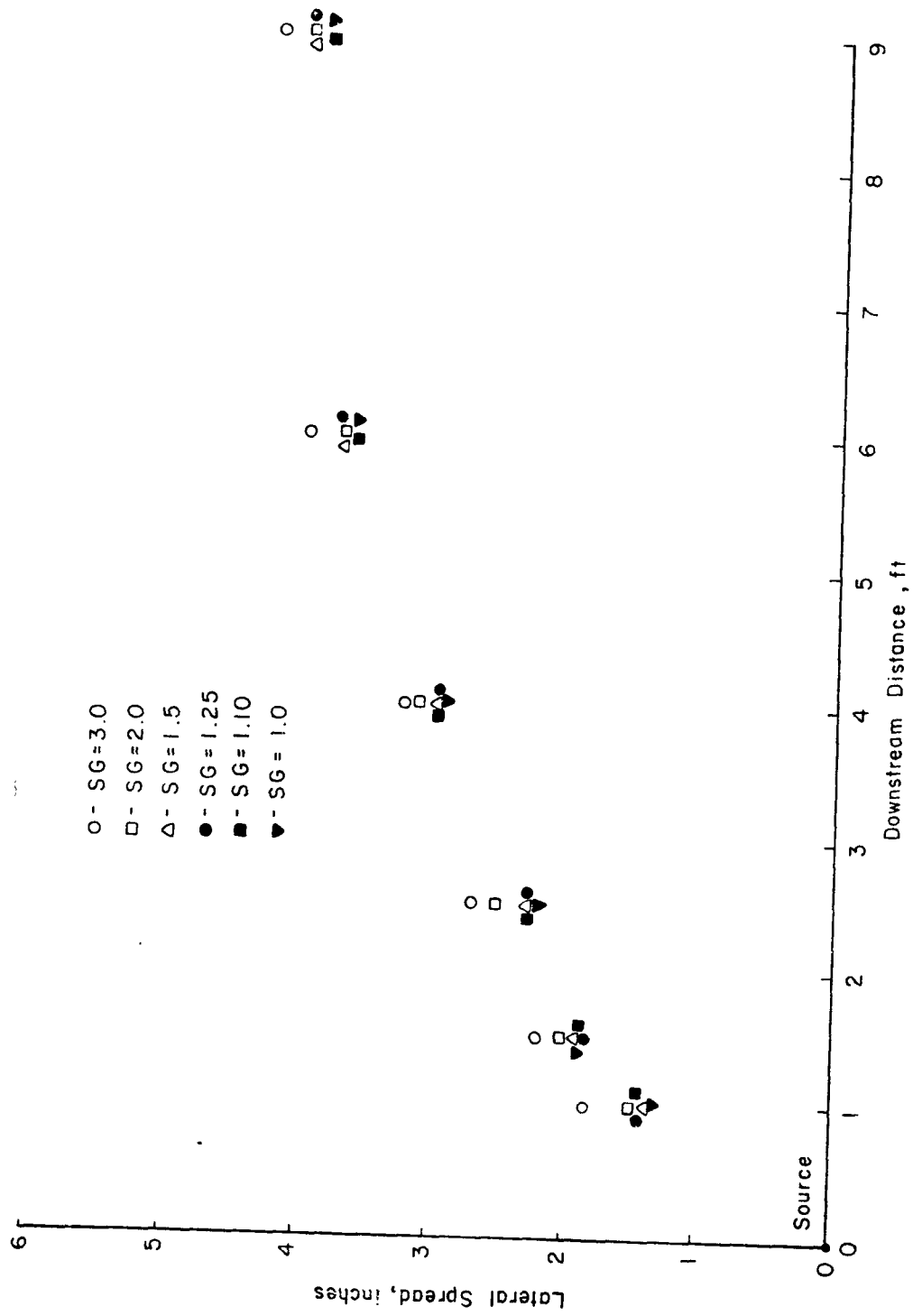


Fig. 25. Lateral Spread 10 Percent Concentration Neutral Stratification

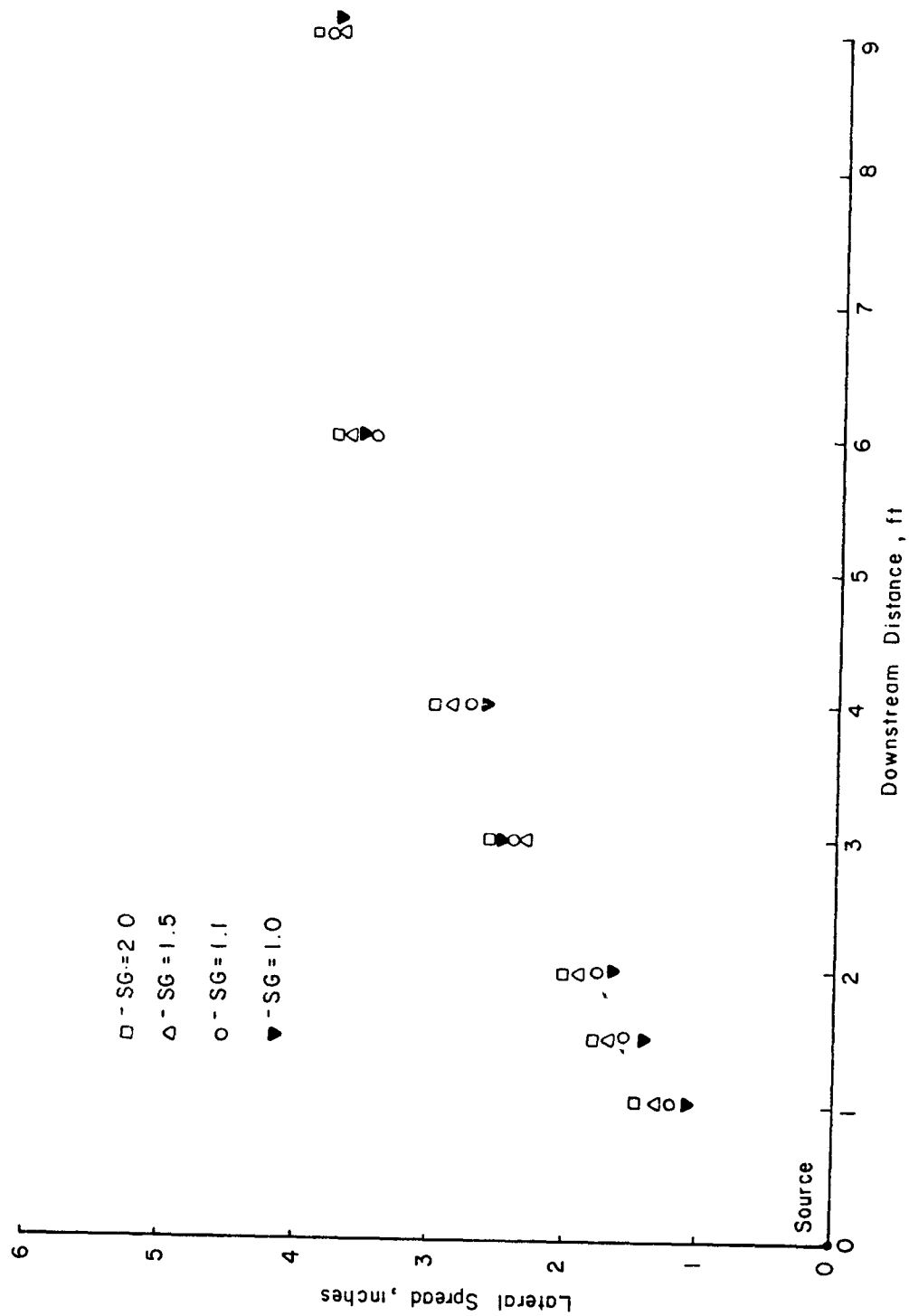


Fig. 26. Lateral Spread 10 Percent Concentration Inversion Stratification

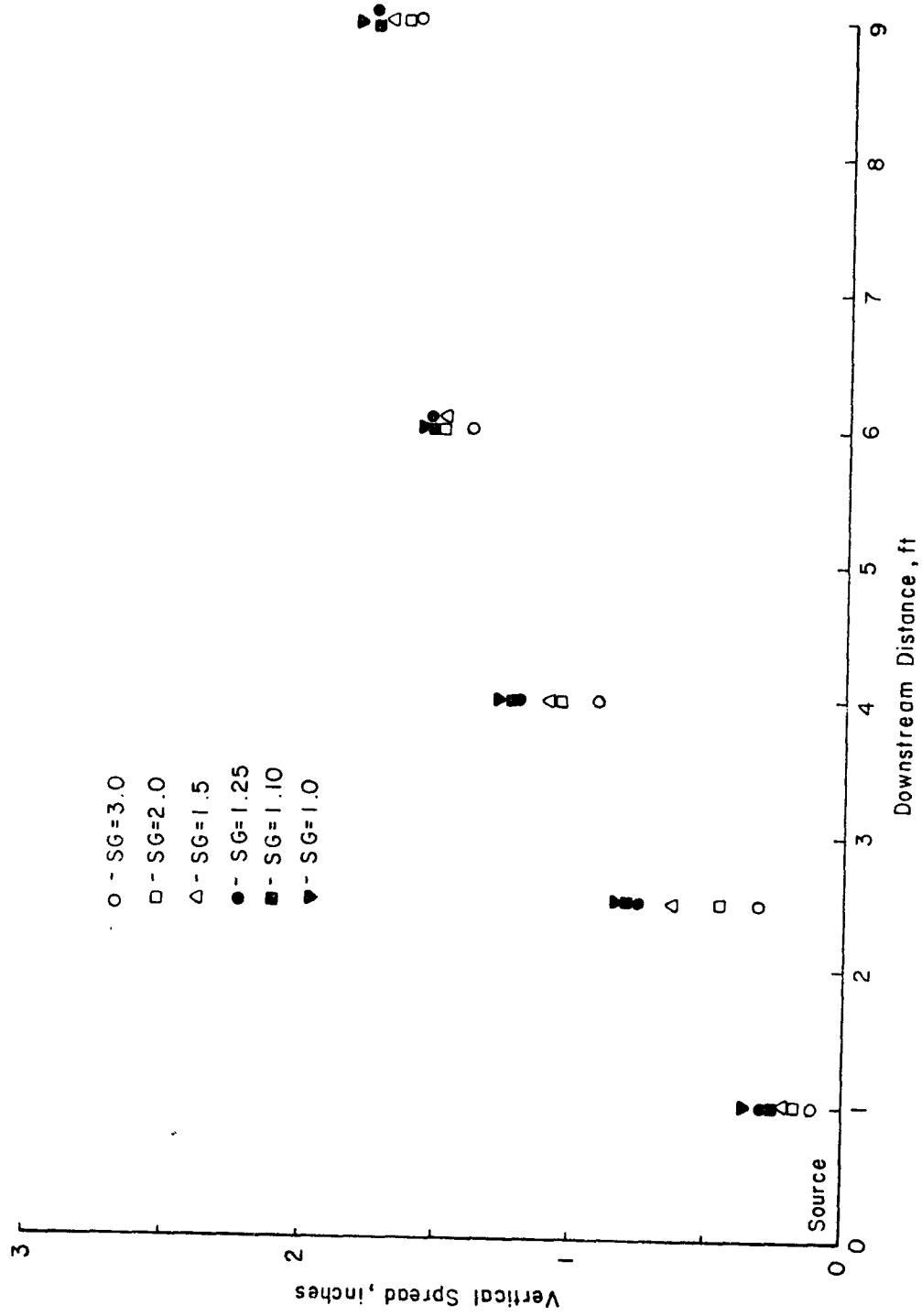


Fig. 27. Vertical Spread 50 Percent Concentration Neutral Stratification

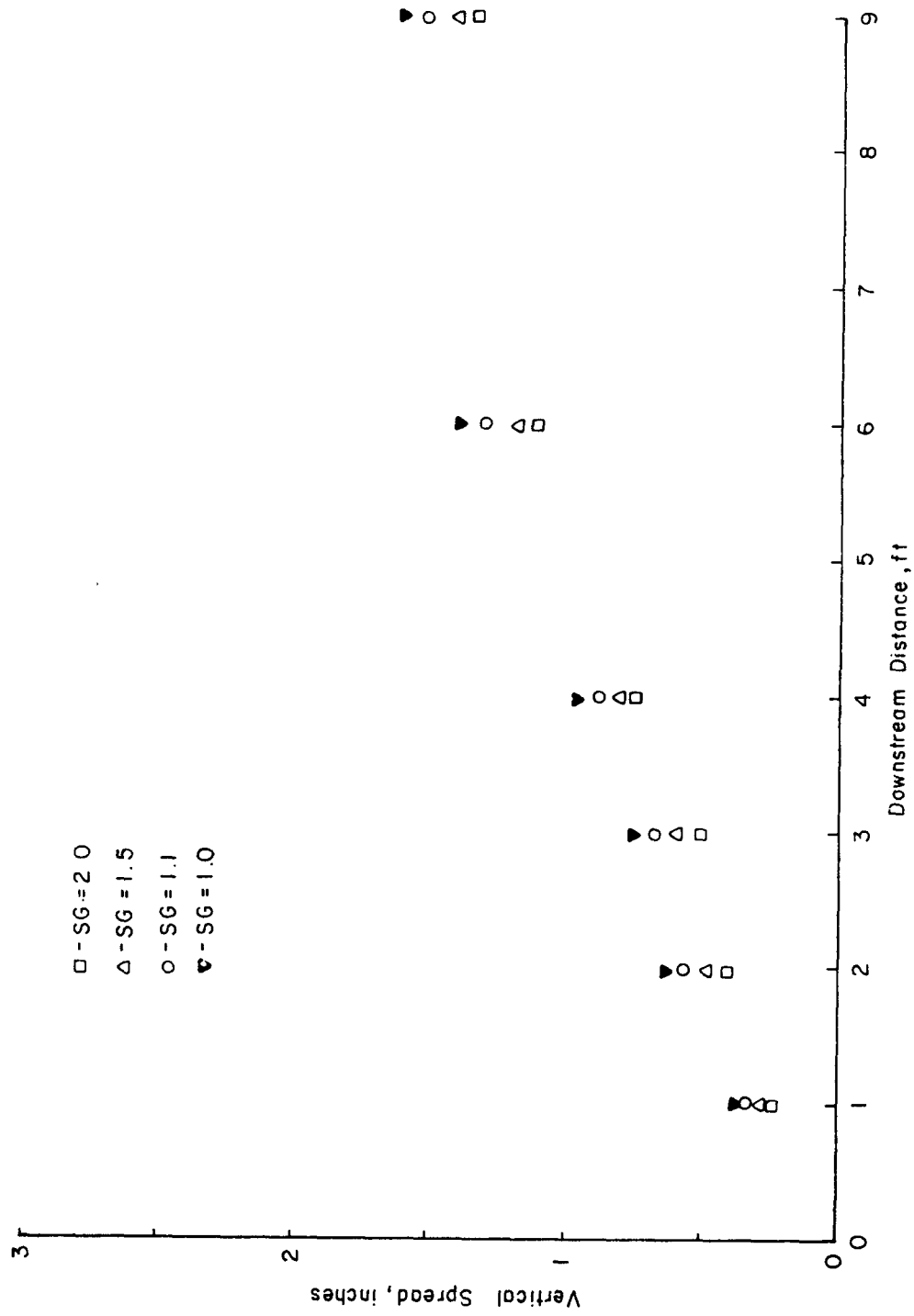


Fig. 28. Vertical Spread 50 Percent Concentration Inversion Stratification

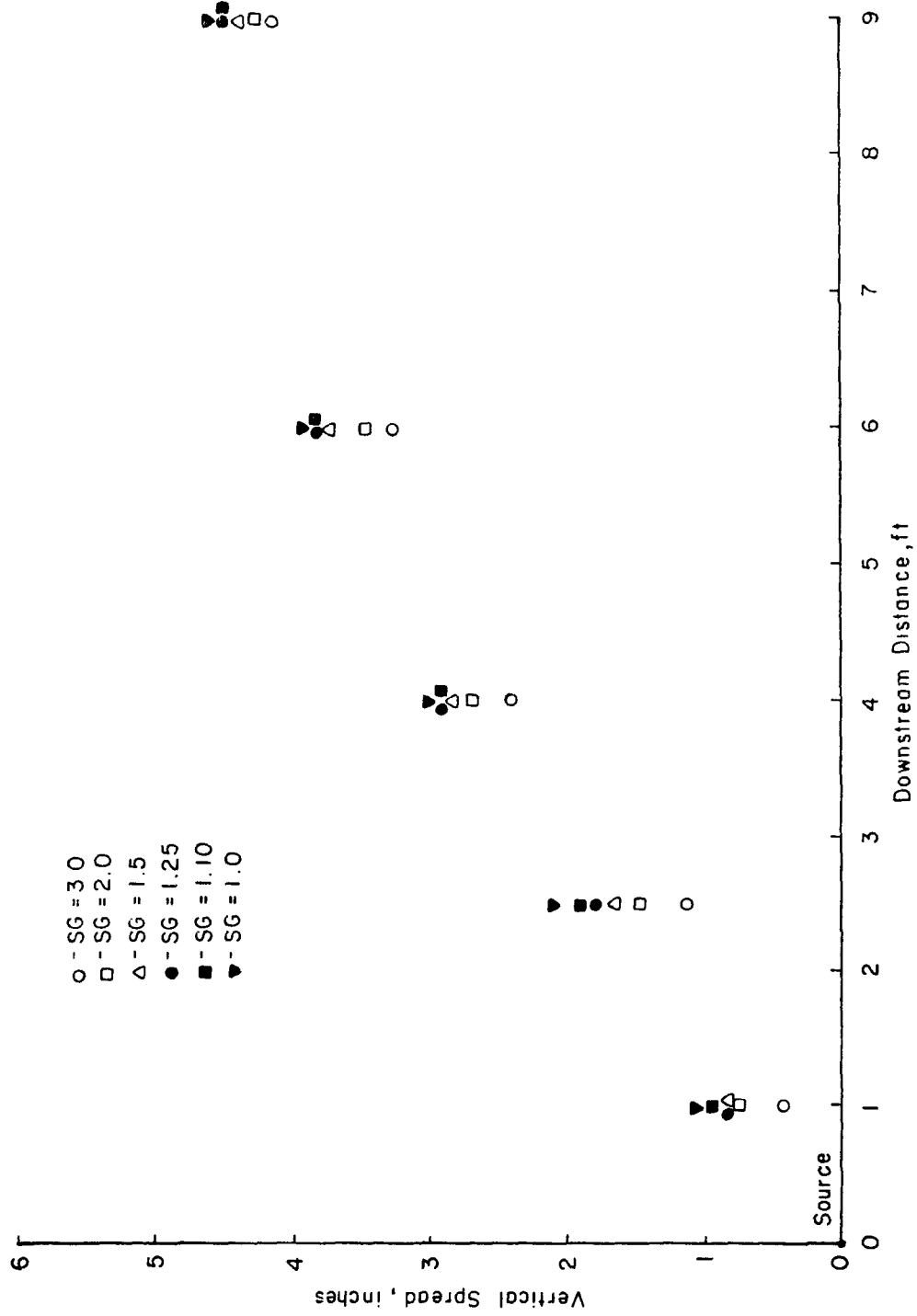


Fig. 29. Vertical Spread 10 Percent Concentration Neutral Stratification

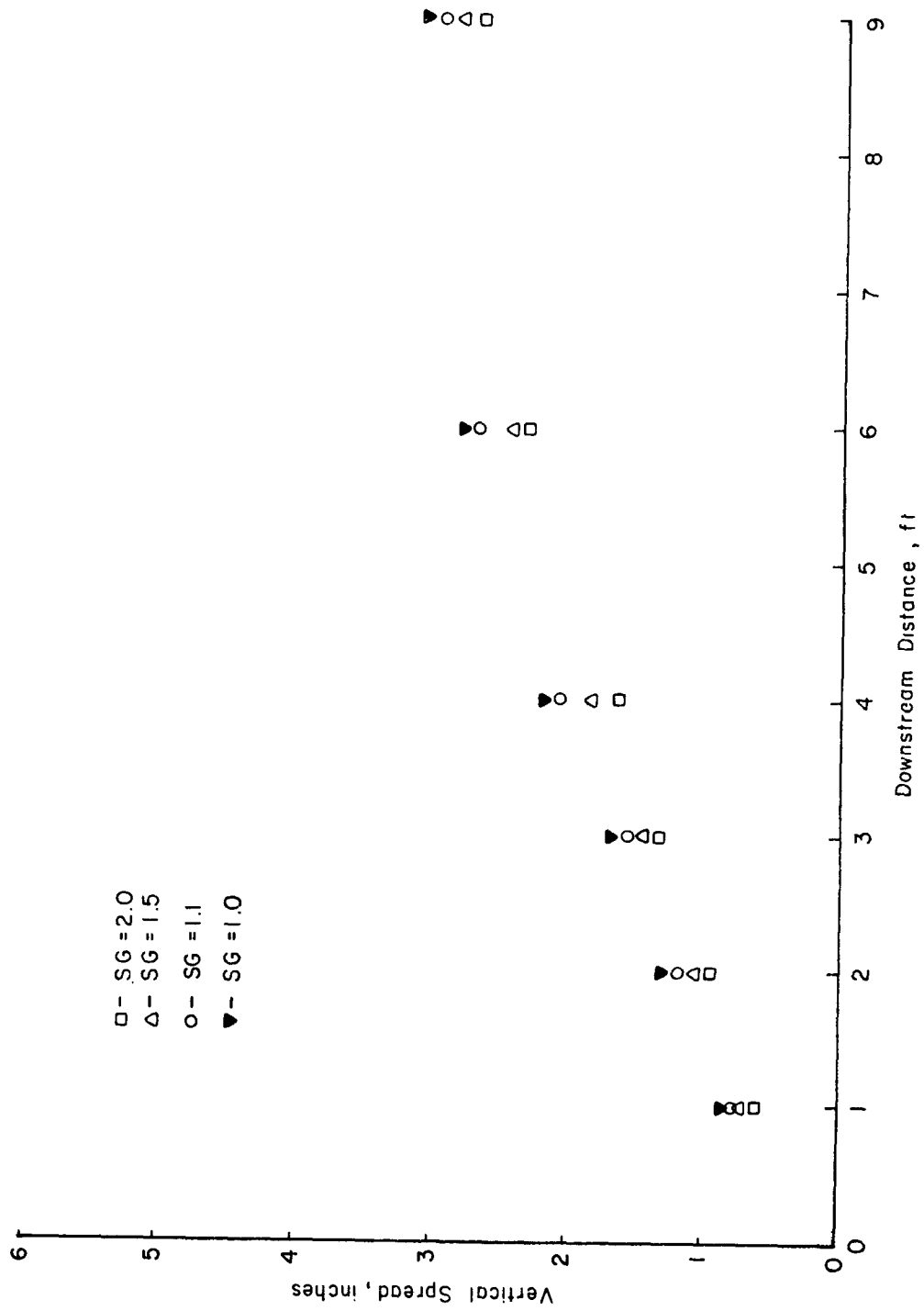


Fig. 30. Vertical Spread 10 Percent Concentration Inversion Stratification

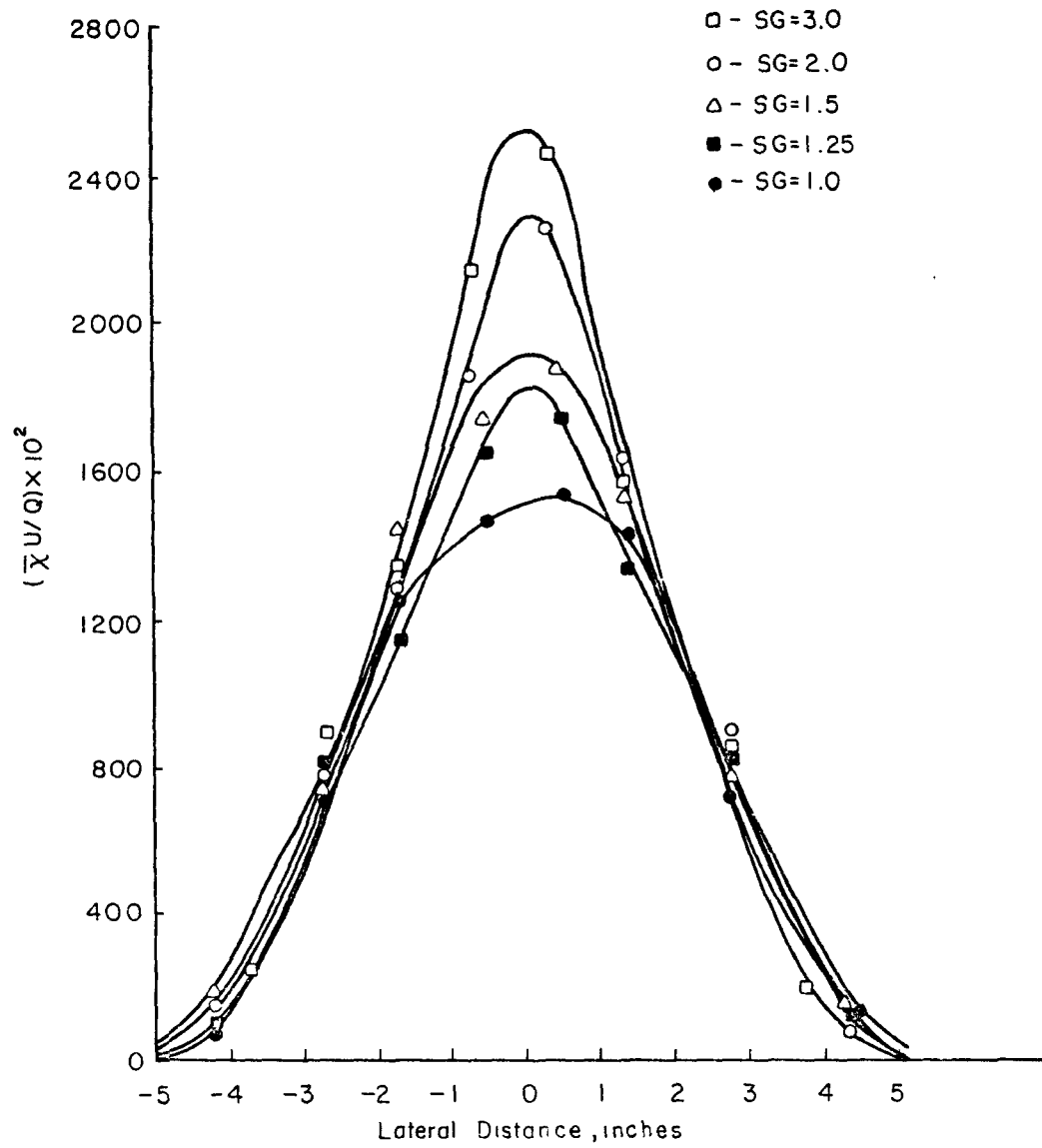


Fig. 31. Cross-sectional Distribution of Concentration, $x=6\text{ft}$. Neutral Stratification

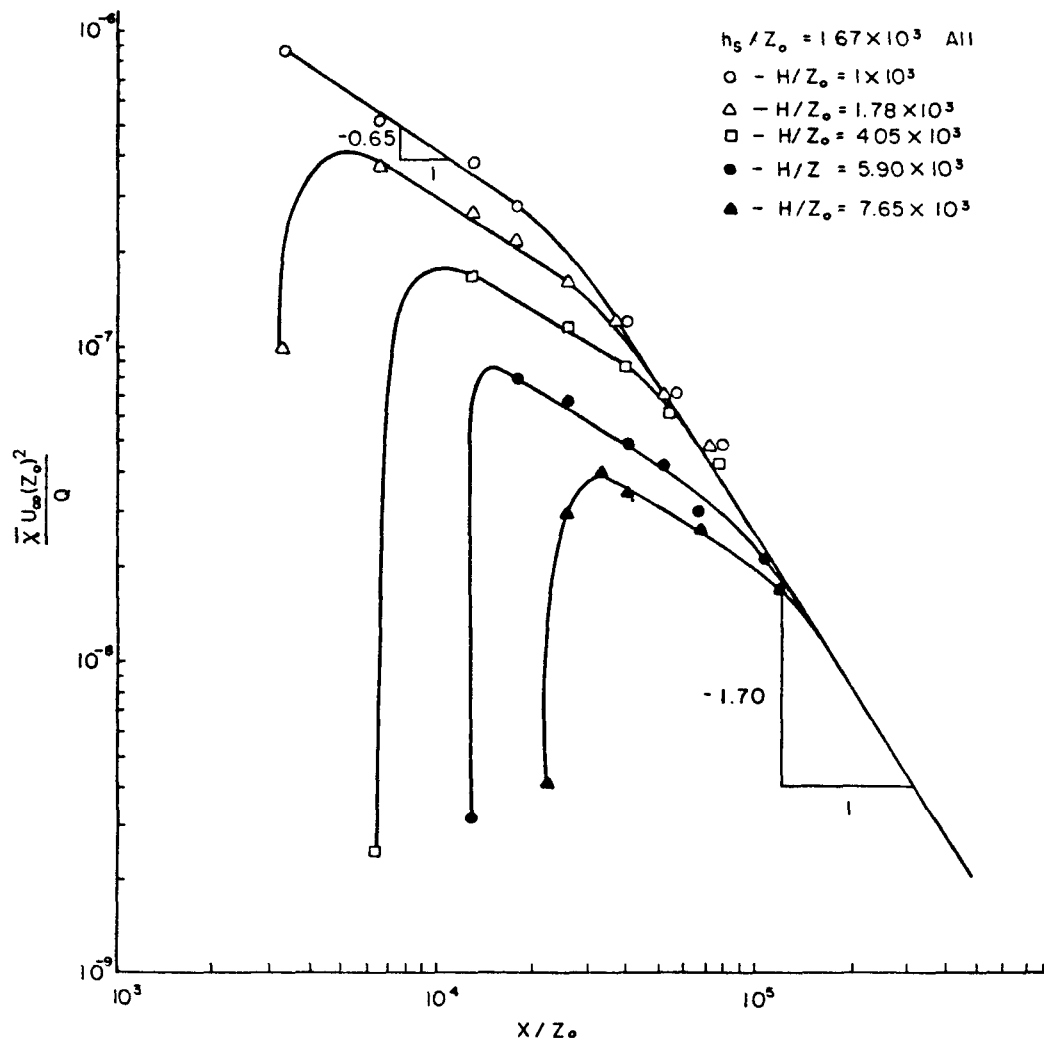


Fig. 32. Decay of Plume Maximum Concentration Downstream from Touchdown Point

TECHNICAL REPORT DATA

(Please read Instructions on the reverse before completing)

1. REPORT NO. EPA-650/3-74-003		2.	3. RECIPIENT'S ACCESSION NO.	
4. TITLE AND SUBTITLE WIND TUNNEL TESTS OF NEGATIVELY BUOYANT PLUMES			5. REPORT DATE October 1973	
			6. PERFORMING ORGANIZATION CODE	
7. AUTHOR(S) T. G. Hoot, R. N. Meroney and J. A. Peterka			8. PERFORMING ORGANIZATION REPORT NO. RNM-JAP-13	
9. PERFORMING ORGANIZATION NAME AND ADDRESS Fluid Dynamics and Diffusion Laboratory Colorado State University Fort Collins, Colorado 80521			10. PROGRAM ELEMENT NO. 1AA009	
			11. CONTRACT/GRANT NO. AP-01186	
12. SPONSORING AGENCY NAME AND ADDRESS Meteorology Laboratory - EPA National Environmental Research Center Research Triangle Park, North Carolina 27711			13. TYPE OF REPORT AND PERIOD COVERED Final	
			14. SPONSORING AGENCY CODE	
15. SUPPLEMENTARY NOTES				
16. ABSTRACT The results of tests made of negatively buoyant emissions into a quiescent medium, laminar crosswind and turbulent boundary layer conducted in a wind tunnel and reported. Measurements include the maximum rise height, horizontal point of descent and behavior of emission characteristics.				
17. KEY WORDS AND DOCUMENT ANALYSIS				
a. DESCRIPTORS		b. IDENTIFIERS/OPEN ENDED TERMS		c. COSATI Field/Group
Wind tunnel tests Negatively buoyant plumes Plume dispersion Plume rise Air pollution meteorology				
18. DISTRIBUTION STATEMENT Unlimited		19. SECURITY CLASS (This Report)		21. NO. OF PAGES 104
		20. SECURITY CLASS (This page)		22. PRICE

ENVIRONMENTAL PROTECTION AGENCY
Technical Publications Branch
Office of Administration
Research Triangle Park, N.C. 27711

OFFICIAL BUSINESS

AN EQUAL OPPORTUNITY EMPLOYER

POSTAGE AND FEES PAID
ENVIRONMENTAL PROTECTION AGENCY
EPA - 335



Return this sheet if you do NOT wish to receive this material ☐,
or if change of address is needed ☐. (Indicate change, including
ZIP code.)